CHALMERS
UNIVERSITY OF TECHNOLOGY

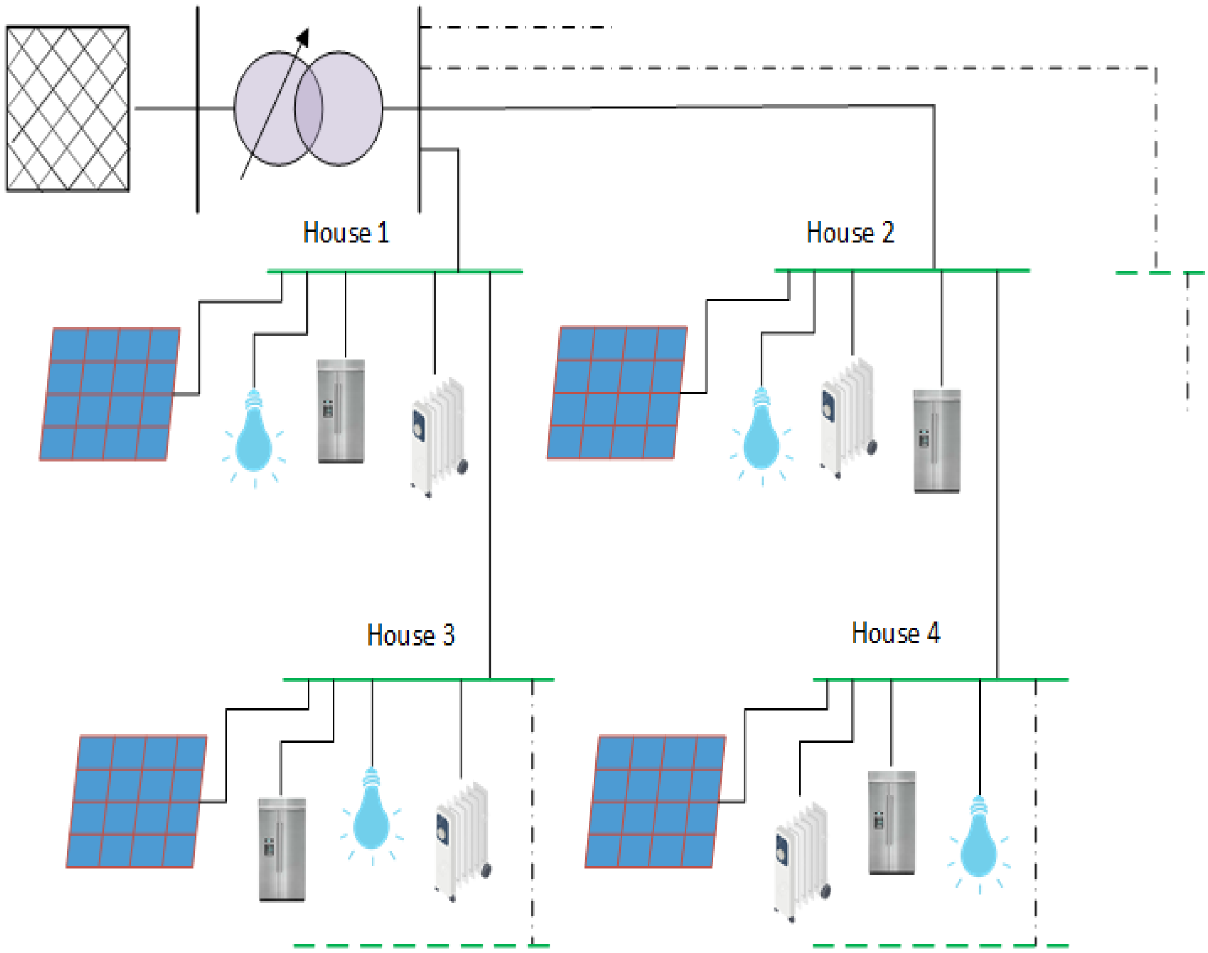

Investigation of Cloud-Effects on Voltage Stability of Distribution Grids with Large Amount of Solar Photovoltaics

Master’s thesis in the program of Electric Power Engineering

Valeriu Cirjaleanu

Department of Energy and Environment
Division of Electric Power Engineering
CHALMERS UNIVERSITY OF TECHNOLOGY
Gothenburg, Sweden 2017

MASTER'S THESIS

Investigation of Cloud-Effects on Voltage Stability of Distribution Grids with Large Amount of Solar Photovoltaics

Valeriu Cirjaleanu

In partial fulfilment for the award of Master of Science degree in Electric Power Engineering, in the Department of Environment and Energy, Division of Electric Power Engineering, Chalmers University of Technology, Gothenburg, Sweden

Supervisor: Jacob Edvinsson
WSP-Sverige SE-402 51
Department-Electrics
Gothenburg, Sweden
Email: jacob.edvinsson@wspgroup.se

Examiner: Anh Tuan Le
Division of Electric Power Engineering
Chalmers University of Technology SE-412 96
Gothenburg, Sweden
Email: tuan.le@chalmers.se

Department of Energy and Environment
Division of Electric Power Engineering
CHALMERS UNIVERSITY OF TECHNOLOGY
Gothenburg, Sweden 2017

Investigation of Cloud-Effects on Voltage Stability of Distribution Grids with Large Amount of Solar Photovoltaics

Master's Thesis in the program of Electric Power Engineering
Valeriu Cirjaleanu

Department of Energy and Environment
Division of Electric Power Engineering
Chalmers University of Technology
SE-412 96 Gothenburg
Sweden
Telephone: + 46 (0)31-772 1000
Fax: +46 (0)31-7721633

Cover: Symbolic diagram for a distribution grid with photovoltaic power integration

Chalmers Bibliotek, Reproservice
Gothenburg, Sweden 2017

Investigation of Cloud-Effects on Voltage Stability of Distribution Grids with Large Amount of Solar Photovoltaics

Master's Thesis in the program of Electric Power Engineering

Valeriu Cirjaleanu

Department of Energy and Environment
Division of Electric Power Engineering
Chalmers University of Technology

Abstract

The Photovoltaic (PV) energy is becoming more and more popular nowadays due to both the awareness of people about environmental concerns and the governmental support schemes which makes it more accessible for the potential PV owners to install PV systems at the residential level. However, the integration of large amount of PV systems at the residential level might bring challenges to the utilities companies regarding the power quality and the reliability of the system. One of the biggest challenges is the power output fluctuation of the PV systems. This fluctuation is caused by the weather condition and especially, by the fast-moving clouds which can be referred as the ''cloud-effect''.

This project work has investigated the ''cloud-effect'' of the solar PV units in a residential grid with regard to voltage stability. The residential network (the real system) is a 10/0.4 kV radial grid located in Mölndal area, Göteborg. The simulations have shown that the Mölndal grid was able to maintain its voltage stability when cloud induced power swings occurred in the network. This outcome can be explained as the distribution network is designed to be a strong grid with high short circuit capacity, short line branches and low load condition during the summer in the Swedish residential houses.

However, in order to investigate the potential negative impacts of the cloud induced power swings on another possible weaker residential network, the operational parameters (the short circuit capacity and the load power) of the real system were modified. The simulations have shown that for the modified system, the network was able to maintain its voltage stability for 20-40 % PV penetration levels. For the 50% PV penetration level, cloud induced power swings caused low operational voltage profiles (voltage instability) within the grid. This instability was not properly identified when the loads were modeled as static loads. Therefore, dynamic load models are recommended to be implemented in impact-studies in order to investigate more accurate the PV impact on the system operation, especially when a relatively large amount of the system load is represented by induction motors.

Different mitigating solutions were proposed and implemented in the simulation for the modified case scenario. Static Var Compensator, STATCOM and Energy Storage Devices were found to improve the voltage stability limits of the network and therefore, to allow a higher penetration level of PV energy. The simulations have shown that ESD are the best mitigating solutions in order to counteract the PV power drops if they are located in close proximity of the electrical loads. For the case with SVC integration, it was found that the placement and the size of the device has to be correlated with the regulating transformer for proper and reliable operation of the grid. For the case with STATCOM integration, it has been shown that its dynamic transient response was superior to SVC when the network was

subjected to PV power drops. This difference was due to both, that the device incorporated an inverter which provided reactive power independent of the grid voltage and also that its dynamic control was roughly modeled as for a PV inverter. By using this type of control algorithm, the reactive power support of the device was injected more casually which led to a better transient response within the system.

Key Words: Photovoltaic (PV), Penetration Level, Induction Motor (IM), Under Load Tap Changer (ULTC), Static Var Compensator (SVC), Static Synchronous Compensator (STATCOM), Energy Storage Devices (ESD).

Acknowledgments

I would like to thank my supervisor at WSP, Jacob Edvinsson for support, patience and understanding during the entire project work. I would also like to thank my examiner at Chalmers, Tuan Anh Le for his professional comments and discussions in order to improve the content of the report. Special thanks go to Tarik Abdulahovic for his assistance and his advices regarding the PSCAD simulation platform which gave me a better insight of the working principle of a PV generation system. Special thanks go also to my classmate, Enock Mulenga for his advices and his involvements during my thesis work.

I would also like to thank the ABB staff for providing the NEPLAN software's license for the study to be conducted and their effort to help me with the activation key during the last steps of the thesis work. Last, but not in the end, I would like to thank the WSP personnel for making the working place a nice work environment.

Contents

List of Figures

List of Tables

List of Symbols, Abbreviations and Acronyms

ETR:	Extra Terrestrial Radiation
CI:	Clearness Index
VI:	Variability Index
ac:	Alternating Current
dc:	Direct Current
V:	Voltage
P:	Active Power
Q:	Reactive Power
Z:	Impedance
R:	Resistance
X:	Reactance
ZIP:	Constant Impedance, Constant Current and Constant Power Loads
ULTC:	Under Load Tap Changer
PV:	Photovoltaic
MPPT:	Maximum Power Point Tracking
P-V:	Power-Voltage Curves
PCC:	Point of Common Coupling
PLL:	Phase Locked Loop
VSI:	Voltage Source Inverter
FACTS:	Flexible Alternating Current Transmission System
SVC:	Static Var Compensator
STATCOM:	Static Synchronous Compensator
IM:	Induction Motor
ESD:	Energy Storage Devices

1 INTRODUCTION

This chapter presents the background and the problems associated with PV energy integration into the distribution grids. It clearly states the objective of the thesis and the specific tasks/limitations that had to be achieved in order for the study to be conducted. It basically provides the main structure for the entire project work.

1.1 Background

In the wake of climate change, more attention is put to ’’green’’ energy production. Renewable energy resources are fossil fuel-less and environmentally friendly. One method to produce energy in a sustainable way is to make use of photovoltaic (PV) panels which convert directly the solar energy into electricity. The active power generated by the PV units is proportional with the irradiation level which reaches the PV panels. Therefore, any fluctuation in the irradiation level (caused by weather conditions) will lead to variation in the output power of the PV systems. Since, the electric energy cannot be stored; any imbalance between the generation and consumption can lead to failures. Hence, due to the intermittency nature of the solar energy, full PV integration is still hard to achieve.

In the recent years, PV power has emerged as a mainstream technology for generating clean and secure electricity in a decentralized fashion, ideally allowing for electricity to be produced on the same premises where it is consumed, albeit often at different times [1]. Integration of large amount of PV solar units, however, might have a negative impact not only on distribution systems but also on transmission and generation systems as well. Grid operators are concerned with the behavior of PV power output fluctuations over various timescales. Opaque clouds cause reductions in output power by 50 to 80% within the time period it takes a large cloud to cover an array, which typically ranges from a few seconds for a kW facility to a few minutes for a large utility scale plant [2].

Cloud effects can cause PV power fluctuations. Due to the fact that the PV units only generate active power, traditionally, power system frequency will be affected and vary with PV power. However, in distribution systems the R/X ratio of lines and cables is much larger than in transmission systems, so real power variation can result in a comparable impact on grid voltage to reactive power

Short-term irradiance fluctuations can cause voltage fluctuations that can trigger automated line equipment (e.g. tap changers) on distribution feeders leading to higher maintenance costs for utilities [2]. In the extreme case, the irradiance fluctuation can cause voltage instability. Therefore, detailed analyses and simulations must be done in order to understand the impacts of PV generation on the electrical grid. Consequently, there is a need to find appropriate solutions to mitigate the PV drawbacks on the system operation and to maximize the use of solar energy.

1.2 Problem description

When it comes about solar and wind energy, big questions arise on their impact on the power system operation due to their power output variation. An important concern, in the power output variation, regarding the PV energy is caused by the so called ’’cloud effect’’. In this case, the operator is unable to predict the weather behavior and back-up solutions must be found for the efficient operation of the system.

The fast moving clouds, which might cover the PV panels in a short period of time, could affect the voltage stability in the distribution systems. The distribution systems have their own characteristics which make them different from transmission systems. Distribution systems are characterized by: heavy loading condition, low voltage level, high R/X ratio, unbalanced structure etc. Moreover, the distribution regulating transformers have a longer time delay for the first tap operation compared with the transmission transformers.

When there is a sudden decrease in irradiance, the power output of the PV panels will be lowered and therefore, a sudden voltage drop will appear along the feeders. In this case, the tap-changer distribution transformer might be unable to control the voltage within the limits due to the fast changing in the active power production by the PV units and the delayed time (30-60 s) in the transformer’s first tap operation. Because of this, the voltage at some remote buses could reach unacceptable low values.

The potential occurred low voltage values could affect the proper operation of the electric loads and especially, constant power loads. Constant power loads tend to restore their pre-disturbance power condition to a specific extent within a relatively short period of time drawing a higher current from the system. This will lead to higher losses and voltage drops in the entire system and inadmissible low voltage violations might occur, especially in the case of induction motor connected load.

The induction motor load is very sensitive to supply voltage variations in that its electromechanical torque is proportional with the square of the supply voltage. If the supply voltage becomes too low, the motor might not able to meet the requirements of the mechanical load torque and the induction motor will stall. Once the induction motor load has stalled, its demand for active and especially reactive power will increase substantially which will cause additional voltage drops in the system. This situation is dangerous in the sense that it can lead to voltage collapse and the protection system could disconnect a part of the system load.

1.3 Objective

The objective of this thesis was to investigate the ’’cloud-effect’’ on voltage stability of a distribution grid with different PV penetration levels and to find appropriate solutions to mitigate their negative effects, if any.

The thesis attempted to answer the following research questions:

1. What could be the maximum PV penetration level into a distribution grid from voltage stability point of view, when cloud induced power swings occur in the network?
2. Is it any difference between the dynamic and static loads operational behavior when the distribution grid is subject to clouds’ disturbance?
3. What could be the possible mitigating solutions in order to increase the PV penetration level in order to counteract the ’’cloud-effect’’ and the potential differences between them?

1.4 Specific Tasks

In order to analyze the dynamic impact of PV energy intermittency on voltage stability, a good theoretical knowledge regarding voltage stability had to be accomplished. After that, a more in depth literature study regarding: distributions systems, PV generation system and load modeling had to be fulfilled as well. The thesis was conducted by implementing the PV generation system, load modeling and grid topology in the Neplan simulation tool and different simulation scenarios were performed. In general terms, the steps of the thesis may be described as:

1. Literature study;
2. Familiarization with the Neplan simulation tool;
3. Data collections/measurements for both PV generation and load characteristics;
4. Implement the investigated network with/without PV energy integration and perform simulations;
5. Analyze the behavior of the grid's characteristics, understand the impact of the different factors on grid's operational parameters and propose mitigating solutions.

1.5 Scope

The scope of the thesis was to analyze the voltage stability of a distribution grid with lots of solar photovoltaics when cloud induced power swings occurred in the network. In order to achieve this, several assumptions/limitations were made:

1. The ''cloud-effect'' was simulated only by a decrease in the irradiation level corresponding to clouds' coverage of the PV systems. The increase in the irradiation level when the clouds could unveil the PV units was not investigated.
2. The PV generation system was modeled simply as a dispersed generation system operated at unity power factor. Therefore, the control system and the involved dynamics inside the PV system were neglected.
3. The regulating transformer was modeled to regulate the voltage mainly at the secondary side and therefore the devices to incorporate line drop compensation (LDC) control were not implemented.
4. PV penetration level was calculated based on the total load demand rather than the potential roof top area of the houses.

1.6 Thesis Layout

The remaining of the thesis is organized as follow:

1. **Chapter 2** presents the background knowledge that had to be achieved in order to understand the challenges of PV energy integration at the distribution level. Solar energy variation, PV generation system, voltage stability concept, FACTS devices and literature review were summarized in this chapter.
2. **Chapter 3** presents the methods and the approaches used in the grid modeling. It presents the network data, load data, PV data and software processing data. Different assumptions and limitations were made in this chapter.

3. **Chapter 4** presents the simulation results of the ´´cloud-effect'' for different PV penetration levels for the real grid as well for the modified grid. The chapter presents also the difference between the dynamic and the static loads modeling subjected to voltage disturbance for the modified network scenario.
4. **Chapter 5** proposes and implements mitigation solutions regarding PV power swings in order for the modified system to maintain its voltage stability.
5. **Chapter 6** is the last chapter and presents the conclusion of the study and it suggests future work that can be done on the related topic.

2 LITERATURE STUDY

This chapter describes the most important characteristics that had to be achieved in order to analyze the effects of the cloud induced PV power swings could have on the voltage stability at the distribution level. The chapter starts explaining the cause of solar variation; it explains the basic operation of a PV generation system; it explains the voltage stability concept and it ends with a short literature review of previous work conducted by other scholars.

2.1 Solar Energy

Since the electric grid does not store any energy by itself, the energy network production and consumption must match perfectly. Any imbalance could cause grid instability or failures. In order to understand and counteract the effects of PV integration, details about the system' characteristics and PV generation must be accomplished.

The huge availability of solar energy around the world makes PV energy an attractive option towards a more sustainable power production. According to [3], the amount of solar irradiation which reaches the earth's surface during a year, it's about 5000 times more than the globe's energy consumption. This energy can be used for many purposes, one of them being the conversion in electricity through the photovoltaic effect. However, the power output in a PV system is strongly dependent on the irradiation level which reaches the surface of the PV panels. Therefore, PV systems are very sensitive in case of moving clouds which leads to intermittency in the output power.

2.1.1 Solar Global irradiation

The cause of solar irradiation variability can be described by means of <u>deterministic</u> and <u>stochastic</u> approaches. The deterministic part can be justified by mathematical formulas and is related to the motion of the earth, both on its own axis and around the sun which leads to diurnal and seasonal aftermaths. Contrary, the stochastic component is related to the weather and in particular to the moving clouds. The change of the weather condition can happen over short time periods from seconds, during partly cloudy conditions, to a few days due to weather fronts [4].

When the solar radiation flux passes the earth's atmosphere, its spectral distribution it is affected by absorption and scattering processes. As a result of its passage through the atmosphere, the extraterrestrial irradiation (ETR) is separated into different components [5].

The beam or the <u>direct component</u> G_n of the solar radiation is that part of ETR which directly reaches Earth's surface. It can be defined as the energy flux density (W/m^2) of the solar radiation incoming from the solid angle subtended by the sun's disk on a unitary surface perpendicular to the rays. <u>Direct horizontal irradiance</u> Gb differs from the direct beam irradiance in that it is measured with respect to a flat horizontal plane. Therefore, if we consider the irradiation flux observer as shown in Figure 2.1, the horizontal component can be derived as:

$$G_b = G_n \cdot cos\theta \tag{2.1}$$

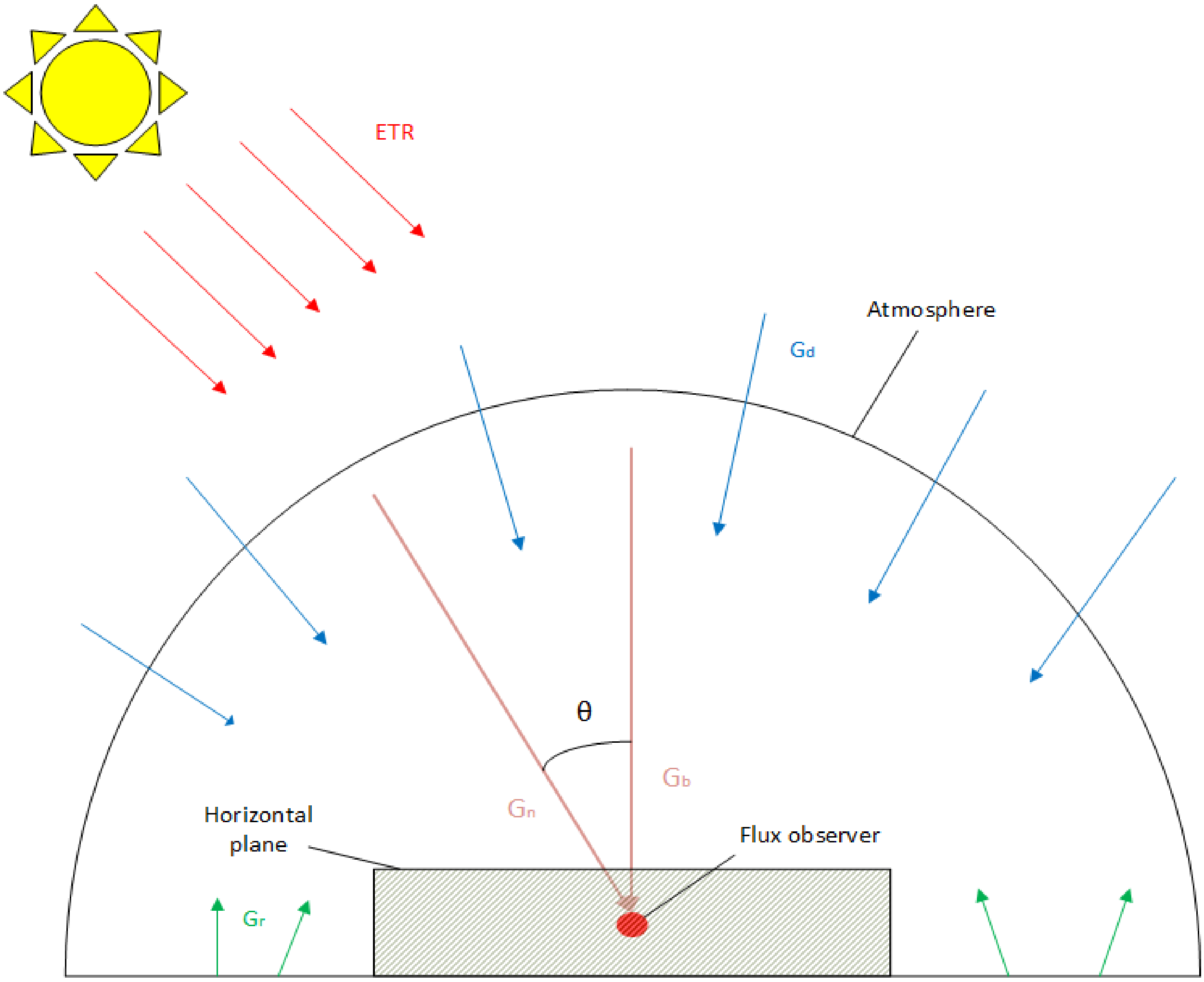

Figure 2.1: Different components for the Global irradiation level

Scattering of the ETR in the atmosphere generates the diffuse component G_d. It can be defined as the energy flux density (W/m^2) of the solar radiation incoming from the entire sky dome on a horizontal surface, excluding the direct beam coming from the Sun's disk.

A part of the solar radiation that is reflected by the ground G_r, can also be present in the total solar radiation especially if the radiation observer is tilted (case of PV systems). Therefore, the global irradiance (G) is the sum of the direct horizontal, the diffuse and the ground reflected component, given as:

$$G = G_b + G_d = G_n \cdot cos\theta + G_d + G_r \tag{2.2}$$

The term ''global'' is associated to the fact that the solar radiation is received from the entire 2π solid angles of the sky vault.

Figure 2.2 shows the variation in the irradiation level for a day in the month of May in the city of Norrköping, Sweden, with a time resolution of 1 minute. As can be noticed, at around 13 o'clock the clouds covered the flux observer. As soon as they covered, the value of the direct component went to zero while the diffuse component increased. Nevertheless, the total (global) irradiation level had to decrease.

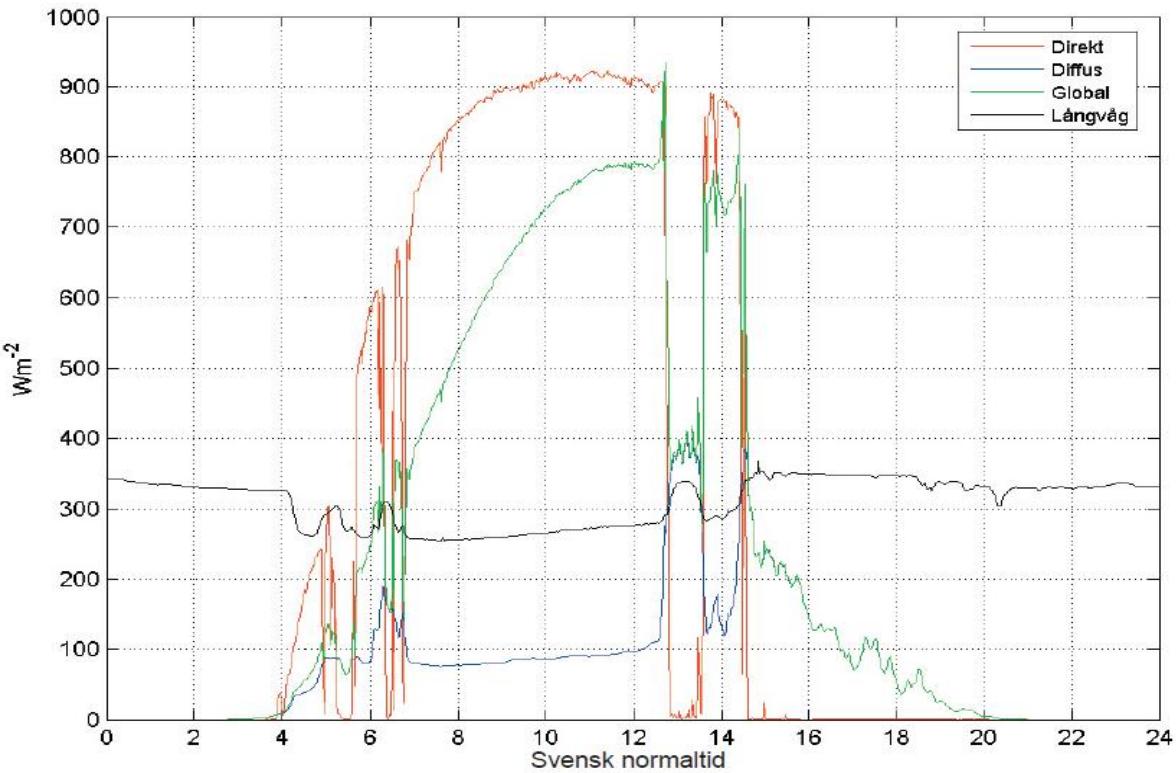

Figure 2.2: Variation in the irradiation level for a day in the city of Norrköping, Sweden, 11th of May, 2004 [6]

2.1.2 Variability index

The performance of solar energy conversion devices is strongly dependent on the incoming flux of solar radiation, which, in turn, is strongly dependent on the state of the sky. Larger amounts of radiation are received when the sky is free of clouds. Moreover, when clouds are present, the incident radiation depends on the cloud types. There are different quantities which describes the state of the sky. One of the most common is the Clearness index CI. Clearness index can be defined as the ratio between the daily global solar irradiation on the earth surface and the total solar irradiation incident on the Earth's surface assuming clear sky conditions (no clouds).

Based on the clearness index, the variability index VI can be defined. Variability index is an important quantity which helps to classify time periods in which the intermittency can be compared, helps to classify sites in terms of timing, frequency and magnitude of variability and helps to provide a metric that can be forecasted in the future (i.e. day ahead) to enable utility planners to ensure generation resources are available to balance out variability on the grid.

According with [7], the ''Variability Index" is the ratio of the "length" of the measured irradiance plotted against time divided by the "length" of the reference clear sky irradiance signal. For an interval of time, VI is calculated as:

$$VI = \frac{\sum_{k=2}^{n} \sqrt{(GHI_k - GHI_{k-1})^2 + \Delta t^2}}{\sum_{k=2}^{n} \sqrt{(CSI_k - CSI_{k-1})^2 + \Delta t^2}} \tag{2.3}$$

Where GHI is a vector of length n of global horizontal irradiance values averaged at some time intervals in minutes, GSI is a vector of calculated clear sky irradiance values for the same times as the GHI data. In other words, the variability index is the ratio of the ''length'' of the measured irradiance plotted against time divided by the ''length'' of the reference clear sky signal.

Figure 2.3 shows different variability index values for different specifics days. The red line represents the global irradiance for a clear sky (reference value) while the blue line represents the real (measured) global irradiance level.

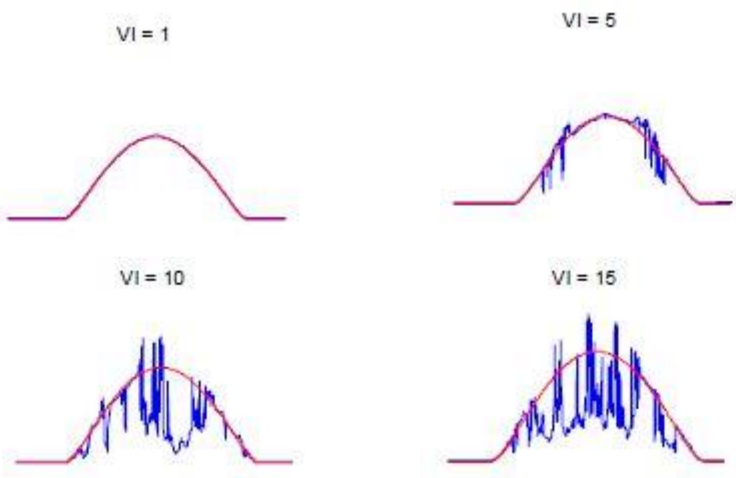

Figure 2.3: Different variability indexes for different days [7]

As can be noticed from Figure 2.3, high VI represents the most unwanted condition for the utility companies while the most preferable case is when VI equals 1. Low values for the variability index can occur both during days without clouds or in case of overcast or rainy days. Higher values will occur when the intermittency in the solar irradiation will have large fluctuations during a day.

2.1.3 Smoothing effect

Due to the fact that PV power generation in most regions is distributed, the PV systems (all the PV units) overall aggregate impact on the power system in the case of irradiation variation (caused by the moving clouds) is different from the impact of a single PV unit. In other words, if there is a ramp in the PVs' power due to the variation of irradiation level, the overall impact of the PV units dispersed across an area is different from the impact of one single PV unit at one specific location. This can be referred as the *smoothing effect* and is important in solar variability studies.

In [8], it is proved that the overall impact of an aggregate PV system in a one dimensional space coordination system is different from a single PV unit in the case of irradiation change.

According with the authors [8], the output variability is the measure of the PV Fleet's power output changes over a selected sampling time interval relative to the PV fleet capacity.

Therefore, if we consider a one dimensional (one string) PV fleet consisting of N identical, equally spaced PV installations, we can express the output variability as:

$$\delta_{\Delta t}^{\sum N} = \left(\frac{1}{C^{Fleet}}\right) \cdot \sqrt{Var\left[\sum_{n=1}^{N} \Delta P_{\Delta t}^{n}\right]} \tag{2.4}$$

Where C^{Fleet} represents the total installed peak power of the PV fleet and $\Delta P^{n}_{\Delta t}$ is a random value that represents the time series of changes in Power at the n^{th} PV installation using a sampling time interval of Δt (i.e. 1 min).

The <u>relative output variability</u> can be defined as the ratio of the output variability for the PV Fleet ($\delta^{\Sigma N}_{\Delta t}$) to the output variability of the same PV fleet concentrated in one location ($\delta^{1}_{\Delta t}$):

$$Rel. Output\ variab. = \frac{\delta_{\Delta t}^{\sum N}}{\delta_{\Delta t}^{1}} \tag{2.5}$$

In order to make further analysis, we define the *Dispersion factor D* which captures the relationship between PV Fleet configuration (i.e. the number of systems and their geographic density), cloud transit speed and the time interval Δt. In other words, the dispersion factor is a dimensionless variable defined as the number of time intervals required for a cloud disturbance to pass across the entire PV fleet:

$$D = \frac{L}{v \cdot \Delta t} \tag{2.6}$$

Where L is the length of the PV fleet in meters, v is the cloud speed in m/s and Δt the time interval in seconds. From the equation 2.6, it can be concluded that the dispersion factor increases as the cloud speed decreases or the length L of the PV fleet increases.

The authors proved that the relative output variability has a minimum and that it stabilizes as soon as the dispersion factor D becomes higher than the number of PV systems N.

Based on the values of the dispersion factor D, four different regions can be defined:

- **Crowded region:** the number of the PV systems N is greater than the dispersion factor D in that a cloud disturbance affects more than one PV system within the PV Fleet in one time interval;
- **Optimal point:** the number of PV systems N equals the Dispersion factor D in that a cloud disturbance affects only one PV system within PV Fleet in one time interval;
- **Limited region:** the number of PV systems N is less than the Dispersion factor D in that a cloud disturbance does not reach the next PV system before the next time interval;
- **Spacious region:** the number of PV systems is much less than the Dispersion factor; PV units are sufficiently far apart such that output variability of an PV unit is independent of the output variability for any other PV unit

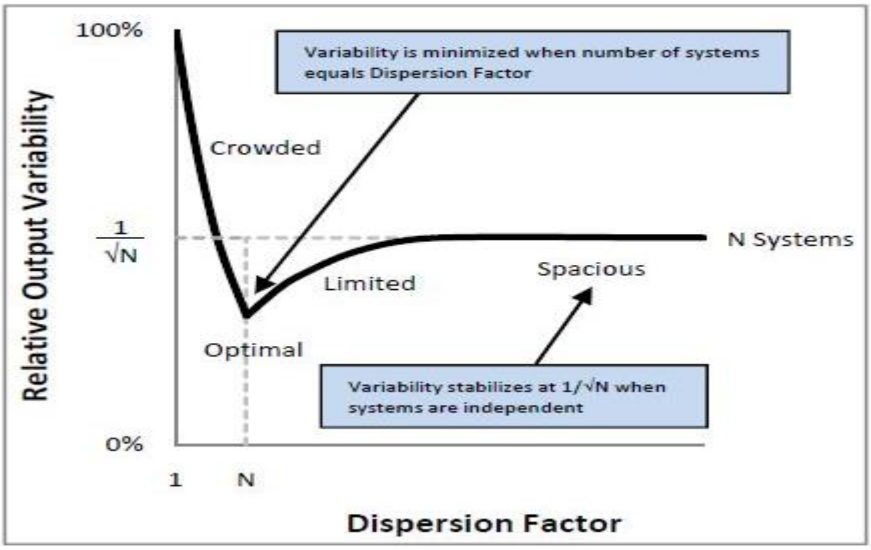

Figure 2.4: The relation between the relative output variability and the Dispersion factor for a PV Fleet containing N PV systems [8]

Therefore, it can be concluded that the aggregated variability of N uncorrelated identical PV units can be expressed as:

$$\frac{\delta^{\Sigma N}{}_{\Delta t}}{\delta^{1}{}_{\Delta t}} = \frac{1}{\sqrt{N}} \tag{2.7}$$

Figure 2.5 shows the overall *smoothing effect* of an 8 site places radiation' sensors displaced within 340 m at one second time resolution for a partly cloudy day in Uppsala, Sweden. As can be noticed, the mean effect of the irradiation level has a lower variability compared to a single site location. For a larger system, the smoothing effect (mean value) becomes more pronounced.

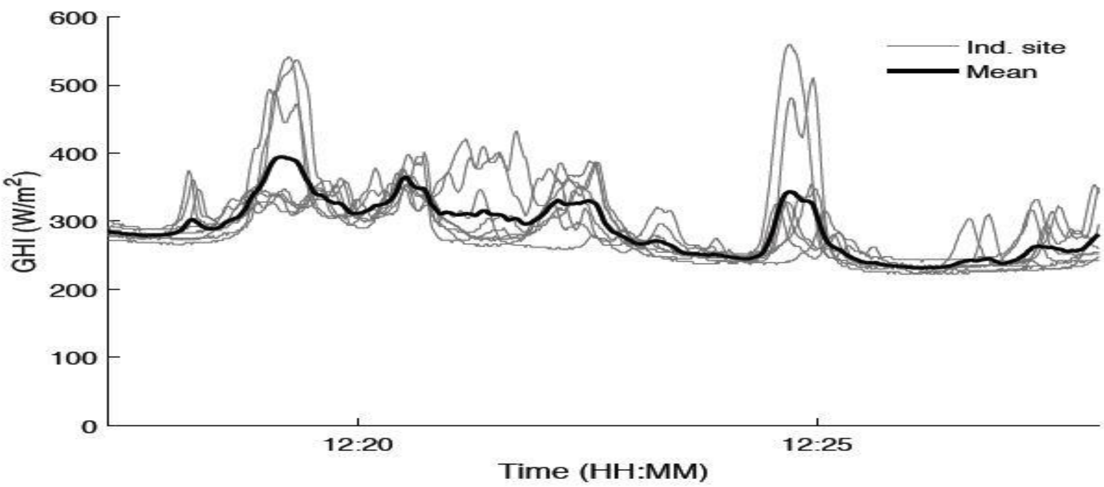

Figure 2.5: Global horizontal irradiance (GHI) with time steps (Δt) of 1 second for 8 sites displaced within 340 meters, on a partly cloudy day in September 2014 in Uppsala, Sweden [4]

2.2 PV Generator

The PV generator system converts the solar energy into electricity and transfers this power to the electrical grid. The system is composed of several components by means of control systems and conversion stages. The PV arrays collect the irradiance from the sun and convert it to dc power through the photovoltaic effect. The DC-DC converter adjusts the voltage level to a specific value and feeds it to the inverter. The DC-DC converter has also incorporated the MPPT (maximum power point tracking) in order to assure that the maximum energy amount is collected from the PV arrays. The inverter converts the dc power to ac power and feeds it to the electrical grid through the transformer. The transformer is needed for galvanic separation between the grid and PV generation system. A generic overview of a grid connected PV generator system is presented in Figure 2.6.

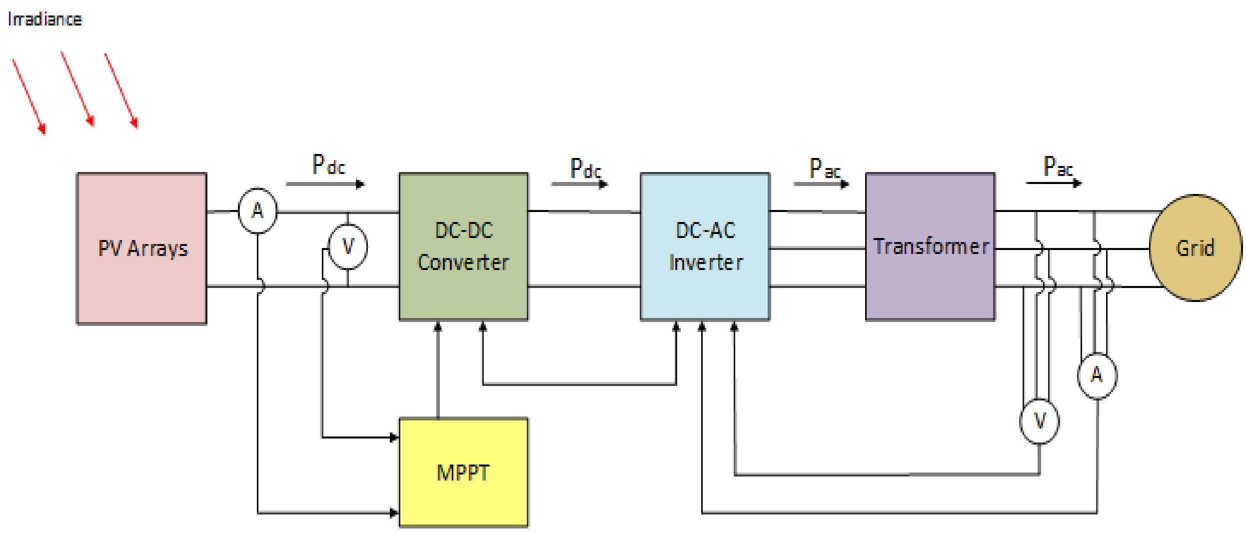

Figure 2.6: Basic overview of a PV generation system

The output power of a PV generation system is strongly affected by the irradiation level which reaches the surface of the PV arrays and can be expressed as:

$$P_{PV} = G \cdot A \cdot \mu_1 \cdot \mu_2 \tag{2.8}$$

Where:

- G is the global solar irradiation level (W/m^2);
- A is the effective area of the PV arrays (m^2);
- μ_1 is the efficiency of the PV arrays;
- μ_2 is the efficiency of the inverter.

2.2.1 PV Panels characteristics

The solar cell functions similarly to a semiconductor and utilizes a p-n junction diode. When the solar cell is exposed to sunlight, a different voltage potential raises across semiconductor' terminals and if a load is connected, a current will start to flow converting the energy from sunlight into electricity. This process of conversion is known as *photovoltaic effect*.

An ideal solar cell can be modeled by a current source connected in parallel with a diode. The current source represents the generated photocurrent when the sunlight hits the solar cell, and the diode represents the p-n transition area of the solar cell [9]. In practice no solar cell is ideal and a shunt resistance R_{sh} and a series resistance R_s component are incorporated in the model.

R_s is made up of surface resistance of the roof of the proliferation, body resistance of the cell, resistance between the top and bottom electrode and PV cell as well as resistance of the metal conductor. R_{sh} is mainly caused by the following factors: the surface leakage current along the edge of the cell, which is caused by the surface spots; the leakage current along the small bridge that caused by the disfigurement of the micro-cracks, grains and crystal after the electrode metal processing, or caused by the dislocation and the irregular spread of the grains [10]. The equivalent circuit of a solar cell is shown in Figure 2.7.

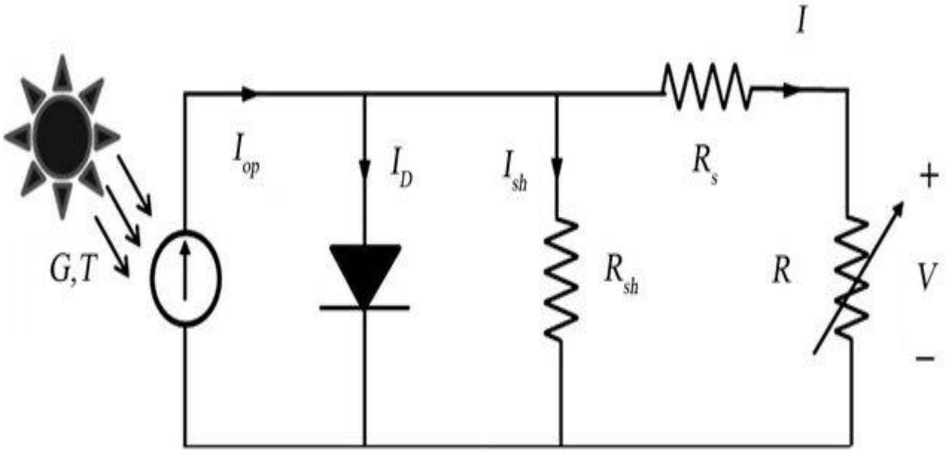

Figure 2.7: Single PV cell equivalent circuit

The output current of the PV cell I can be expressed in terms of diode current I_D and leakage current I_{sh} as:

$$I = I_{op} - I_D - I_{sh} \tag{2.9}$$

Where I_{op} is the photon generated current, I_D is the diode current and I_{sh} is the leakage current.

The diode current can be expressed using Shockley's diode equation:

$$I_D = I_0 \cdot e^{\left[\frac{q\cdot(V+I\cdot R_s)}{n\cdot k\cdot T}-1\right]} \tag{2.10}$$

Where T is the absolute temperature in Kelvin, q is the charge of an electron, k is the Boltzmann's constant, n is the diode ideality factor which depends on the certain PV technology and I_0 is the reverse saturation current.

Substituting the equation 2.10 in equation 2.9, we can express the electrical characteristic of the solar cell in terms of output voltage and current as:

$$I = I_{op} - I_0 \cdot \left[e^{\frac{q\cdot(V+I\cdot R_s)}{n\cdot k\cdot T}-1}\right] - \frac{V + I \cdot R_s}{R_{sh}} \tag{2.11}$$

The electrical output of a single cell is dependent of the device design and the semiconductor material chosen, but it is usually insufficient for most applications. To increase the voltage level, the cells are connected in series and to increase the current level, the cells are connected in parallel. Figure 2.8 shows the variation of current and voltage for different configuration of the PV cells.

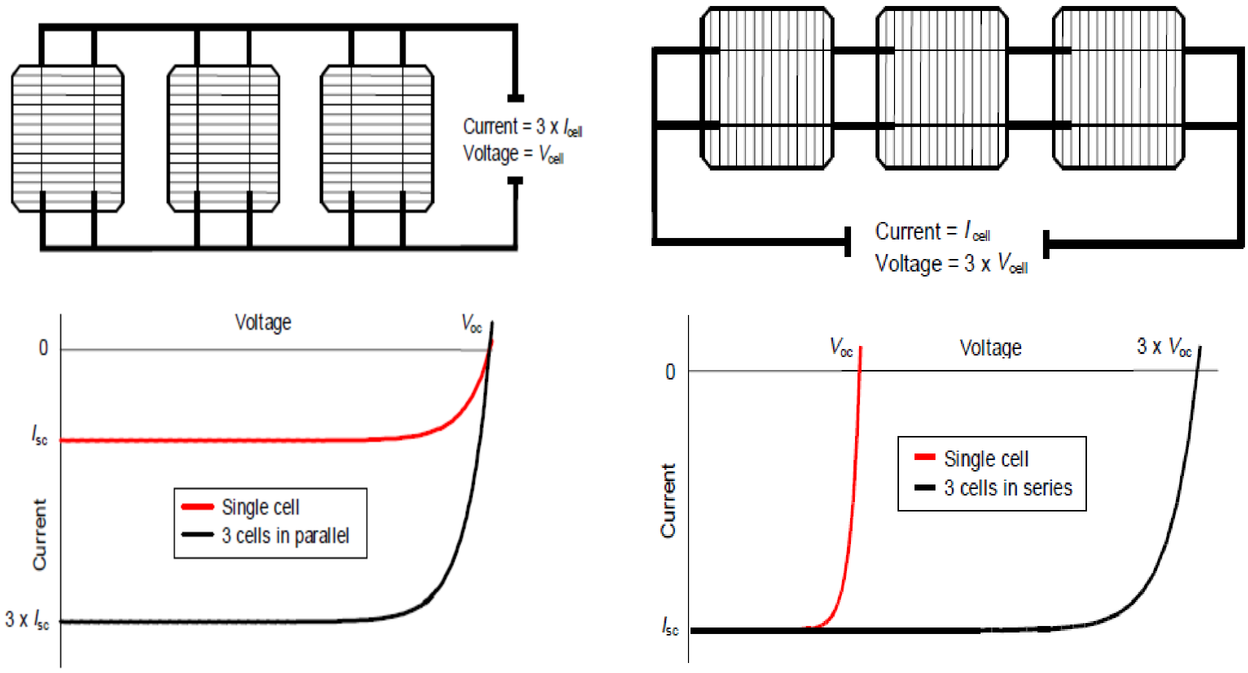

Figure 2.8: Series and parallel connection of solar cells [11]

Combinations of series and parallel connections of solar cells form the module. In order to provide a specified amount of output power, the PV modules are electrically connected also in series and in parallel to form a PV array.

The characteristic I-V curve of a module is highly nonlinear. During the short circuit condition, the maximum current from the PV module is obtained. In the case that we attach a load resistance and increase it, the current start to decrease at a low rate until a knee point. Beyond the knee point the current falls drastically to zero (where $V=V_{OC}$). The variation of solar irradiance and the operating temperature, to a less extent, are the dominant factors which are affecting the electrical characteristics of the solar module according to the equation 2.11. While the increase in irradiation level increases the power output of a PV module, the opposite effect happens for the temperature. Figure 2.9 and Figure 2.10 shows typical variations in the electrical output of a PV module with different irradiation and temperature levels.

The power versus voltage can be found by multiplication of the current I and the voltage V for each operating point. Figure 2.10 shows the P-V characteristics for different insolation levels and temperature values.

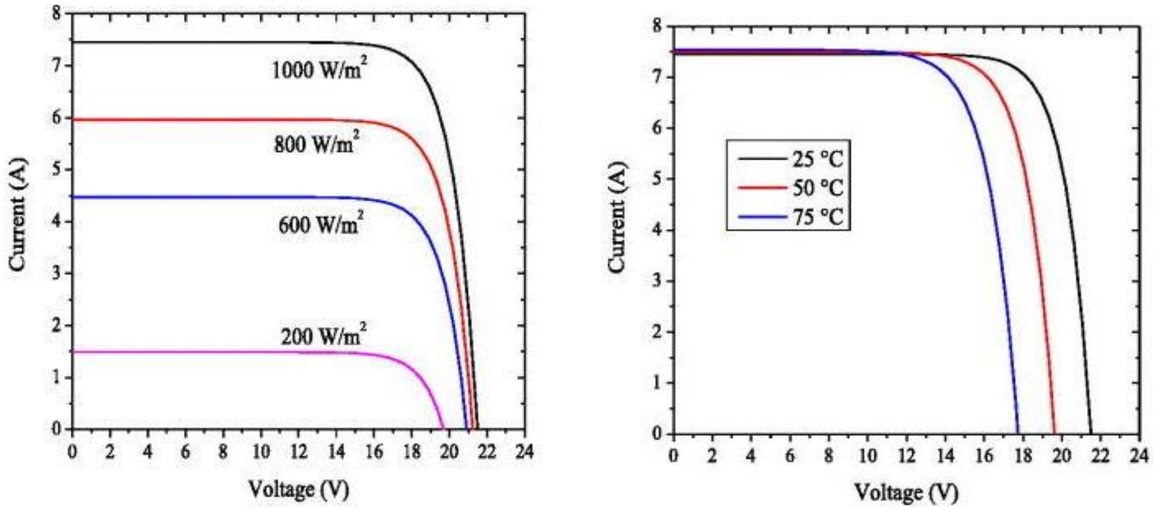

Figure 2.9: I-V characteristics of a typical module with different insolation and temperature levels [12]

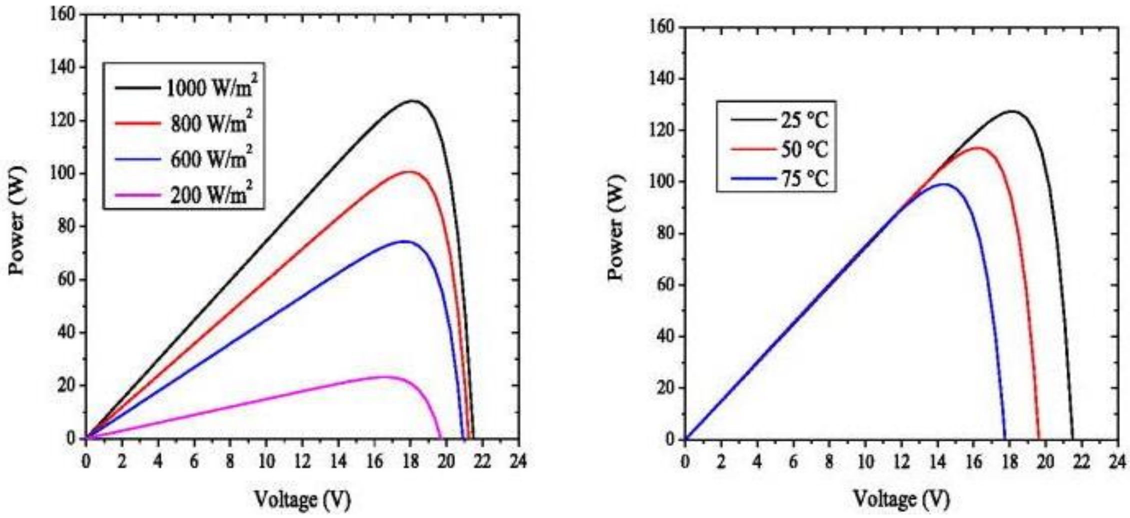

Figure 2.10: P-V characteristics of a typical module with different insolation and temperature levels [12]

2.2.2 DC-DC converter

The DC-DC converter is an electronic circuit that is used either to step down the input dc voltage coming from the PV panels (buck converter) or to step up the input dc voltage (boost converter). Combinations of buck-boost converters are usually the perfect choice since the converter incorporates the Maximum Power Point Tracking MPPT. MPPT is a control algorithm which extracts the maximum power coming from the solar panels under different transient conditions as change in the irradiation level or change in the operating temperature condition of the PV panels. This is achieved by first creating a reference voltage that is then supplied to a PI controller which creates switching signals that force the voltage across the PV array to follow the reference voltage. There are different control strategies for obtaining MPPT, two of the most known are the *incremental conductance tracking* algorithm and *perturb and observe* algorithm. Both of the methods have their advantages and disadvantages.

2.2.3 DC-AC inverter

In order to connect a PV system with the utility grid, the dc power of the DC-DC converter should be converted into ac power and fed to the grid. To achieve this, an inverter is used. The inverter can be both, single phase or three-phase depending how the connection is implemented. Usually for small PV systems (below 10 kW), the connection is made through single phase system and therefore the inverter is single phase. For higher PV systems (above 10 kW), the connection is made through 3 phase inverters. There are different topologies and control strategies regarding the inverters. The most common used is full bridge inverter with unipolar PMW control strategies. Aside the topology, there are different control strategies regarding the synchronization (usually PLL is used) and operation of the inverter under different transient conditions (variation of P and Q). Additionally, different types of filters are used in order to assure that the harmonics injected into the grid are below certain values. All these aspects belong to power electronics and are out of the scope of thesis. Good information can be found in [13].

2.3 Voltage Stability

Power system voltage stability involves generation, transmission and distribution systems. Voltage stability is closely associated with other aspects of power system steady-state and dynamic performance. Voltage control, reactive power compensation and management, rotor angle (synchronous) stability, protective relaying, and control center operations all influence voltage stability [14].

According to [15], the concept of voltage stability is the ability of the system to maintain steady state acceptable voltages at all buses in the system under normal operating conditions and after being subjected to a disturbance. In the case when PV energy is integrated in an electrical network, the disturbance can be considered as variation in the PV output power. This variation is affected by weather conditions and especially by the fast moving clouds.

2.3.1 Voltage drop phenomenon

The concept of voltage stability and the voltage drop of a system can be well explained by making use of power flow between two buses of a system. Therefore, we consider the bus number 1 as the sending end bus with voltage magnitude V_1 and voltage angle δ and bus number 2 as the receiving end bus, with S_2 consumed power, voltage magnitude V_2 and a reference voltage angle equal to 0. The buses are connected each other through a line with the impedance $\underline{Z}$ representing the resistances and the reactances properties of the electrical line. In addition, we consider a PV generation unit connected at bus 2 which produces power locally and which operates at unity power factor (cosφ=1).

The load current which flows through the impedance of the electrical line produces a voltage drop at the load bus. Relating to Figure 2.11, the sending end voltage can be expressed as the voltage at the receiving end bus plus the longitudinal and the transverse voltage drops occurred in the system due to the impedance of the line. The longitudinal and the transverse voltage drops are due to the resistance and the reactance through which the load current is flowing.

$$\underline{V_1} = V_2 + \underline{I} \cdot \underline{Z} \tag{2.12}$$

If we develop equation 2.12 further and incorporate PV power generation at the load bus, the voltage at the receiving end can be expressed as:

$$|V_2| = |V_1| - \Delta V = |V_1| - \frac{R \cdot (P - P_{PV}) + X \cdot Q}{V_2} \tag{2.13}$$

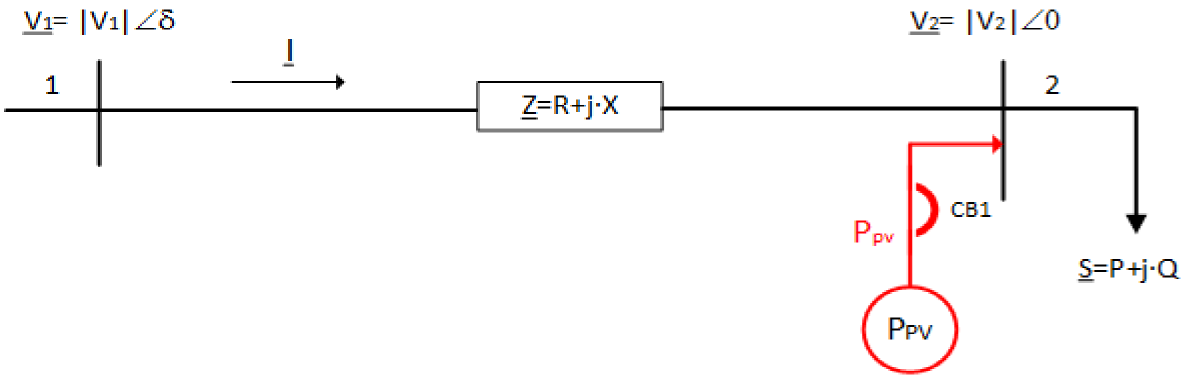

Figure 2.11: Two port system

Contrary to the transmission systems, the distribution systems have high R/X ration and from equation 2.13, we can notice that as soon as active power P_{pv} produced by the PV plant decreases (due to the decrease in the irradiation level) and the load demand remains constant, more power will flow through the electrical line which will cause a higher voltage drop at the receiving end bus 2. This relation is very important, since it shows the potential negative impact the PV units have on distribution systems with high R/X ratio under different weather conditions.

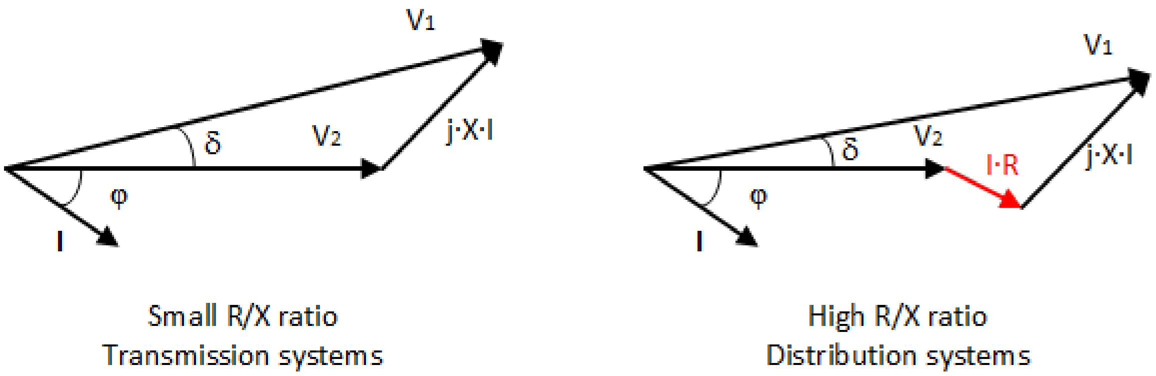

Figure 2.12: Phasor diagrams for small and high R/X ratio

From equation 2.13, we can notice as well that in cases in which the PV power increases substantially (due to the increase in the irradiation level), a reverse power flow might occur leading to a voltage rise at the receiving end bus V_2. In this situation, the corresponding phasor diagram is affected as it can be seen in Figure 2.13. Therefore, if the PV unit operates at unity power factor, only the active power is reversed back to the sending bus V_1 while the reactive power flow remains unchanged (flows to the receiving end bus V_2) due to the inductive characteristics of the electrical loads.

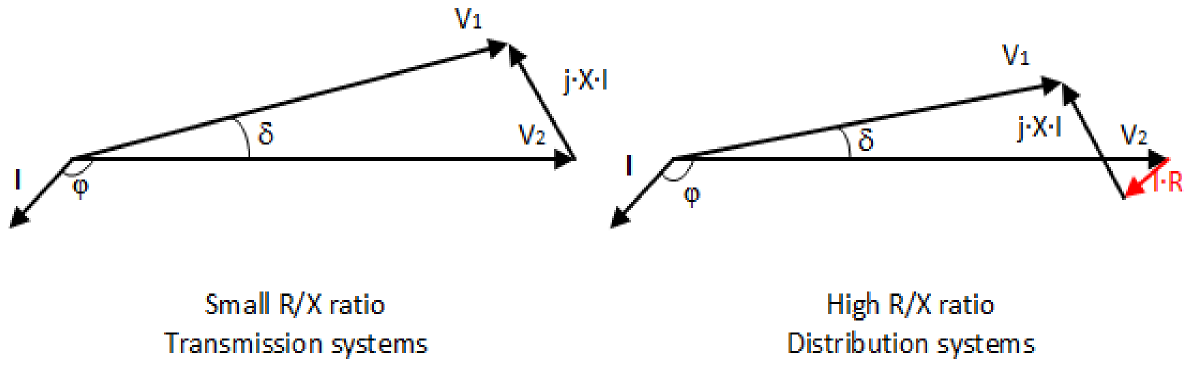

Figure 2.13: Phasor diagrams for small and high R/X ratio with reverse power flow

2.3.2 P-V curves

P-V curves help to explain the relation between the voltage level and the consumed active power at a load bus and also give the insight of how much active power can be consumed until the system becomes voltage unstable. If we consider the same two port system (Figure 2.11), but neglect the resistance term (for stability purposes, R can be neglected), the voltage at the bus 2 can be expressed as [16]:

$$V_2 = \sqrt{\frac{{V_1}^2}{2} - Q \cdot X \mp \sqrt{\frac{{V_1}^4}{4} - X^2 \cdot (P - P_{pv})^2 - X \cdot {V_1}^2 \cdot Q}} \tag{2.14}$$

Equation 2.14 has two solutions, one representing the stable solution (upper part) and one representing unstable (lower part) solution.

By expressing the voltage at the bus V_2 for different values of load power under a constant power factor, one is able to illustrate the voltage dependence with regard to the consumed active power P. This is known in literature as ''the famous P-V curves'' [16] and represents the core of voltage stability studies. Figure 2.14 shows different P-V characteristics under different power factors. As can be noticed, compensating reactive power locally (at the receiving end), improves the P-V capability in that more active power can be transported. However, the nose point (critical point) occurs at higher voltage values which make the system more prone to instability. This situation is dangerous in the sense that maximum transfer capability may be reached at voltage close to the nominal values.

2.3.3 Load characteristics

The characteristics of the loads play an important role regarding voltage instability. They represent the sensitivity of the active and reactive power regarding the voltage variation at the load bus. The behavior of the loads modeling when there is a variation in the voltage can be analyzed from a *static* and a *dynamic* perspective. According to [14] static load models can capture the transient behavior of the loads for low voltage variations (±10 %). For higher voltage variations, the static approach fails to give accurate results and a more detailed approached for load modeling must be used. This approach is called the *dynamic* load modeling and it takes into consideration the differential equations of the dynamic loads under transient conditions.

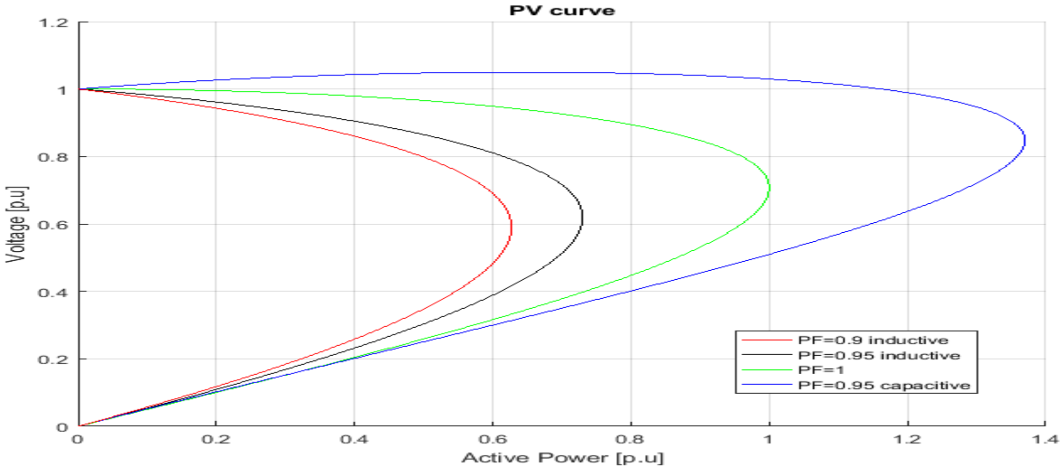

Figure 2.14: P-V curves for different power factors

2.3.3.1 Static loads

A static load model does not depend on the time, and therefore it describes the relation of the active and reactive power with the voltage at that specific time [17]. In other words, when there is a voltage deviation into the system from the nominal voltage, the static model takes in consideration the sensitivity of load power at that instance of time and it assumes to be constant for the rest of the remaining time until a new variation in voltage occurs. A widely used static load characteristic is the well-known *exponential* load model [16], which has the general form as:

$$P = z \cdot P_0 \cdot \left(\frac{V}{V_0}\right)^a \tag{2.15}$$

$$Q = z \cdot Q_0 \cdot \left(\frac{V}{V_0}\right)^b \tag{2.16}$$

Where z is a dimensionless demand variable, V_0 is the reference voltage and the exponents a and b depend of the type of the load. P_0 and Q_0 represent the consumed active and reactive power for the nominal voltage V_0 and P and Q represent the consumed active and reactive power when there is a voltage variation.

The exponents a and b determine the sensitivity of load power to voltage. With these exponents equal to 0, 1 and 2, the model represents constant power, constant current and constant impedance characteristics (ZIP model).

2.3.3.2 Dynamic loads

Contrary with static loads, the dynamic loads' dependence on voltage may be varying with time, exhibiting a power restoration tendency. Induction motors and thermostatically controlled loads are types of loads which exhibit power restoration after a voltage disturbance occurred in the system. While the induction motors have a fast restoration process, the thermostatically loads have a longer (prolonged) restoration tendency. Nevertheless, both of them are important in voltage stability analysis.

In power system studies, the induction motors are usually represented as constant power loads. Although this is a valid representation for steady state operation, induction motors do not always operate under constant power, especially when large deviations of voltage occur. In reality induction motors in steady state operate at a point where the electro-mechanical torque of the motor equals the mechanical torque of the electric load [18].

2.3.3.2.1 Induction motors

The induction motor can be defined as an electromechanical device which converts electrical energy into mechanical energy by means of electromagnetic induction. Its construction consists of two main components: stator (static part) and rotor (rotating part). The stator has a 3-phase windings which are phase shifted 120 geometrical degrees in space. When the stator windings are connected to a 3-phase supply system, which are 120 electrical degrees phase shifted, a resultant constant flux will start to rotate in the machine.

The resultant flux will interact with the rotor windings and by means of electromagnetical induction a current will be induced in the rotor. The interaction between the rotor current and the stator flux creates an electromechanical torque in the machine which forces the rotor to rotate in the same direction as the stator flux. As soon as the machine reaches its synchronous speed (in reality it will be small behind due to the friction losses), no current will flow in the rotor. However, if we apply a load torque at the shaft of the machine, the rotor will decelerate and a current will be induced again in the rotor which will form the electrical torque. The relation between the electrical torque Te and load torque T_L can be described by means of motion dynamics as:

$$J \cdot \frac{d\Omega_r}{dt} = T_e - T_L \tag{2.17}$$

Where:

- J is the inertia of the machine [kg·m^2]
- Ω_r is the mechanical rotor speed [rev/min].

Based on the values of the load torque, the rotor will rotate slightly behind the synchronous speed. A quantity which describes the relative position of the rotor regarding the stator is the *slip*. The slip can be defined as the difference between the synchronous speed and the rotor speed divided by the synchronous speed as:

$$s = \frac{\Omega_s - \Omega_r}{\Omega_s} \tag{2.18}$$

Where:

- Ω_s is the synchronous speed in rev/min.

When all the transients have died out, the motor is said to operate in the steady-state condition. The equivalent circuit of an induction motor in steady-state is composed by the rotor and stator resistances, rotor and stator leakage reactance and magnetizing inductance as can be seen in Figure 2.15.

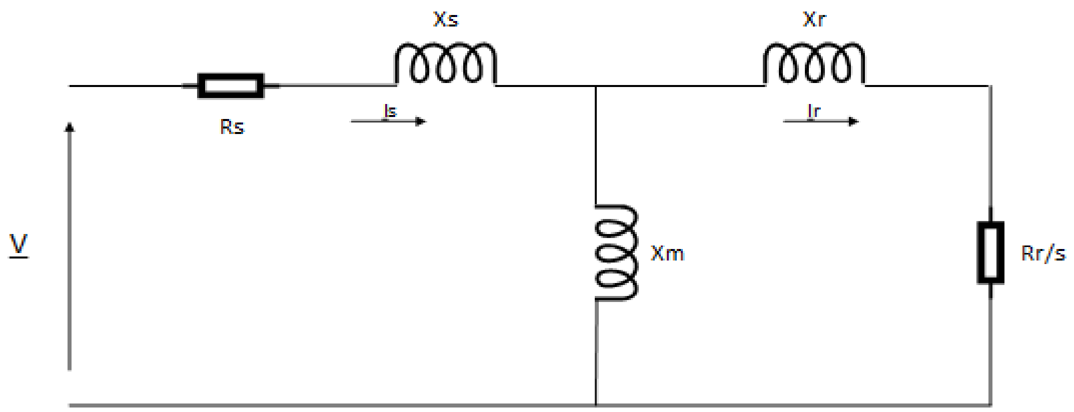

Figure 2.15: Steady-state equivalent circuit of induction motor

Where:

- R_s and R_r represents the resistance of the stator and the rotor coils;
- X_s and X_r represent the leakage reactance of the stator and rotor coils;
- X_m represents the magnetizing reactance.

The slip at which the machine operates depends on the characteristics of electromechanical and the load torques. While the electromechanical torque is dependent on the supply voltage which produces the magnetizing flux, the load torque depends on the load characteristics. The load torque can have a speed dependent (i.e. fans, pumps etc) characteristic and a constant torque characteristic (i.e. refrigerators, air-conditioners etc) or a combination of both. Constant torque loads are the most demanding from voltage stability point of view.

When different disturbances will occur, there will be both electrical and mechanical transients in the machine. According with [16], the electrical transients are much faster than mechanical transients and can be neglected in voltage stability studies.

2.3.3.2.2 Thermostatic loads

Loads such as space heating, water heating and air conditioning are usually controlled by the thermostats which make them to have a constant power load tendency. Their thermostatic control is based on the reference value of the temperature of a system (i.e. room temperature, water temperature etc). Based on the temperature value, the thermostat connects or disconnects the electrical equipment from the grid.

If we consider a parallel number of thermostatic loads with conductance G which are connected to the system from a supply voltage V as shown in Figure 2.16.

Then, we can express the required active power by all the devices as [16]:

$$P = \sum f_n \cdot G_n \cdot V^2 \tag{2.19}$$

The term f_n represents the thermostat duty cycle at the nth device and can be expressed as [16]:

$$f_n = \frac{t_{on}}{t_{on} + t_{off}} \tag{2.20}$$

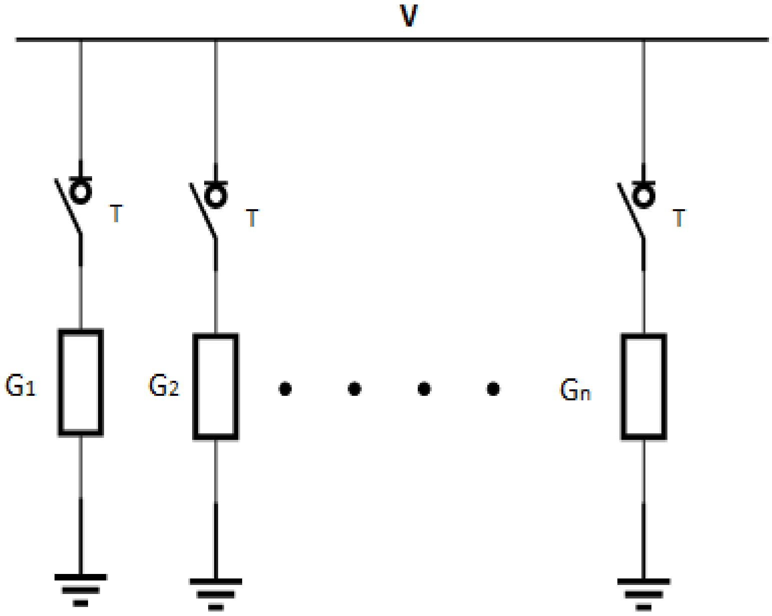

Figure 2.16: Thermostat controlled devices in parallel

Where t_{on} represents the time on which the device is ’’on-cycle’’ and the t_{off} is the time on which the device is ’’off-cycle’’.

In case of a voltage disturbance in the system, it is important to acknowledge that not all of the thermostatically controlled loads will be in the ’’on’’ position (might depend on the weather condition). There will a portion of loads which will be in the ’’off’’ status.

Therefore, right after the voltage disturbance, the possible variation in the input power of the devices which are ’’on’’ does not affect the referenced temperature and therefore the devices are behaving as a constant impedance load. However, after some seconds the heat produced by the thermostatic equipment will start to decrease and this will lead to a prolonged interval for the ’’on cycle’’ in order to recover the temperature. The temperature will increase slower than during normal condition.

On the other hands, those devices which are in the ’’off’’ cycle will not respond to the voltage disturbance until they will enter in the ’’on cycle’’. If more and more devices will operate in the ’’on’’ position in order to recover the temperature (the case for severe voltage disturbances), there will be a power restoration process. However, if all of the devices are in the ’’on’’ position and the temperature did not reach the referenced value, then all of the thermostatic devices will start to behave as constant impedance loads and power restoration process is lost.

2.3.4 Network characteristics vs Load characteristics

The intersection between the network characteristic and the load characteristic gives the operating point on the P-V curve. The solar power integration improves the P-V curve but questions arise how the load behaves when there is a disturbance in the output power of the PV units. The disturbance in case of PV integration can be considered as the ramp down in the PV output power caused by the change in the irradiation level (due to the moving clouds).

Let's assume that the system operates in a relatively stressed condition and consist mainly constant power loads. Initially, the system operates at point A (Figure 2.17) and it is a stable operating point. However, due to the cloud coverage, the network P-V characteristic is affected and the system jumps from point A to point B reaching a new state of operation. But operating at point B involves a lower operating voltage which means that the consumed power of the load is affected. The constant power loads, however, will have a power load restoration tendency and will move the operating point on the P-V curve to point C (their pre-disturbance demanded power). At this point the system is in a critical condition in that any increase in the load demand will cause voltage instability (voltage collapse).

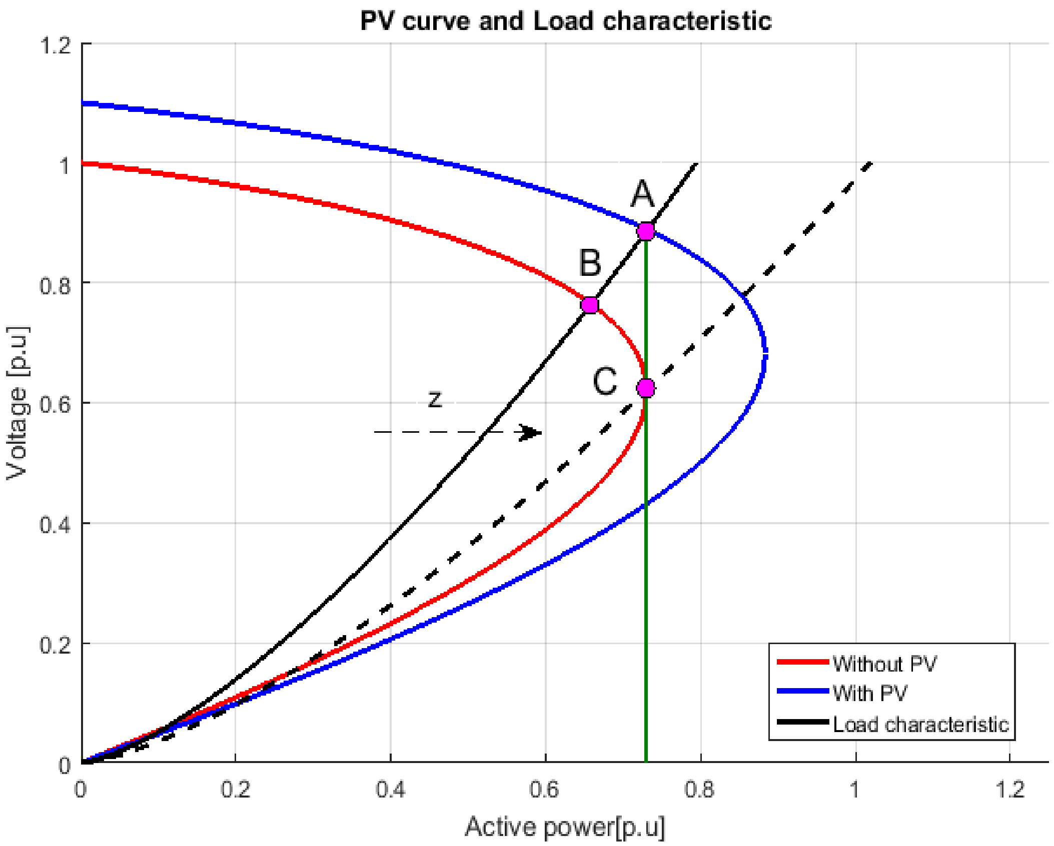

Figure 2.17: Network and load P-V curve

2.4 FACTS Devices

FACTS devices are power electronic devices which are able to change the natural electrical characteristic of the network in order to improve the system stability under different transient conditions. This system improvement can be achieved by adjusting the shunt and the series impedances of the network without performing any change in the network topology. In other words, FACTS devices are able to control the power flow through the electrical line and the bus voltage by means of power electronics in a fast and continuous way. There are different configurations regarding the control systems, most known ones are: shunt and series control or combination of both. The shunt control is achieved through static var compensator (SVC) and synchronous compensator (STATCOM) devices.

This section presents a general overview of the working principle of the SVC and STATCOM devices. More detailed and elaborated information can be found in [19].

2.4.1 Static Var Compensator (SVC)

The SVC operation principle is based on a thyristor switched capacitor (TSC) in parallel with a thyristor switched reactor (TSR) which adjusts the overall shunt impedance of the device in order to keep the voltage at the PCC under a predefined value. Therefore, if we consider a Thevenin equivalent circuit with source voltage E and a series reactance X, the voltage at the PCC can be expressed as:

$$V_{svc} = E - j \cdot X \cdot I_{svc} \tag{2.21}$$

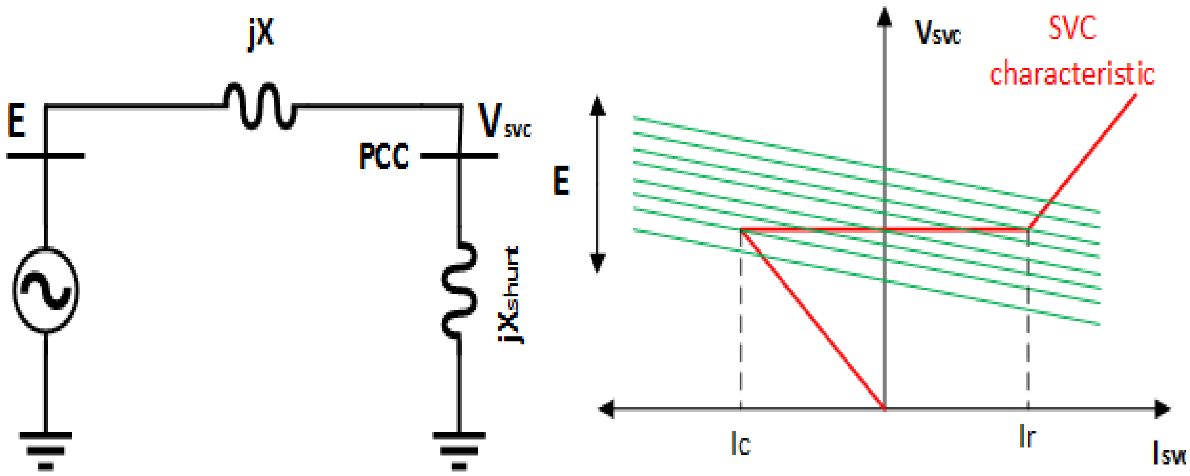

Figure 2.18: SVC characteristics for different system conditions

If the source voltage E increases, the voltage at the PCC will be above the reference value, then SVC's shunt impedance will be predominantly reactive and absorption of reactive power will take place. Contrary, if the source voltage decreases, then the voltage at the PCC is below the reference value, the SVC's shunt impedance will be predominantly capacitive and injection of reactive power will take place. In other words, based on the value of the voltage at the PCC, the SVC absorbs or injects reactive current into the network in order to keep the voltage under control. However, if the SVC hits its power rating, it will start to behave as a constant capacitor/reactor and the voltage control is not possible anymore. The SVC can incorporate a droop characteristic (usually 1-5%) to increase the voltage control range but as well to coordinate with other possible SVC units connected to the same system for better load sharing.

2.4.2 Static Synchronous Compensator (STATCOM)

The STATCOM is a power electronics device based on the voltage source converter principle. It is able to provide a path for the line currents to flow between the phases and therefore to inject or absorb reactive power. Its control is made through the synchronous coordination system (d-q system). Therefore, by using a PLL system, the reference d-q currents are calculated and are fed to the current controller which gives the reference voltages for the converter. The STATCOM device is also able to inject active power if it is equipped with energy storage devices (ESD).

If we consider the same Thevenin system as in the SVC case, then the characteristics of the STATCOM are obtained under different voltage deviations.

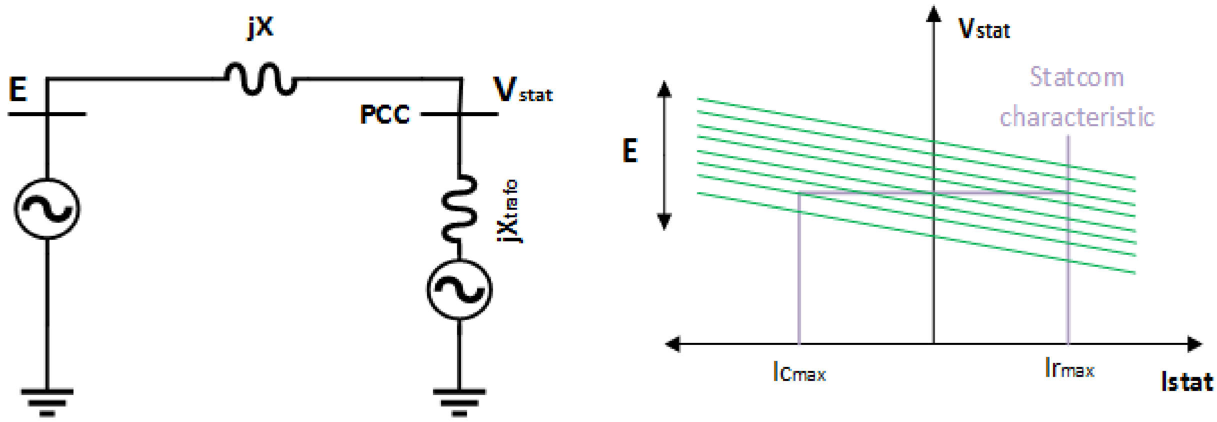

Figure 2.19: STATCOM characteristics for different system conditions

As it can be seen in Figure 2.19, once the STATCOM hits its capacitive limit, it will continue to provide the same compensating current independently of the grid voltage. This is a major characteristic which makes STATCOM to have a better transient response compared with the SVC, especially connected to weak grids. Additionally, the ratings for reactive and capacitive operation are always equal which it is not always the case for the SVC.

2.5 Literature Review

A relatively large penetration level of PV energy may lead to severe impacts on different areas of distribution systems planning and operations, including effects on active and reactive power flows, voltage profiles, interaction with voltage control and regulation equipment, equipment maintenance and life cycle, feeder loading, overcurrent and overvoltage protection, electric losses, power factor and power quality [20].

Therefore, in order to integrate more distributed PV energy at the residential level, better coordination control between the system and the PV units have to be achieved. In addition, different power electronic devices (SVC, STATCOM etc) could also be incorporated into the grid for improved performance of the system with PV integration. Also, different standards and grid topology might be needed to be changed as well.

In order to assess the impact of PV energy integration, several studies have been conducted around the world. These studies attempted to investigate the impact of PV intermittency at the distribution level and proposed different mitigating solutions in order to increase the hosting capacity and the reliability of the PV energy.

2.5.1 Cloud-effect impact on the voltage stability for distribution grids

In [21], the authors investigated the dynamic response of a PV generation system, due to the rapid change in irradiance, for a large power system. They concluded that the PV generators that are not equipped with voltage regulator control, the respective connected PV bus voltage fluctuates during periods of large change in the irradiance. These fluctuations become more significant with higher penetrations of PV generation.

In [22], it has been investigated the ''cloud-effect'' for a potential 720 kWp PV power on an urban network in Australia. According with the authors, the grid design, PV power fluctuations and the load behavior are ones of the major characteristics which decide the amount of PV power to be integrated. The authors have concluded that the 720 kWp can be integrated without any voltage related problems but this situation may change in the future if more PV units will be integrated into the same grid.

In another study [23], the ''cloud-effect'' was simulated on a test-distribution network. The authors concluded that the ''cloud-effect'' is a potential threat to the voltage stability of the system due to the rapid power ramps down of the PV units but also due to the delayed time for the first tap operation of the distribution transformer. In addition, the behavior of the loads, and especially induction motor loads, when cloud induced power swings occurs, plays an important role regarding the voltage stability of the system. Therefore, the load behavior subjected to cloud disturbances might be an important parameter regarding the hosting capacity of PV energy.

In another study [24], the ''cloud-effect'' was investigated on a test-distribution network with unbalanced structure. It is stated that low voltage distribution systems have an unbalanced nature and uneven mutual coupling, which result in different voltage drop for each phase. This unbalanced structure might come not only from the different loading levels or tap positions in the three phases but also from the asymmetrical geometry with non-transposed geometry of the electrical line. The authors proved that an increase in the voltage level (due to cloud unveil of the PV units) at one phase might lead surprisingly to, a decrease of the voltage level of the others. It has been concluded that balanced assumption may not be adequate for analyses of distribution systems with high PV penetration levels.

2.5.2 Possible Mitigating Solutions

<u>Firstly</u>, networks which are not equipped with Under Load Tap Changer Transformer (ULTC), might need to be redesigned to incorporate such regulating devices for improvement of voltage profile during low and high load as well due to the PV intermittency. <u>Secondly</u>, custom power devices such as STATCOM (with/without energy storage), have a big potential for power quality improvement and enhancing PV penetration level. <u>Thirdly</u>, some specific standards might need to be changed or adjusted in order to allow voltage regulation control of the PV units at residential level, sometimes even at the expense of active power. <u>Finally</u>, the energy storage devices (ESD) are the most efficient solution in order to integrate high amount of PV systems. However, due to their high purchasing and maintenance price, this method might not be economically viable. Several studies investigated these aspects and different solutions and control algorithms were proposed.

In [25], it has been observed that STATCOM is effective in compensating reactive power, load balancing, harmonic elimination and improving the power quality of a distribution system with distributed generation. In [26], the authors looked up at one residential grid with PV potential without ULTC control located in Australia. They concluded that, in order to integrate more PV energy, the grid needs to incorporate ULTC transformer or STATCOM for improving the voltage stability of the system. However, to have a suitable balance between the ULTC transformer operation frequency and the STATCOM size and system losses, correlation between these two devices exists and there is a best economic and technical solution which incorporates both of the devices. The same conclusion was drawn in [27], in which the authors have also demonstrated that the most optimal solution is to design a coordinated voltage control method based on ULTC action and STATCOM reactive power compensation.

In other studies as [21], [23] the potential reactive power support from the PV units was found to be extremely efficient for voltage regulation purposes despite the skepticism of some scholars, which stated that the potential PV reactive power support for distribution grids it might not be effective due to the high R/X ratio. Therefore, the authors concluded that if the current standards will change in order for the PV systems to provide reactive power, the voltage stability concern might be solved.

In [21], [28] the another possible solution as ESD were found to buffer the PV generation, capturing a portion of energy produced during light load and exporting it back onto the network as required. This possible mitigating solution can be utilized to load shift and regulate the network voltage. The authors have also concluded that, the optimal placement of EDS should be located in the near vicinity of the loads for an improved performance of the system.

3 GRID MODELLING AND SYSTEM STUDY

This chapter describes how the entire project work has been conducted. Different approaches and assumptions are made during the implementation and data collection regarding the entire system (grid data, solar data, load demand data, standards etc) for the simulations to be performed. It clearly describes each step in the implementation of the model to be simulated.

3.1 Study Methodology

The methodology of the study was based on the theoretical knowledge gathered in the literature study and on the investigated/real grid which was simulated in the Neplan simulation tool [29]. The software is able to perform load-flow calculations and in addition it has the ability to perform dynamic analysis regarding PV output fluctuations as well to model the load transient behavior under different disturbances. Moreover, the software's library is equipped with FACTS devices and the user is able to model their control system as well. Figure 3.1 illustrates the study methodology adopted for the model to be simulated.

The analyses started with verifying and implementing the grid data. After that, the implementation of the detailed dynamic load models based on different studies' data was accomplished (portion of induction motor, thermostatic and resistive load). The cloud-effect was simulated based on combination of measurement data and statistic data. The simulation was conducted in the time frame in which the maximum solar power output occurred in the grid and the corresponding loading status at that time interval.

The simulations started with a load flow analysis for the base case scenario (No PV energy integration) and the voltage values were determined. The study proceeded adding different PV penetration levels into the network and the cloud-effect was simulated until the system become voltage instable. A comparison and discussion between the static and the dynamic load modeling was made for the case with the PV penetration level which made the system voltage unstable.

The case with the PV penetration level which caused voltage instability was investigated further and different mitigating solutions were proposed and implemented. Differences and comparisons between the proposed mitigating solutions were discussed and analyzed.

3.2 Distribution Grid Modeling

The investigated grid represents a distribution grid located in Mölndal area. It is a radial grid which provides energy to 39 residential houses. It is fed through a 3 phase transformer 10/0.4 kV with a capacity of 500 kVA. The houses are fed through 3 phase underground cables. The grid consists of 55 branches which have different resistances and reactances as can be seen in Appendix 1. The grid has an average ratio of R/X equal to 9.66 which makes it sensitive to PV power variations as explained in Chapter 2, section 2.3.1. The network has a total peak load of 240 kW and it is operated at 0.95 lagging factor. It has also a short-circuit capacity of 80 MVA.

However, due to the fact that the grid is designed to be a very strong grid and also because it is operated at low load condition during the summer, its short circuit capacity has been changed to 4 MVA for the modified grid case in order to investigate the cloud effect. In addition, its spot loads has been increased to 360 kW and distributed along the residential houses. The load demand, for the modified network, of each residential house can be found in Appendix 2.

Figure 3.2 shows the investigated grid implemented in the Neplan software.

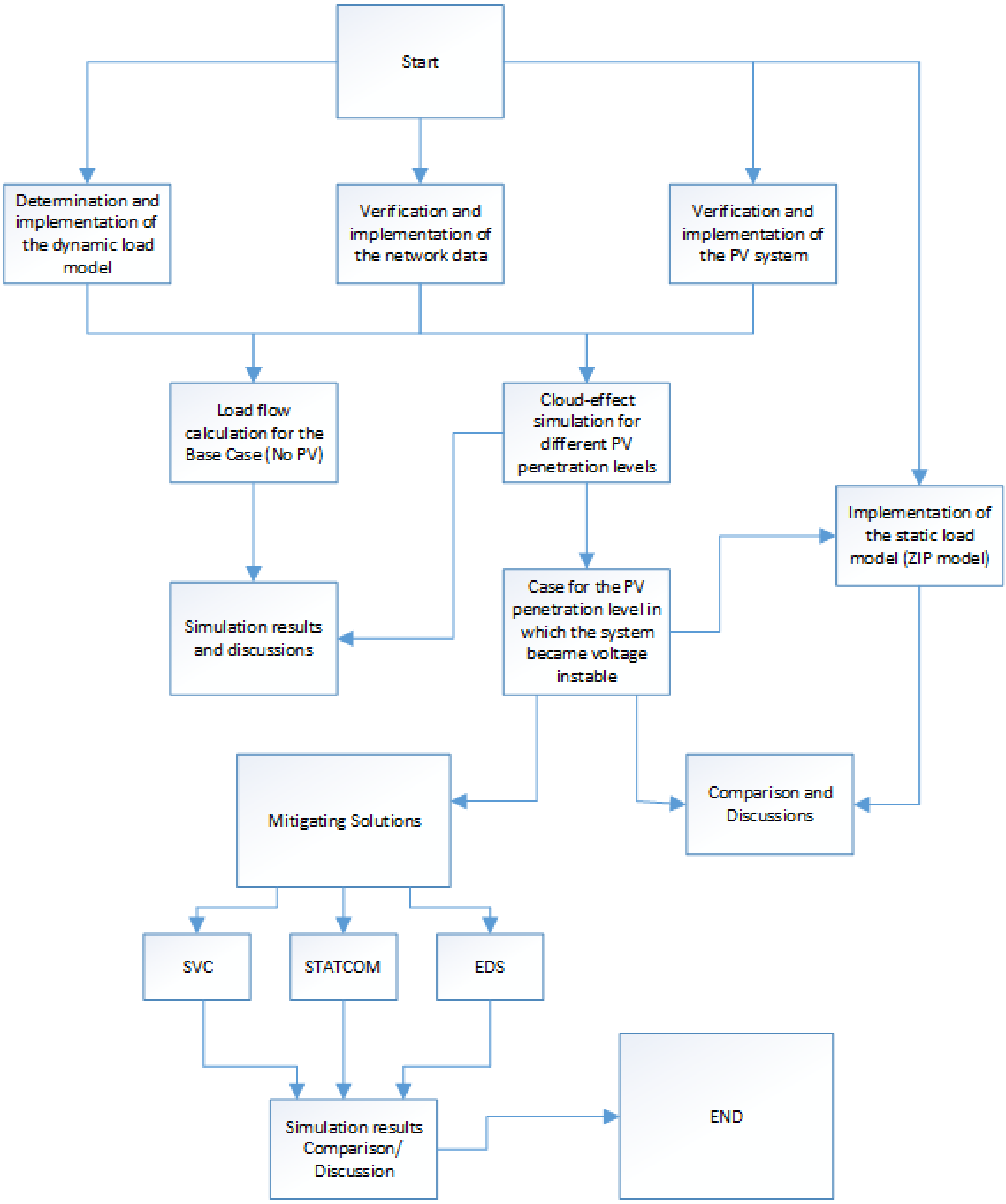

Figure 3.1: Study Methodology flowchart

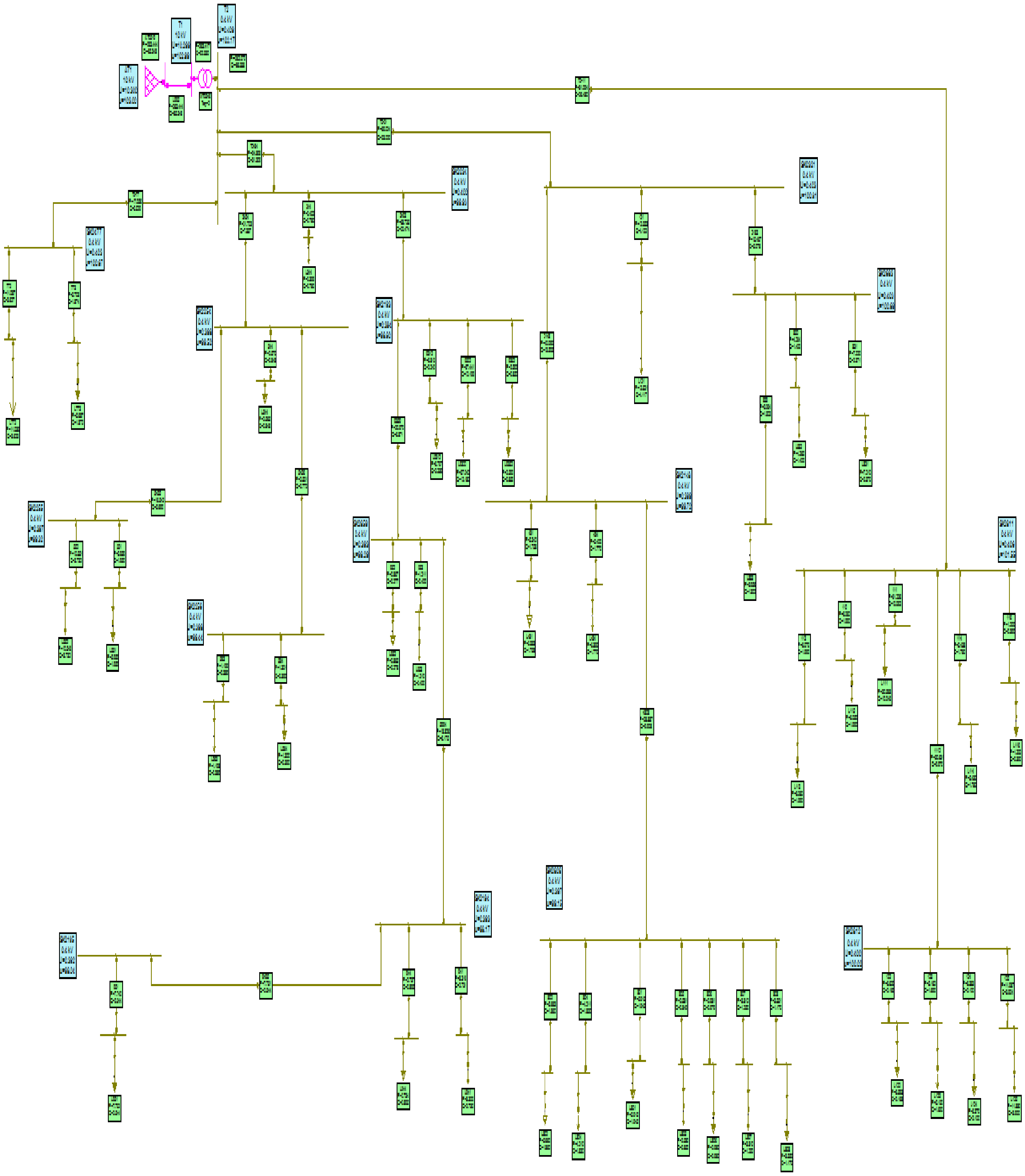

Figure 3.2: Mölndal 10/0.4 kV distribution grid

3.3 PV System and Cloud-Effect Modeling

The operation principle of a PV generation system has been described and explained in Chapter 2, section 2.2. When there are transients inside the generation system (due to the change of the irradiation level or operating temperature), the control system of the generation unit changes its operational characteristics in order to extract the maximum power potential from the PV arrays but also to follow the imposed standards regarding the connection with the grid.

However, due to the fact that the PV generation system incorporates power electronic devices which operate at high switching frequency (much higher than the grid frequency), any transients inside the PV unit will be executed almost immediately compared to the network scale. In addition, the high switching frequency on which the PV units work require high amount of CPU memory and time for the simulation to be performed.

Therefore, the PV generation system can be modeled simply as a generation system which injects power into the grid based on the irradiance values.

3.3.1 PV Generation System Modeling

The PV generation system has been modeled as 3 phase disperse generation system operated at unity power factor. Due to the fact that the PV generation system is equipped with an inverter, it is able to inject both active and reactive power into the grid. However, reactive power support from the PV inverter is usually not paid by the utility companies at the residential level and therefore the PV generation system is normally operated at unity power factor. Moreover, the potential reactive power support from the inverter put more stresses on the switches of the inverter which might affect its life cycle operation. Therefore, in the simulation, all the PV units inject only active power into the grid based on the irradiance values.

3.3.2 Cloud-Effect Modeling

The causes of solar irradiance variations has been explained in Chapter 2, section 2.1. While the seasonal and diurnal prediction in the irradiance variation can be explained quite well based on mathematical formulas, the prediction in the irradiance variation due to the weather condition (moving clouds) is still hard to understand. Therefore, measurement data and statistic data had to be correlated together in order for the cloud-effect to be simulated.

In [23], it has been reported that the quickest ramp rate of the irradiation level can reach as 705 W/m^2 and it takes only a few seconds for a clear sky to be heavily covered by clouds. Therefore, a geographically small network can be shaded by the moving clouds within a relatively short period of time.

Figure 3.3 [30] shows the measured output power on a 15.7 kW PV facility located in the Chalmers campus. As can be noticed, when the clouds started to cover the PV arrays (between 50 and 70 s), the PV power output dropped to low values and after some time (between 74 and 80 s), when the clouds started to unveil the PV system, the PV output power increased again to rated values.

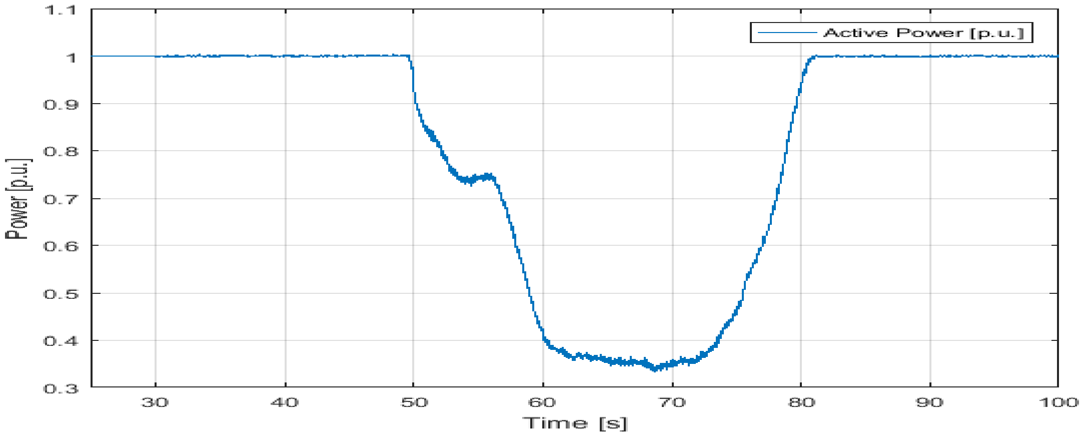

Figure 3.3: Cloud-effect on a 15 kW PV facility located in the Chalmers's campus [30]

Therefore, the cloud-effects on the Mölndal grid with different PV penetration levels were investigated. PV units were integrated into buses with spot loads in the network. As discussed in Chapter 2, section 2.1.3, there is a smoothing effect in case of cloud coverage over a network. But due to the fact that the investigated grid is a relatively geographically small network, the cloud coverage effect is assumed to be the same for all the PV units. In addition, the diffuse term G_d in the Global irradiation level G has been neglected in order to obtain a higher voltage drop in the system.

In this study, the clouds transients were simulated by a decrease in the solar irradiation from 1000 to 0 W/m^2 over a 20 seconds period of time (from 10 to 30 seconds) and the power of all the PV units declined proportionally with the sunlight intensity as it can be seen in Figure 3.4. In reality, the active power of PV units is also affected by the operating temperature, which might decrease with the irradiation level. However, this aspect was neglected in the simulation. Therefore, the PV power is only affected by the irradiance intensity.

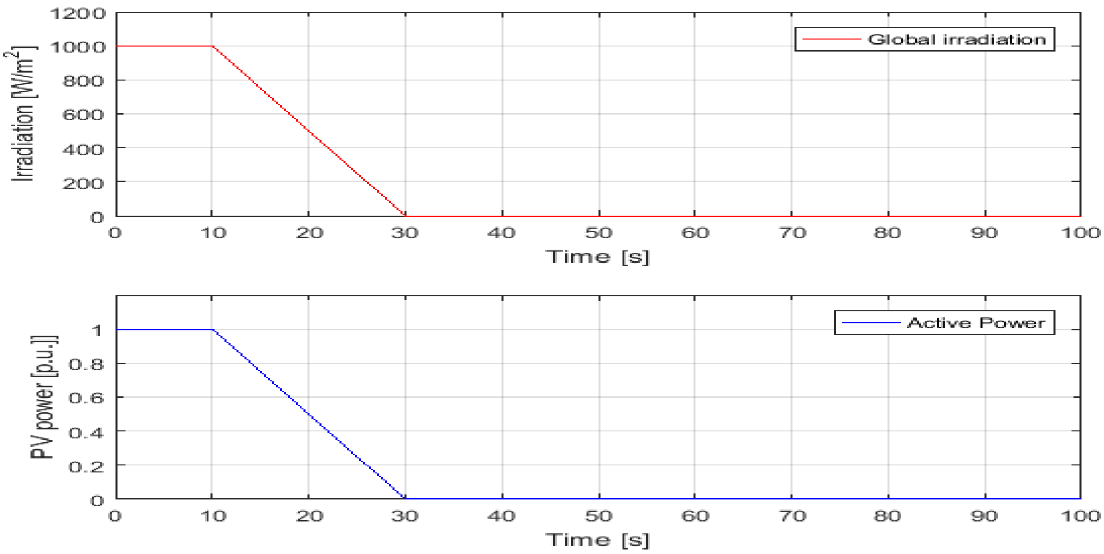

Figure 3.4: Power change with sunlight irradiation level

3.4 Voltage Regulator Modeling

The investigated grid it is not equipped with under load regulating transformer (ULTC). However, in order to integrate more distributed energy resources, the future distribution grids will incorporate the ULTC transformers. Therefore, the grid is modeled with an ULTC for the modified grid case scenario.

The regulating transformer in the simulation adopts the characteristics of a typically transformer for distribution systems. It has 32 positions (±16) with 0.625% regulating voltage per tap (corresponds to 2.5 V per tap) and ±10% voltage regulation range. Normally, the regulating distribution transformers are incorporated with line drop compensation devices LDC. They are able to regulate the voltage at each phase separately and incorporate a line drop compensator. The purpose of the line drop compensator is to compensate the voltage drop of the distribution line from the regulator to the load center which makes the regulation more precise.

Due to the fact that the tap changer transformer is a mechanically device, it requires some time to change between each step. Commonly this mechanical time period is 5-10 s [14]. In large power systems, every voltage level has its own tap changer. In order to reduce the possibility of the tap changer transformers hunting each other and establishing a better coordinated response, the common practice is to make the higher voltage-level tap-changers to respond faster than those in lower voltage networks [16]. Usually, the first tap time delay for distribution tap changers is from 30-60 seconds [14] but it can be longer if the utilities companies have their own additional standards.

In this study, due to the fact that the system is assumed to be phase-balanced, but also because there are several feeders which leave the main transformer (making the LDC harder to implement), the regulated voltage is performed at the secondary side of the main transformer. The reference voltage is set to 101.5 % and has a deadband of 1.25% which represents a typical parameter [16]. The first tap time operation delay was chosen to be 30 s and 10 s for following successive tap operations. All the dynamic features of the voltage regulator can be seen in Table 3.1.

Table 3.1: Dynamic characteristics of the voltage regulator

Reference voltage V_{ref} [%]	**Mechanical time delay T_m [s]**	**Intentional first time operation delay T_f [s]**	**Intentional time delay between two successive steps T_s [s]**	**Step voltage δU [%]**	**Deadband d [%]**
V= 101.5	5	25	5	0.625	1.25

Different utilities companies have different standards regarding the voltage allowable limits. The regular standard for Europe and Sweden is the standard EN50160 [31] which states that: ''*the 10 minute average RMS voltage at the point of common coupling (PCC) must lay within the ±10% Unom limits for 95% of the time, with Unom = 230 VRMS*". After discussing with my supervisor, ±10% was chosen as a reasonable upper/lower limit.

3.5 PV Power Potential and Spot Loads

In order to determine the worst case scenario in which cloud induced power swings could have a potential to cause voltage instability, the PV power profile for the PV systems and the load demand profile for a house during a day were analyzed and correlated. Based on these two curves, the time interval for the simulation to be conducted, with its specific PV power and load demand, was determined.

3.5.1 PV Power Potential

Figure 3.5 shows the PV generation profile during a day in June for the residential area of Mölndal [32]. As it can be seen, the PV power output is varying during a day due to the variation of the solar irradiation level. The PV systems start to produce active power when the sun is rising (between 3 and 4 am) and reach a maximum value when the irradiation level is the highest (between 10 and 11 am). After this interval, the PV power declines with the sun's radiation and around 8 pm no PV power can be produced anymore.

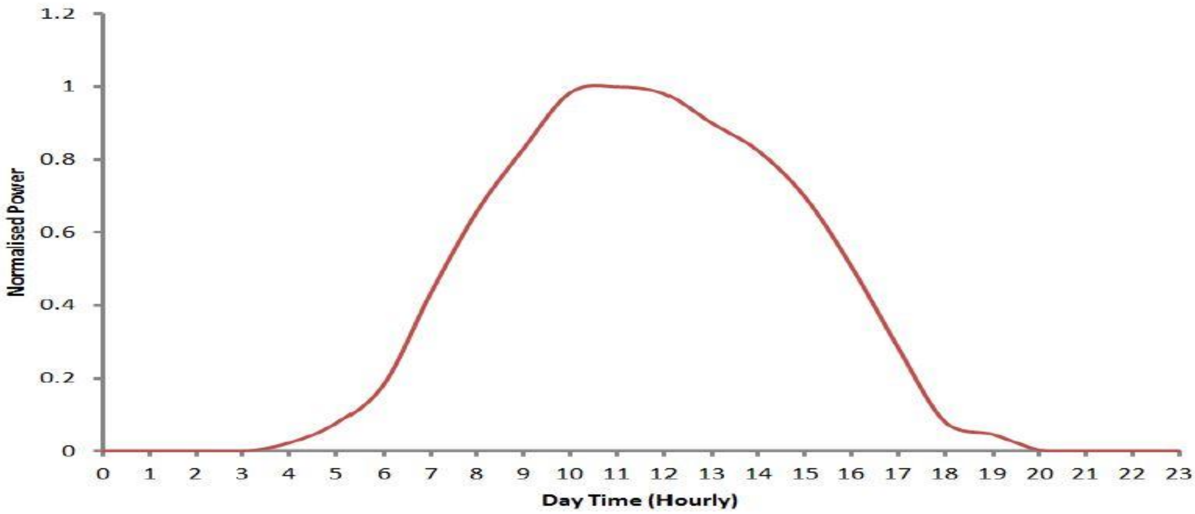

Figure 3.5: PV Power output for Mölndal area during a day in June [32]

As explained in Chapter 2, section 2.2, the active power of a PV system is directly proportional with the effective area of the PV arrays and the global irradiation level which hits the surface of the PV arrays. Therefore, the potential penetration level into the grid of the PV systems could be calculated regarding the total roof-top area of the houses and their PV power capacity. For reliable results, every house's geometrical construction (roof-shape, tilt, position regarding the sun etc) has to be modeled as precise as possible.

Nevertheless, the penetration level can also be calculated based on the load demand. This approach has been used by many scholars [23], [32] and therefore this study has focused and implemented it. Therefore, in this study, the penetration level is defined as the ratio of total installed PV Power to total system real power of all nominal loads, as well for each spot load. For example, if the nominal/spot real power demand at one bus is 5 kW, then 50% PV penetration at this bus load corresponds to 2.5 kW PV power from the PV system.

$$Penetration\ level = \frac{P_{PV}}{P_{load}} \cdot 100\ \% \tag{3.1}$$

3.5.2 Spot Loads

Of next concern is to determine the spot loads and their share of motor loads, thermostatic loads and resistive loads at the time of the simulation. This however, is a difficult task because household energy consumption is affected by many different factors such as building and appliances efficiency, location, occupants' behavior and socio-demographical characteristics (income, age, occupancy patterns, etc.). Seasonal changes in the domestic energy consumption are common in the Nordic countries and have been reported by many authors. Electricity consumption is usually higher during the winter in comparison to the summer period, especially in countries that, as Sweden is, are characterized by long and dark winters [33].

Figure 3.6 shows the average load profile for a residential house in Sweden without electric heating. As can be noticed, the load demand varies during a day and it has its peak demand between 8 and 9 pm. Interesting to notice is that the power demand from the cold appliances is almost constant during a day while the demand for lightning and cooking is more pronounced in the evening.

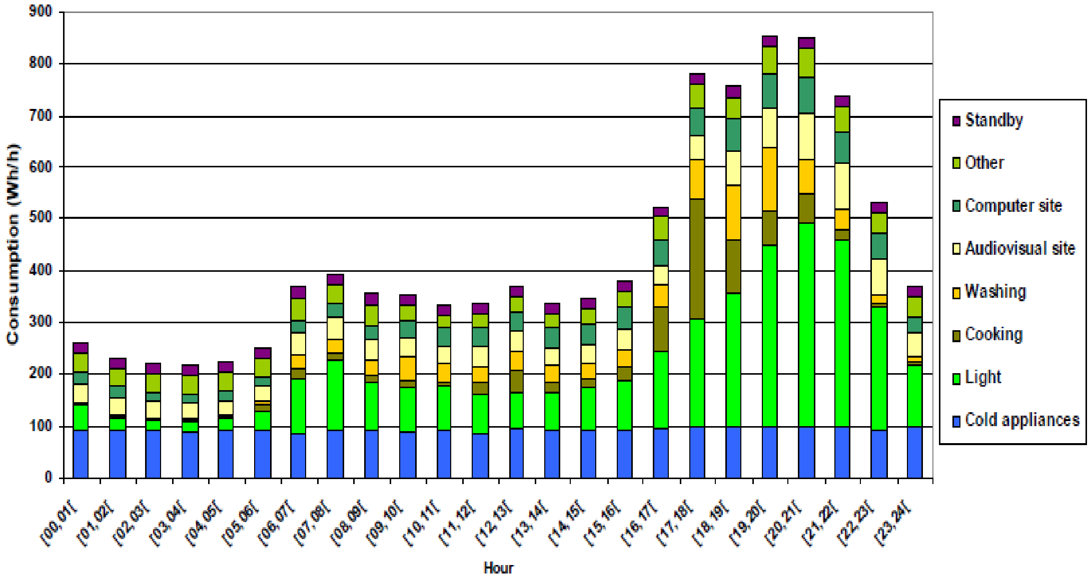

Figure 3.6: Average load profile for a residential house in Sweden [34]

Based on the PV power generation profile and the load power demand, the worst possible case was found out to occur between 10 and 11 am. Therefore, investigations of cloud-induced power swings have been performed between this time intervals, in which it has been assumed that the PV systems produce their rated power.

Figure 3.7 [34], shows the relative distribution of the load demand without electric heating. As it can be seen 20-24 % of energy in a residential house/apartment is consumed by the refrigerators and freezers while 21-25 % of energy is consumed for lightning. The relative energy consumption does not take in consideration the energy used for electric and water heating. However, according with [35] most of the annual energy consumption for electrical heating is consumed during October to April, with only about 11% in the period May to September.

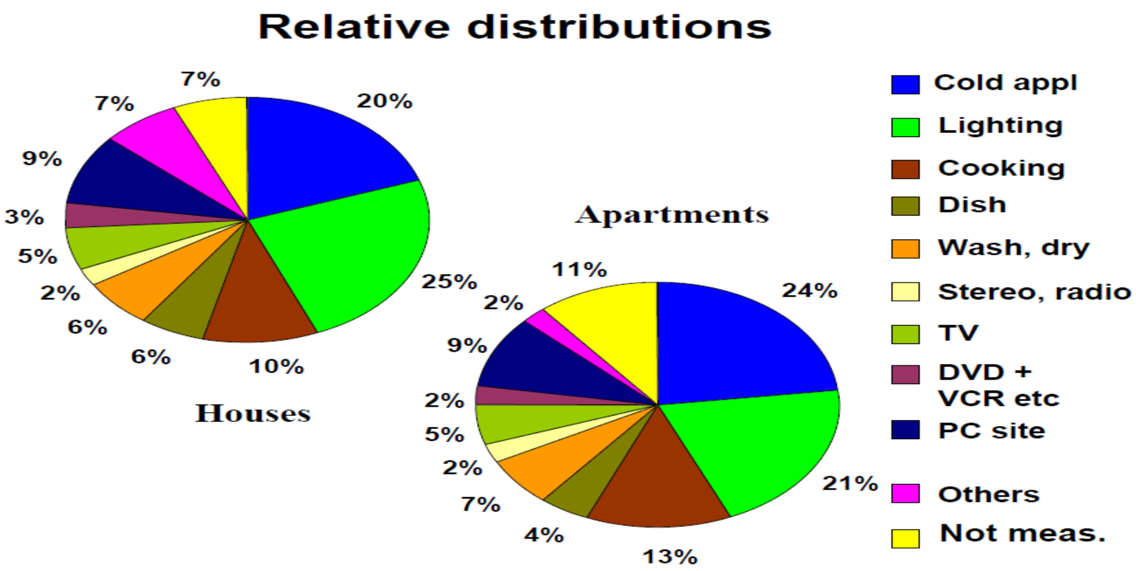

Figure 3.7: Relative load distributions in a house/apartment in Sweden [34]

According with [36], incandescent and halogen lamps account for 85% of installed lightning capacity in a house while the remaining 15% account for fluorescent lightning. Incandescent lamps are often assumed to have a constant resistance characteristic. However, due to the large temperature swing that occurs in the filament when voltage changes, the filament resistance changes with voltage. The result is active power that varies with about the 1.55 power of voltage; about halfway between constant current and constant resistance [37].

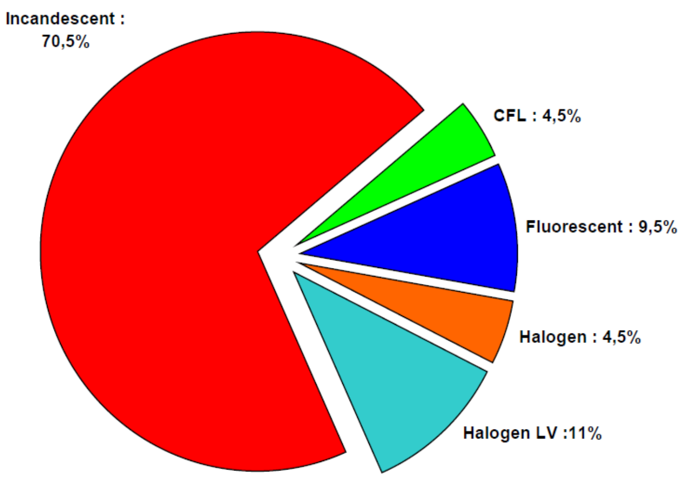

Figure 3.8: Part of each light source in the total installed capacity-houses in Sweden [36].

The total spot load of 360 kW has been distributed across the entire network based on the roof-top area of the houses as in [32] and detailed information can be found in Appendix 2. Based on the previous reports [34,35,36], it has been assumed that the overall load (load seen from the substation) comprises 45% motor loads and 25% thermostatic loads which accounts for 70% constant power loads. The remaining 30% of the loads used for the lightning was simulated simply as incandescent lamps with constant impedance load characteristics despite their half impedance and half constant current transient behavior.

3.6 Dynamic loads modeling

Dynamic loads models are implemented in the simulation. The residential load equipments are usually connected through single phase ac sockets. However, the load at each house it is assumed to be equally divided between phases and therefore three phase analysis is performed in the software.

3.6.1 Induction motor Load

The induction motors account for 45% of the total power demand. For voltage stability concerns, it is very important to include the dynamic characteristics of induction motors in the analyses. However, due to the fact that induction motors exhibit different characteristics based on their application (size, design, torque load etc), it is very difficult to include all these parameters in the simulation. Therefore, a 1 kW, three phase, third order induction motor was simulated in the analyses. According with [14], [19], for the system's voltage stability concerns, it is usually enough to model a third order induction motor. The third model neglects the differential terms in the stator equation.

The 1kW induction motor was assumed to operate at full load torque as refrigerators and air-conditionings require almost constant torque to drive the compressor. According to [14], [15], their stalling voltage is around 0.87-0.88 p.u. The induction motors in the simulation were set to stall at 0.9 p.u.

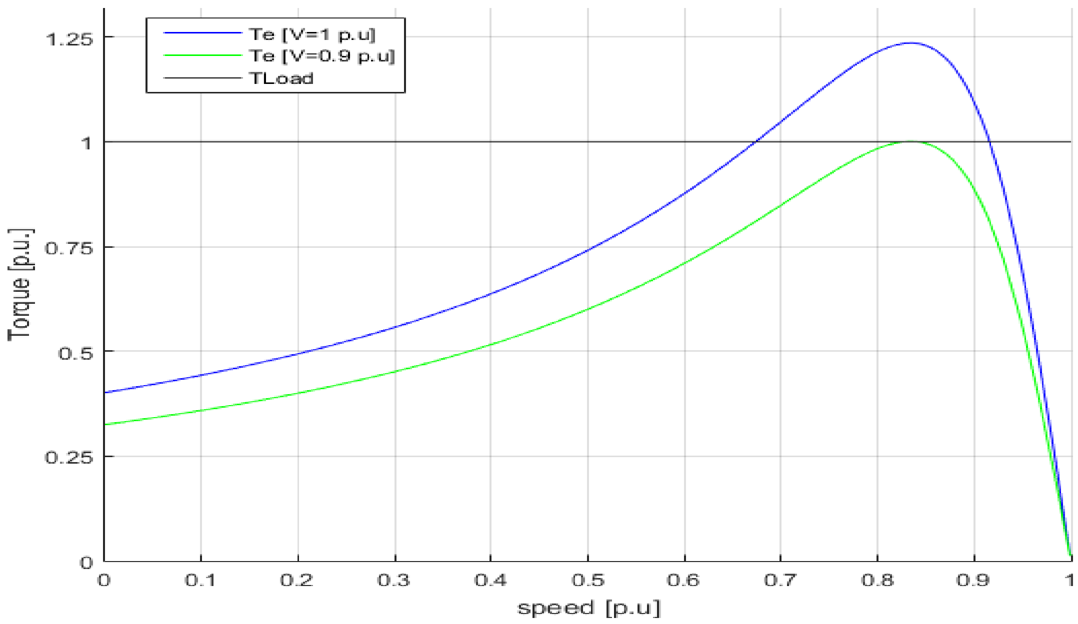

Figure 3.9: Torque vs speed characteristics under different voltage disturbances for a 1 kW IM

Usually small residential motors are only equipped with thermal protection which disengage the motors when the accumulated heat into the motor reaches certain limits. The time to disengage the motors depends on their design and performance characteristics. According to [14], the thermal protection disengages the stalling motor between 3-30 seconds. In the simulation this time was selected to be 5 seconds.

3.6.2 Thermostatic loads

Thermostatic loads which account for 25% of total power demand are also simulated. When the grid voltage drops, more thermostatic loads will be ’’on’’ for a longer period, thus they collectively tend to restore the power. However, if the thermostatic loads are ’’on’’ for the entire period, their power recovery tendency will be affected and their pre-disturbance power target will not be possible. This is mainly because, when they are fully ’’on’’, they will behave as constant impedance loads when voltage variations occur. The recovery time constant is set to 100 s and the maximum thermostatic power under the nominal voltage is 1.5 times the rated load. Figure 3.10 shows the thermostatic loads response under different voltage disturbances.

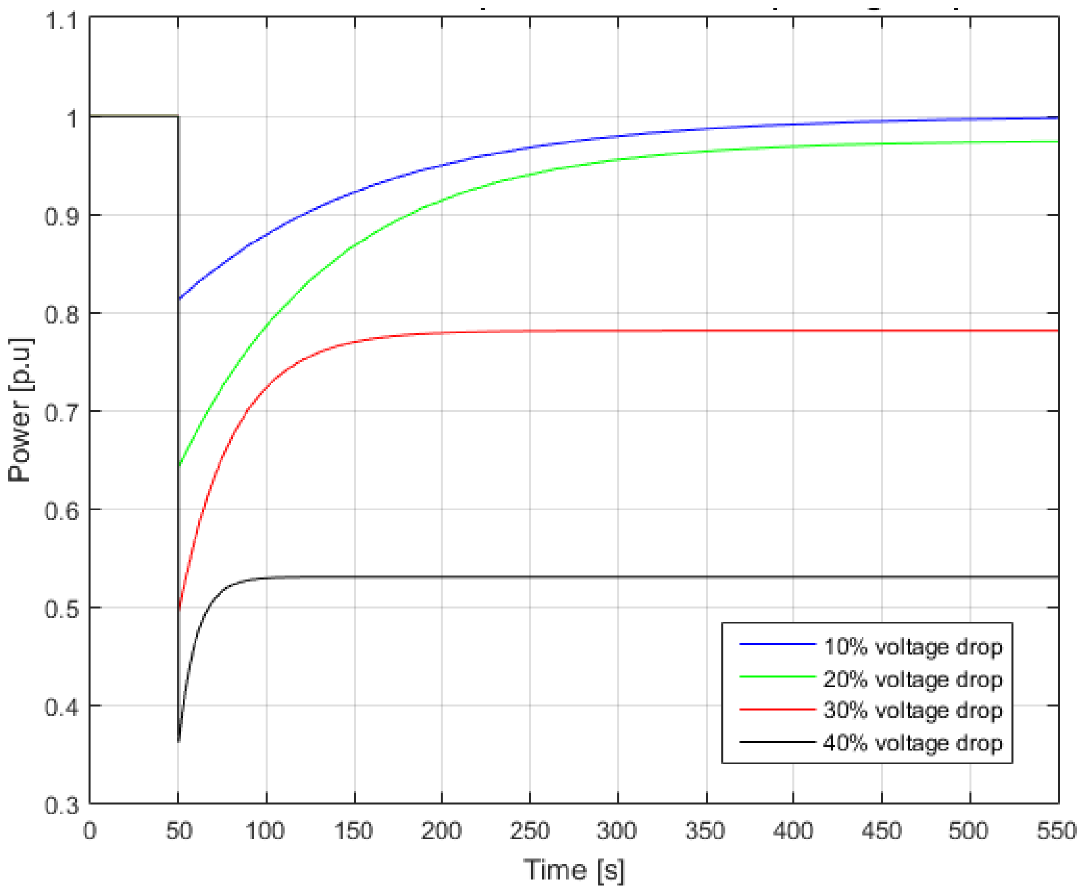

Figure 3.10: Thermostatic load response under different voltage disturbances

4 SIMULATION RESULTS AND DISCUSSION

This chapter presents the simulation results for the Mölndal network as well for the modified grid. The analysis investigated different case scenarios in which the Penetration level from the PV systems has been gradually increased until voltage instability in the modified distribution grid has occurred. The voltage instability was caused by the cloud induced power swings of the PV units; by the time delay of the regulating transformer for the first tap operation and also by the characteristics of the dynamic loads. In addition, it presents the comparison between the static and dynamic loads for the instable case scenario. The chapter ends with a short summary of the simulation results and a comparison table.

4.1 Mölndal grid

Without any PV integration on the investigated grid, the system is a traditional network for which has been designed. After performing load flow calculations, the voltages profiles for all the busses of the network have been determined. As it can be seen in Figure 4.1, the voltage values of the network's buses are close to the nominal values. This can be explained that the network is operated under low load condition during the summer and also the grid is designed to be a strong grid.

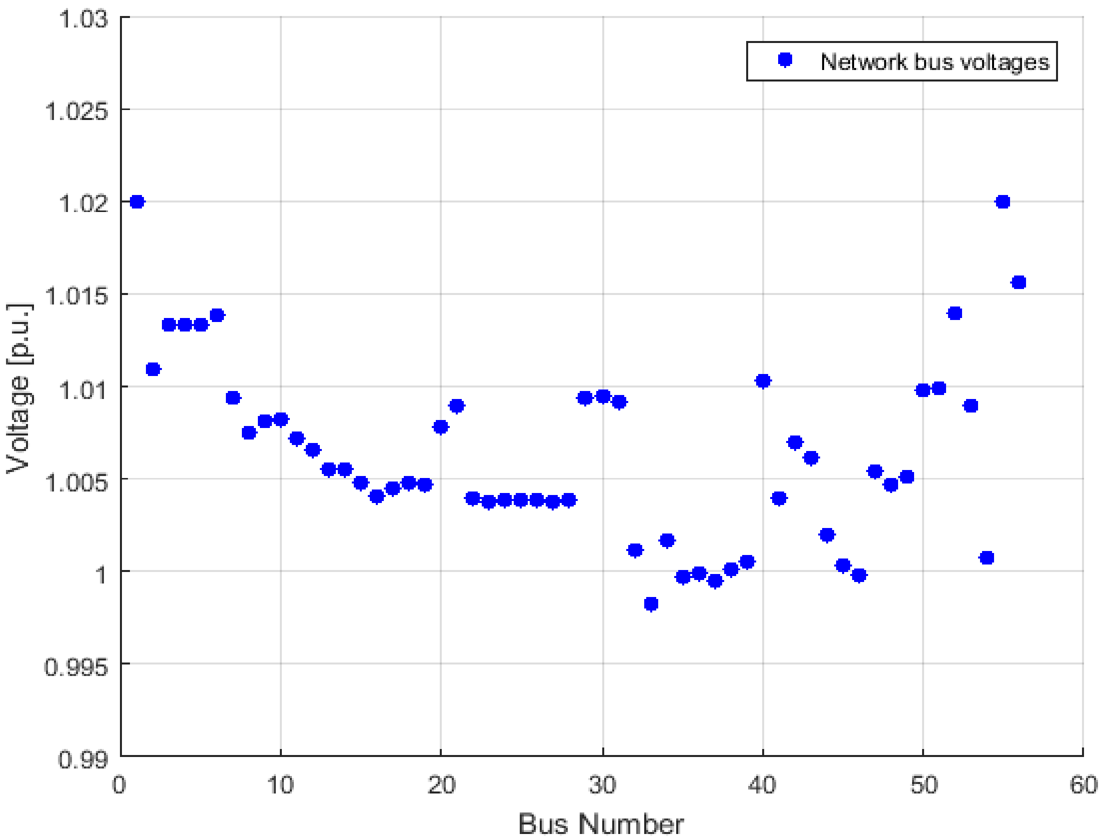

Figure 4.1: Steady-state network's bus voltages for the Mölndal grid (No PV integration)

4.1.1 Case with 30% PV integration

For the investigated grid, 30% PV power were integrated into the network. The clouds were assumed to cover the PV arrays from 10 to 30 seconds. Figure 4.2 shows the voltage variations for some of the most sensitive buses of the network. As it can be noticed the voltage drop was relatively small (approximately 1.2 %) and the grid operated well when it was subjected to clouds ’disturbance.

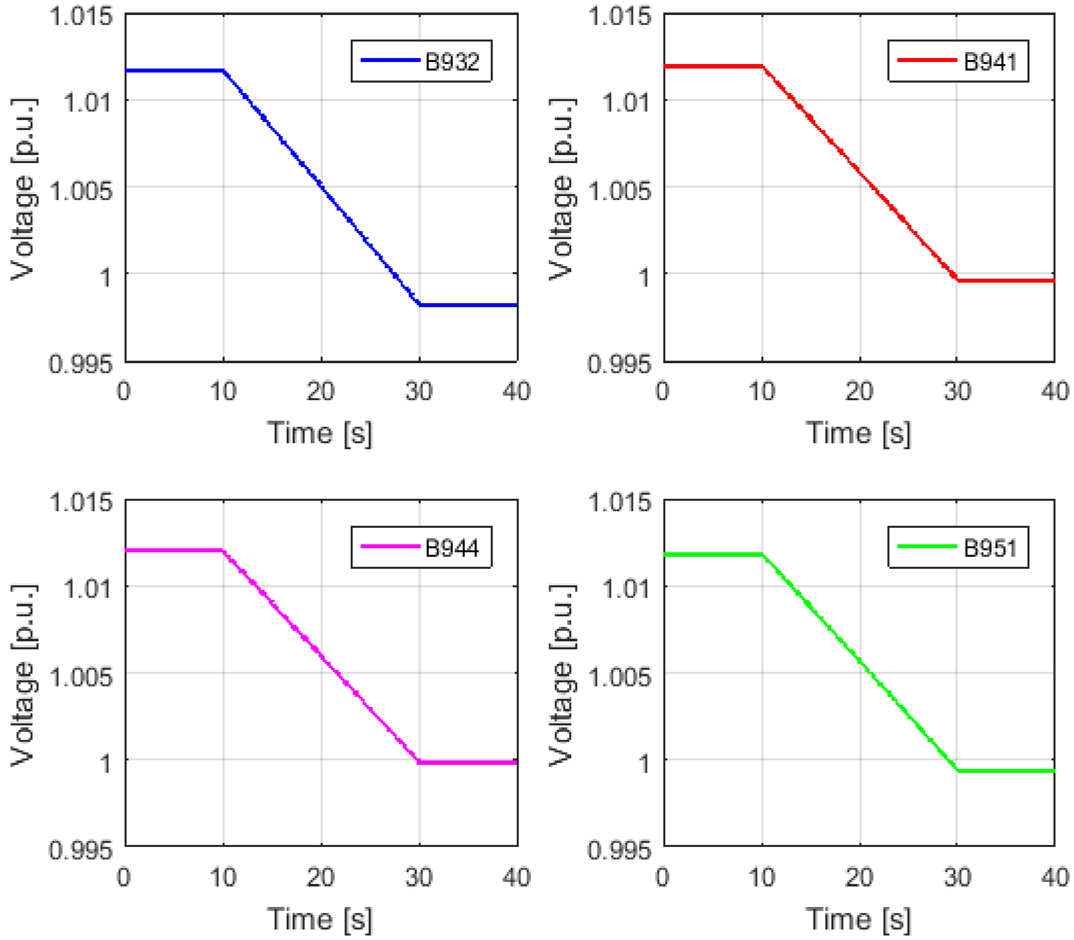

Figure 4.2: Selected system’s bus voltages for the Mölndal grid with 30% PV integration

4.1.2 Case with 60% PV integration

The PV penetration level has been increased to 60% and the cloud-effect was simulated as in the previous case. As it can be seen in Figure 4.3, the steady state voltages of some selected buses have increased due to the higher PV penetration level. However, as soon as the clouds covered the PV arrays, the voltage drop was relatively higher compared with the 30% PV penetration level (approximately 2.5 %). Nevertheless, the voltage after the cloud coverage of the network was still close to the nominal value. A comparison between the 60% and 30% PV penetration level is also illustrated in Figure 4.3.

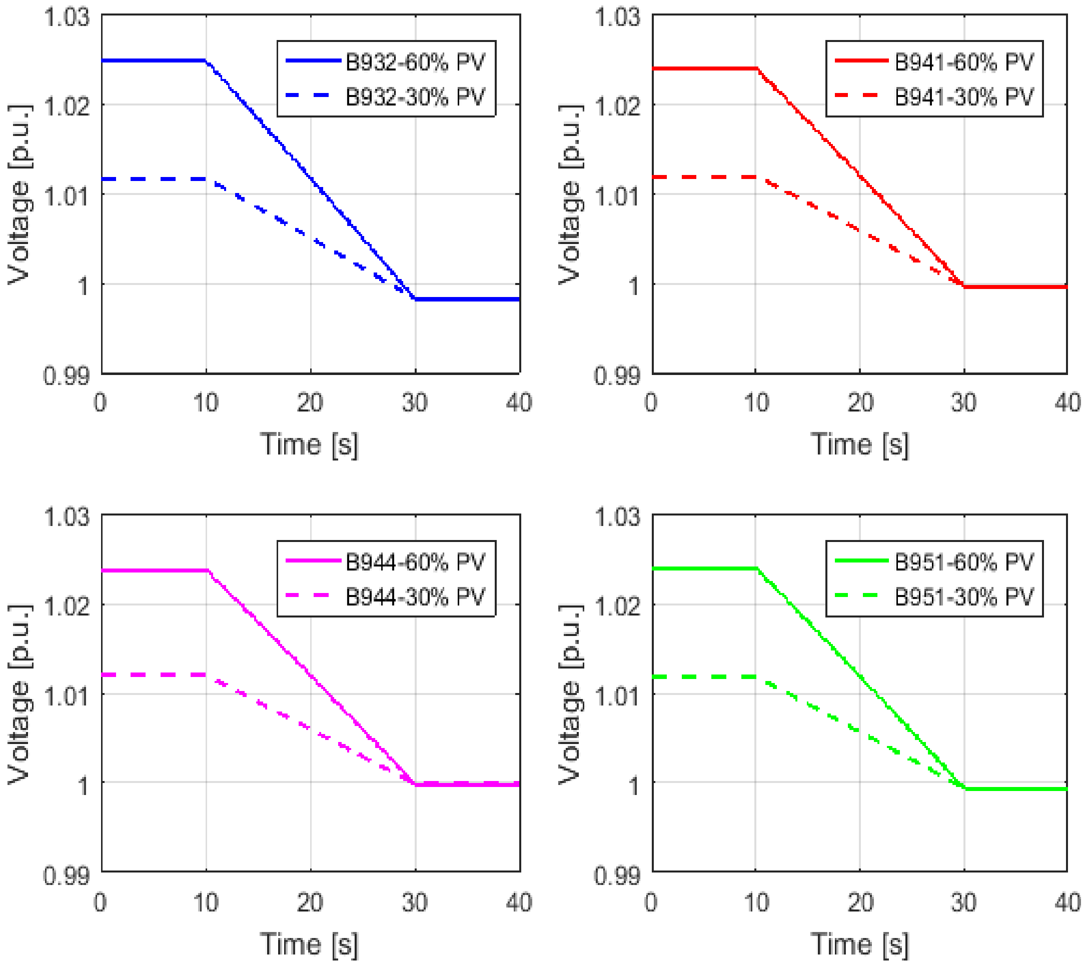

Figure 4.3: Selected system's bus voltages for the Mölndal grid with 60% PV integration

4.1.3 Case with 90% PV integration

The case with 90% PV integration has been investigated as well. The cloud-effect was simulated in the same manner as before and the voltage drop phenomenon has been investigated. As it can be noticed in Figure 4.4, the steady-state voltages of the network have been increased compared to the previous two cases. As soon as the clouds covered the network, voltage drops occurred in the network. However, the grid operated again well when it was subjected to clouds' disturbance and no voltage related problems were encountered.

4.2 Modified grid

In order to investigate the potential negative impact on voltage stability of the cloud induced power swings on distribution grids with high R/X ratio, the operational parameters of the Mölndal's network were modified in order to make the grid to be a relatively weaker grid. Therefore, the short circuit capacity was changed from 80 MVA to 4 MVA and the peak/spot load was increased to 360 kW. In addition, the modified grid was equipped with an ULTC transformer as explained in Chapter 3, section 3.4. The cloud disturbance was modeled to be the same as for the Mölndal grid (real grid) case.

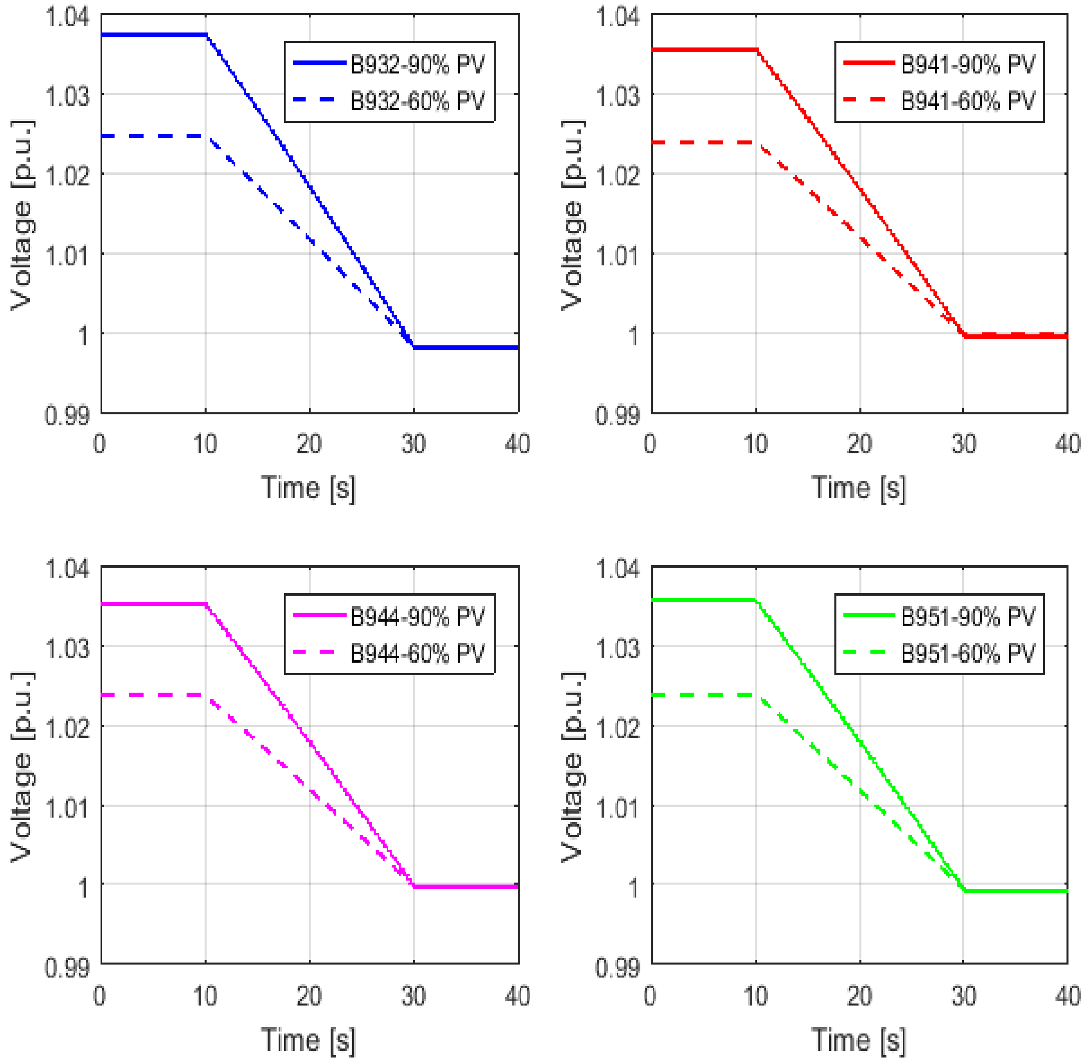

Figure 4.4: Selected system's bus voltages for the Mölndal grid with 90% PV integration

4.2.1 Base case (0% PV integration)

After performing load flow calculations, the voltages profiles for all the busses of the network have been determined as it can be seen in Figure 4.5. The simulation showed that the system operated under a loaded condition without any voltage violations. However, in the case of PV integration into the system, affected by the cloud coverage, the voltage values at some specific buses can violate the standard voltage limits due to both, additional active power flowing through the lines as well as due to the dynamic load characteristics (constant power loads which tend to recover their pre-disturbance power).

Of concern are the most sensitive buses, which can be located far away from the substation, can have a higher loading status or both. If there will be voltage violations, they will occur firstly at the weak buses and therefore these buses have been located and are investigated further in detail.

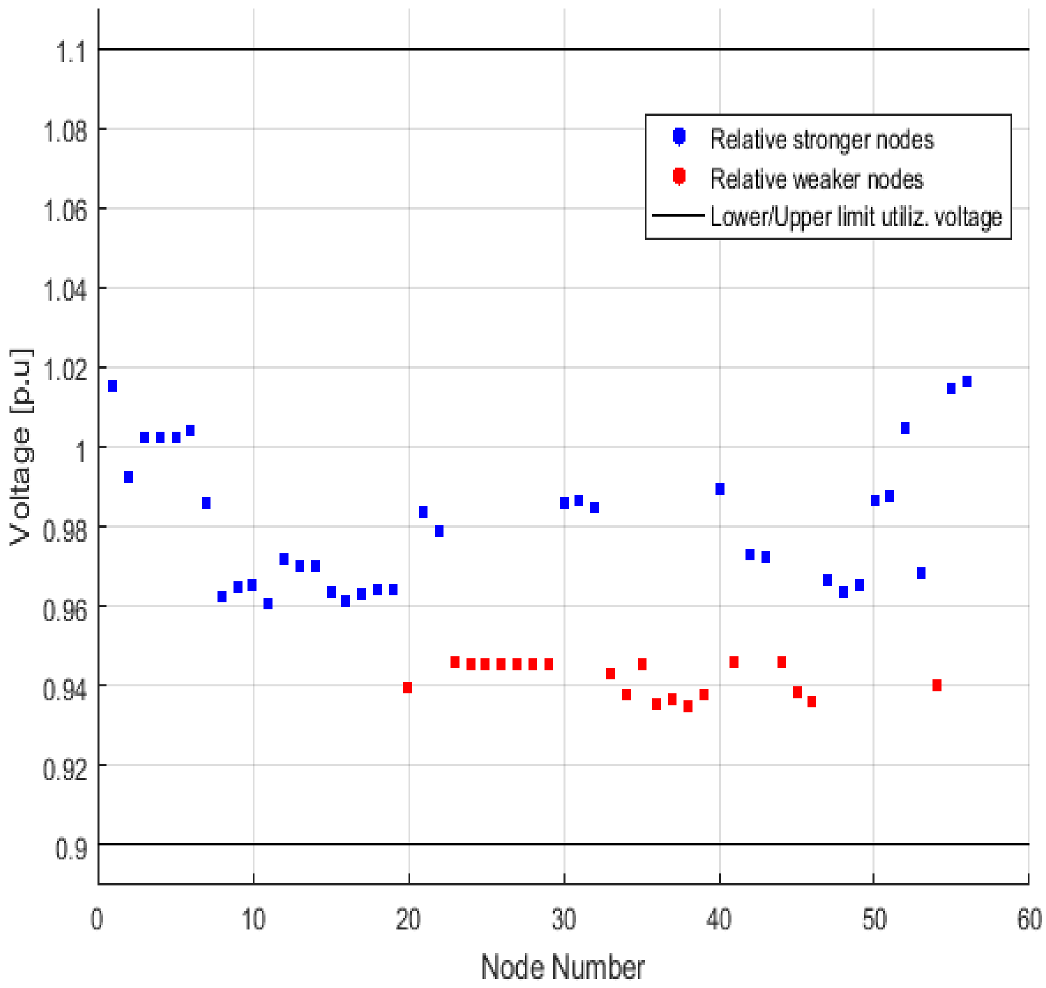

Figure 4.5: Steady-state network's bus voltages for the modified grid (No PV integration)

4.2.2 Case with 20% PV penetration

In the Figure 4.6, it is ilustrated the cloud coverage impact at the substation. Between 0 and 10 seconds, the system is operated in steady-state condition. The regulating transformer had its tap operation at position Tap=-4. As it can be seen, at 10 s when the clouds started to cover the network, a voltage drop occured in the network. However, the voltage drop was not enough to cross the imposed deadband and the regulating transformer didn't operate by keeping its timer turned off.

The voltage profiles for the most sensitive buses with 20% PV penetration are illustrated in Figure 4.7. As it can be noticed, the PV cloud induced power swings caused a voltage drop (between 10 and 30 seconds) at the investigated buses. In addition, the thermostatic controlled load caused an additional small voltage drop (between 30 and 100 seconds) in their attempt to restore the pre-disturbance power level. However, the voltage drop caused by the cloud effect and the thermostatic recovery process, was still within the voltage allowable limits and no potential voltage instability occurred.

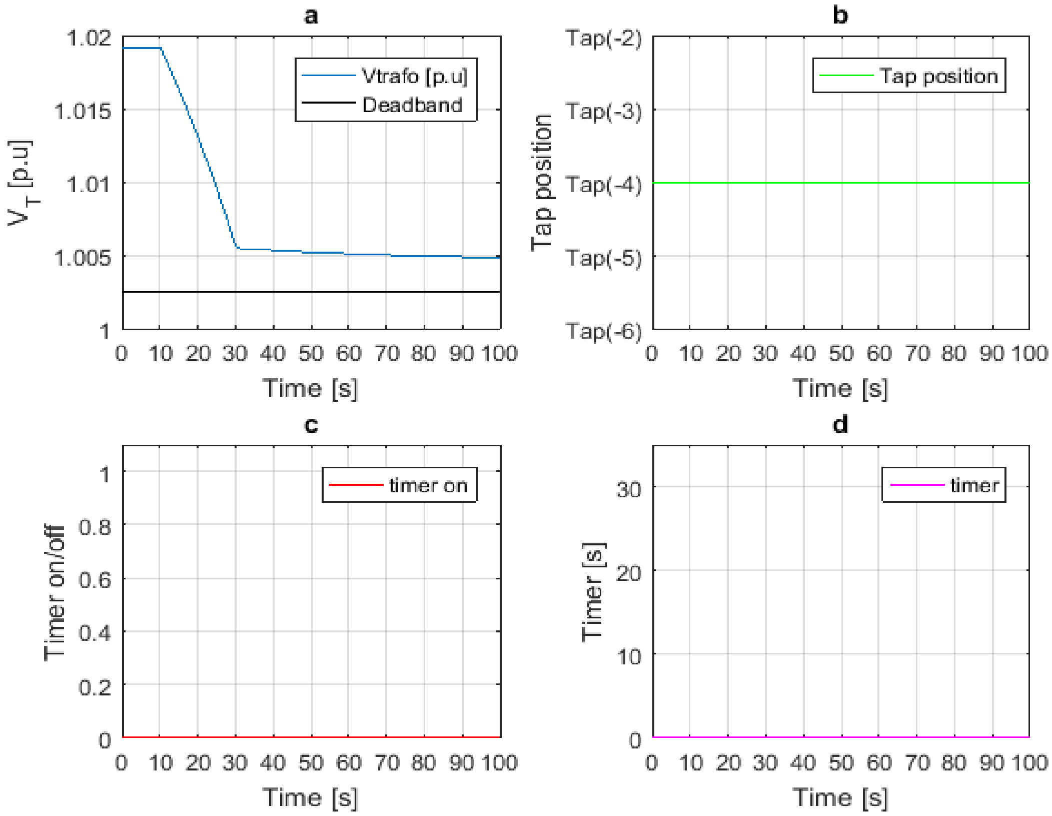

Figure 4.6: Regulating transformer's reaction for the <u>modified grid</u> with 20% PV integration

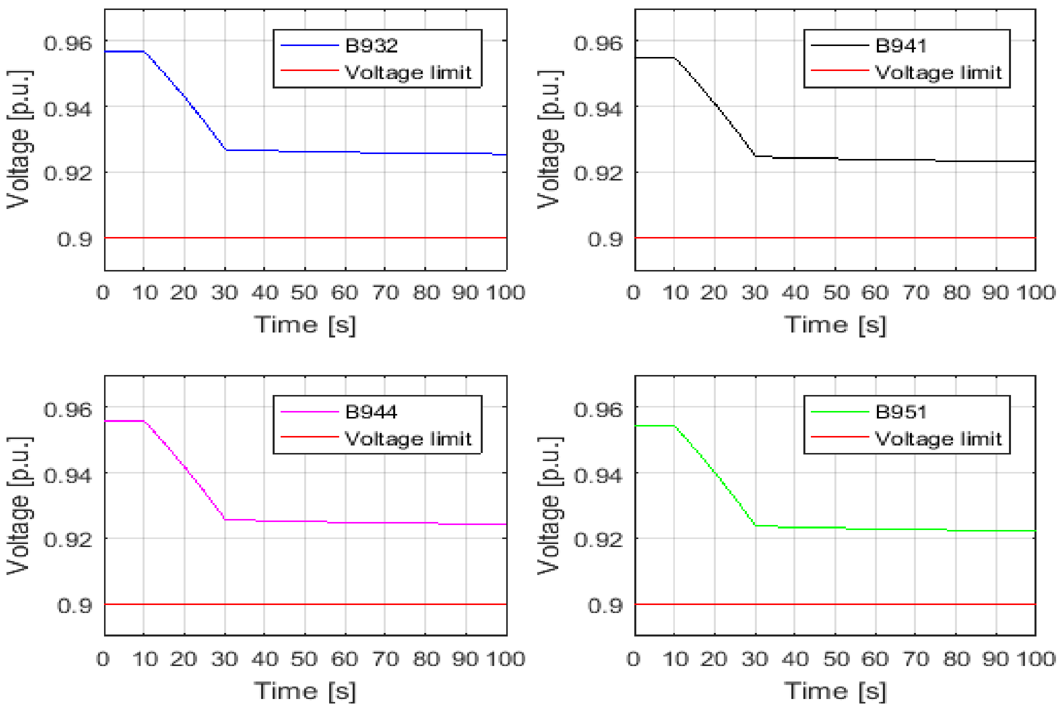

Figure 4.7: Selected system's bus voltages for the <u>modified grid</u> with 20% PV integration

4.2.3 Case with 30% PV Penetration

In this case, due to the higher amount of dispersed energy integrated into the grid, the regulating transformer sensed a less load current and it operated at a higher tap position (Tap=-3) compared with the previous case.

As can be seen in Figure 4.8, as soon as the voltage drop occurred at the secondary side of the transformer crosses the deadband, the tap changer relay is energized (at around 24 s) and it starts counting and at 54 seconds first tap operation is performed. However, after the first tap operation, the voltage at the secondary side of the transformer was still outside the deadband and the regulating transformer operated one more time to bring the voltage within the imposed limits.

The voltage profiles with 30% PV penetration level are illustrated in Figure 4.9. A comparison between the 30% and 20% PV penetration level is also shown. As it can be noticed the steady state voltage values for the 30% were improved compared to the 20% PV integration. However, as soon as the clouds covered the residential houses (between 10 and 30 seconds), the voltage drop was higher than the case with 20% PV integration.

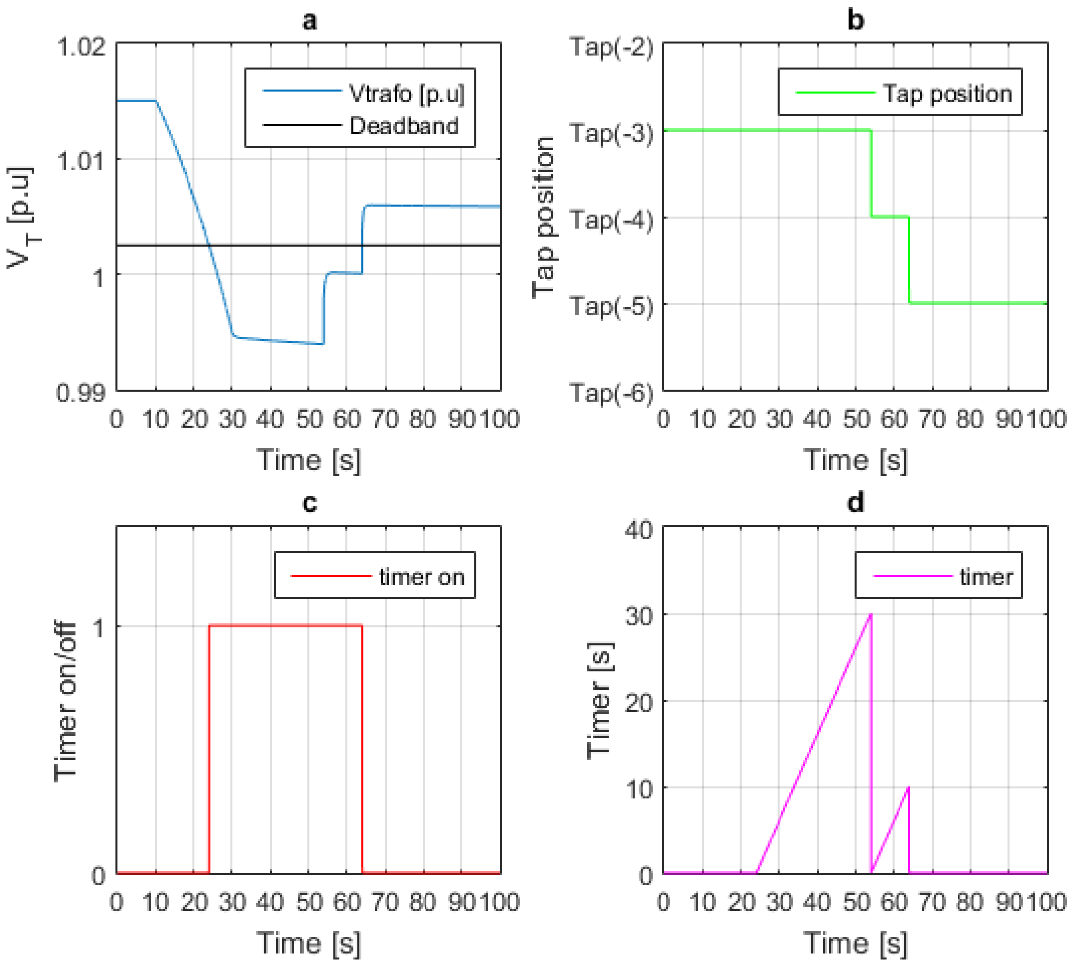

Figure 4.8: Regulating transformer's reaction for the modified grid with 30% PV integration

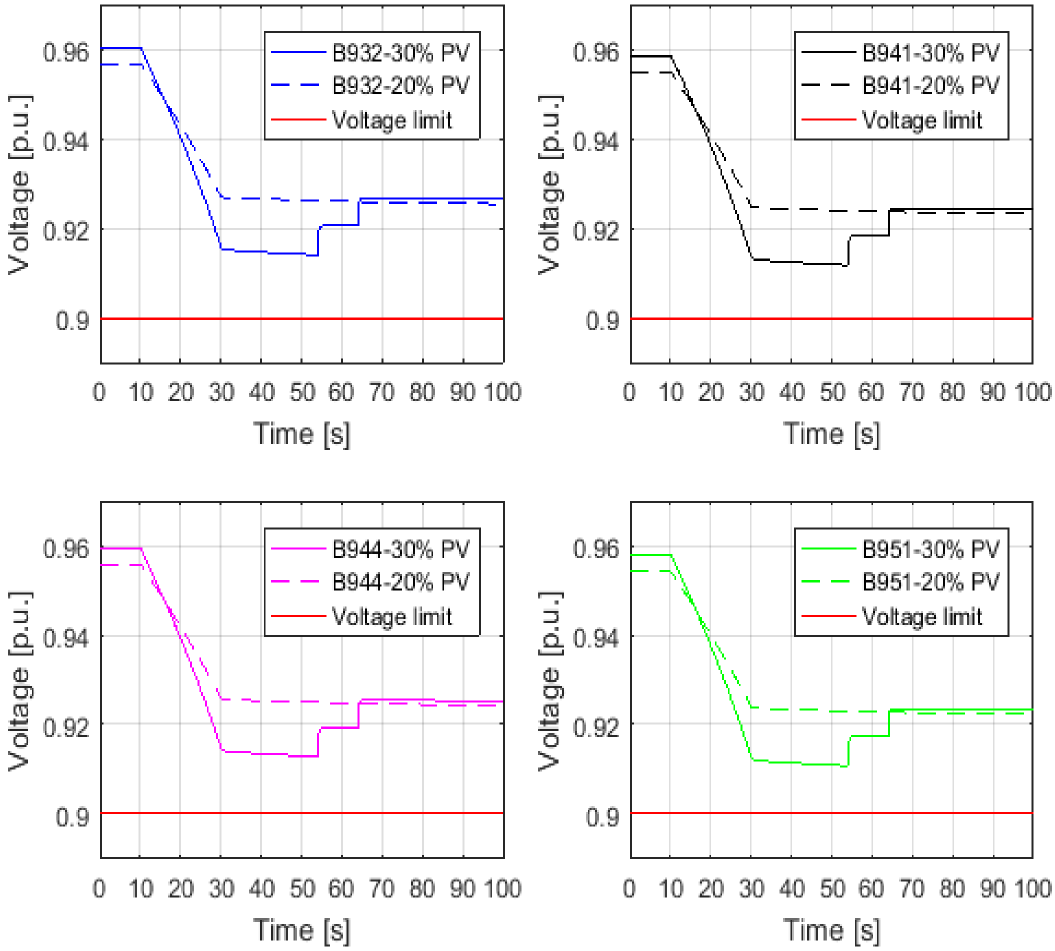

Figure 4.9: Selected system's bus voltages for the <u>modified grid</u> with 30% PV integration

4.2.4 Case with 40% PV Penetration

For the 40% PV integration case, the voltage level at the secondary side of the transformer was slightly higher than in the previous case due to the higher amount of dispersed generation integration. However, it was not enough for the regulating device to operate at a higher tap position and the tap was operated at the same position (Tap -3) as in the previous case.

Nevertheless, as it can be seen in Figure 4.10, as soon as the clouds covered the network (at t=10 s), the resulted voltage drop occurred at the secondary side of the regulating transformer was higher due to higher active power flowing through the regulating device. The transformer was able to restore the voltage level and operated three times.

The voltage profiles before clouds' coverage were improved for the entire network as it can be seen in Figure 4.11 due to the higher penetration level as compared with the previous cases. However, when the grid was subjected to clouds'disturbance, the occurred voltage drop in the system was higher and close to the voltage limit of 0.9 p.u. Nevertheless, the regulating transformer was able to regulate the voltage and no voltage instability occurred

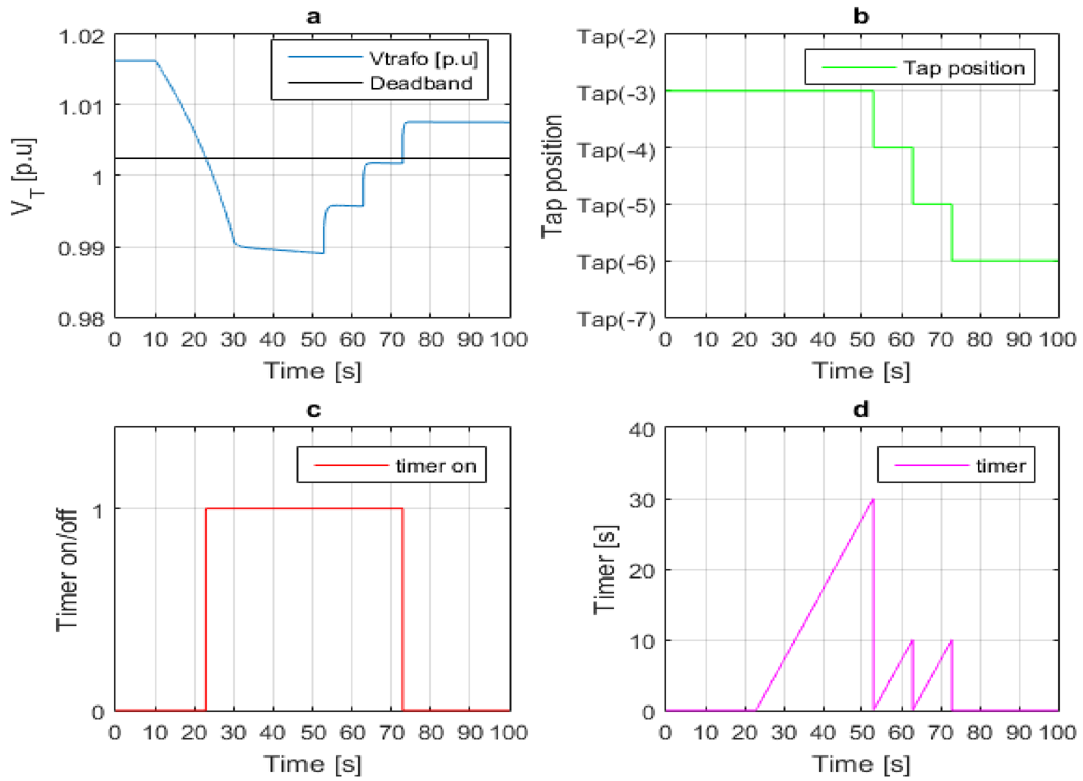

Figure 4.10: Regulating transformer's reaction for the <u>modified grid</u> with 40% PV integration

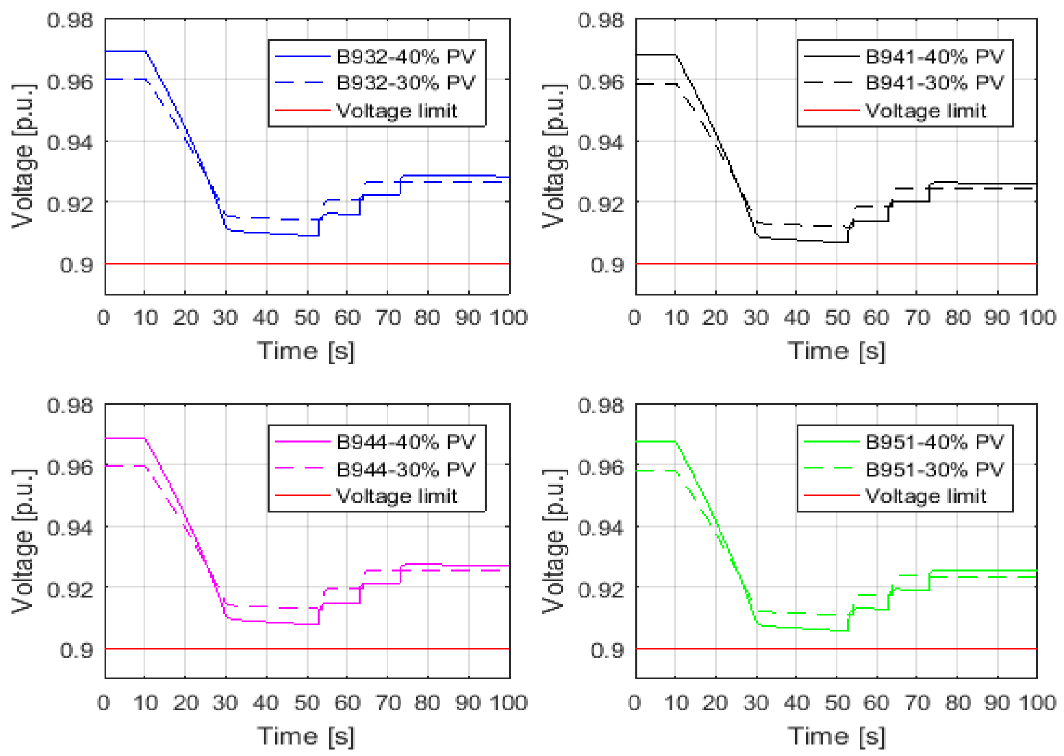

Figure 4.11: Selected system's bus voltages for the <u>modified grid</u> with 40% PV integration

4.2.5 Case with 50% PV Penetration

For 50 % PV integration, the consequences of clouds' coverage are more dramatic. Figure 4.12 shows the characteristics of an induction motor at one of the most sensitive buses, at bus B944. The system operated in steady state condition until 10 seconds. After that, the clouds started to cover the distribution grid, which caused the voltage at the bus 944 to decrease and at 30 seconds it reached the value of 0.905 p.u. At this value, the induction motor load connected at this bus is at the limit but it doesn't stall. However, the thermostatic loads started to recover their pre-disturbance power which caused more voltage drops in the system and when the voltage at bus B944 reached the value of 0.9 p.u (at around 34 s), the induction motor began to stall.

The electrical torque of an induction motor is the product between the stator flux and the rotor current. The stator flux is directly proportional with the square of the supply voltage. As the voltage at bus B944 decreased, the electromechanical torque potential of the machine decreased as well which in turn gave new operational characteristic between the load torque and the electrical torque. This, however lead to an increase in the slip which increased the losses in the machine. To cover both, the losses and to produce the required mechanical power, the motor drawn higher current from the network as can be seen in Figure 4.12.b

As soon as the voltage reached the value of 0.9 p.u, the electrical torque was not able to meet the requirements of the load torque (there was no intersection between electrical and mechanical characteristics of the induction motor) and the motor began to stall.

As far as the induction motor at bus B944 has stalled, it started to draw higher active and especially reactive power, which has tripled as can be seen in Figure 4.13. This led to more voltage drops through the entire system. When the voltages at other induction motors connected at other buses reached the values of 0.9 p.u, they started to stall as well.

During the stalling processes (between 34 and 39 seconds) of all the induction motors in the entire grid, the system was not able to maintain its stability and unacceptable low voltage values occurred. Figure 4.14 shows the stalling process of some selected buses. As it can be seen, the induction motors stalled at relatively different time periods.

As can be seen in Figure 4.15, the regulating transformer did sense an increase in the load current which caused a voltage drop at the secondary side of the regulating device, but due to the fact that the control mechanism prevented it to react fast enough, the regulating transformer failed to prevent the voltage collapse and the system became voltage instable. Successive inefficient tap operations were performed by the regulating device for voltage restoration process.

Figure 4.16 shows the voltage values before and after the transformer's regulation for the entire network. The voltage levels at some of the remote systems reached as low as 0.68 p.u. Worth mentioning here is that, there is a small tendency to increase the voltage by the regulating transformer at some of the remote buses, but as soon as the voltage is relatively increased, the induction motors draw higher active and reactive power in their attempt to accelerate. This leads to a further decrease in the voltage level and no significant improvement is made.

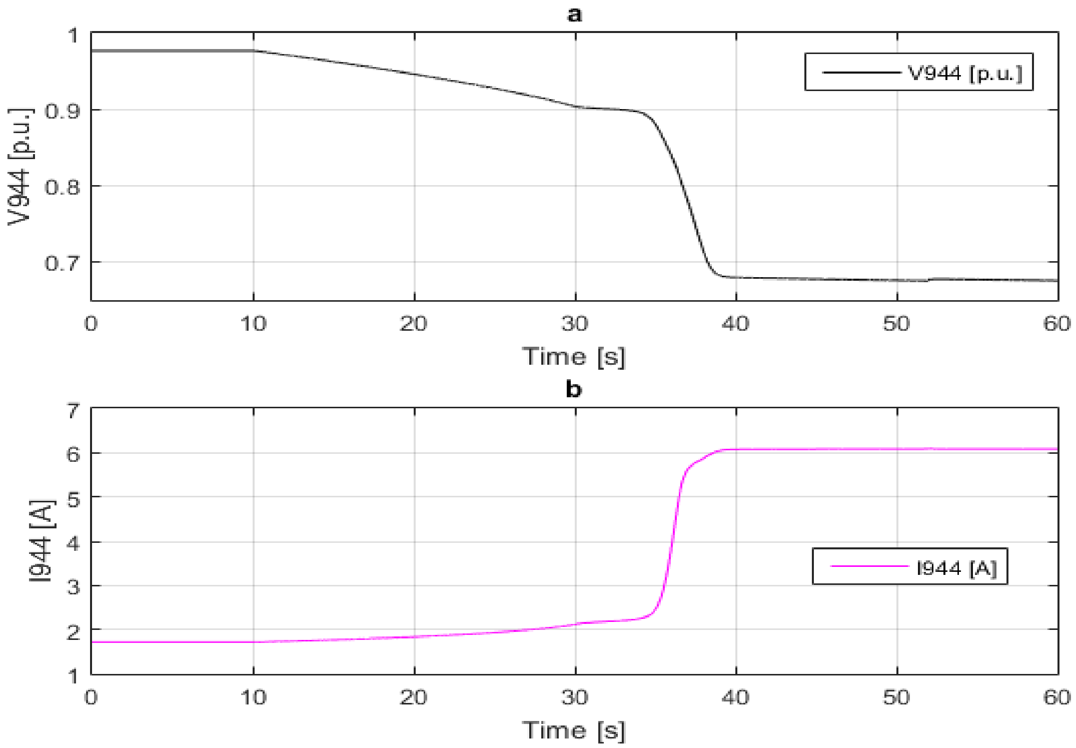

Figure 4.12: Induction motor at bus B944; a: Voltage, b: Current

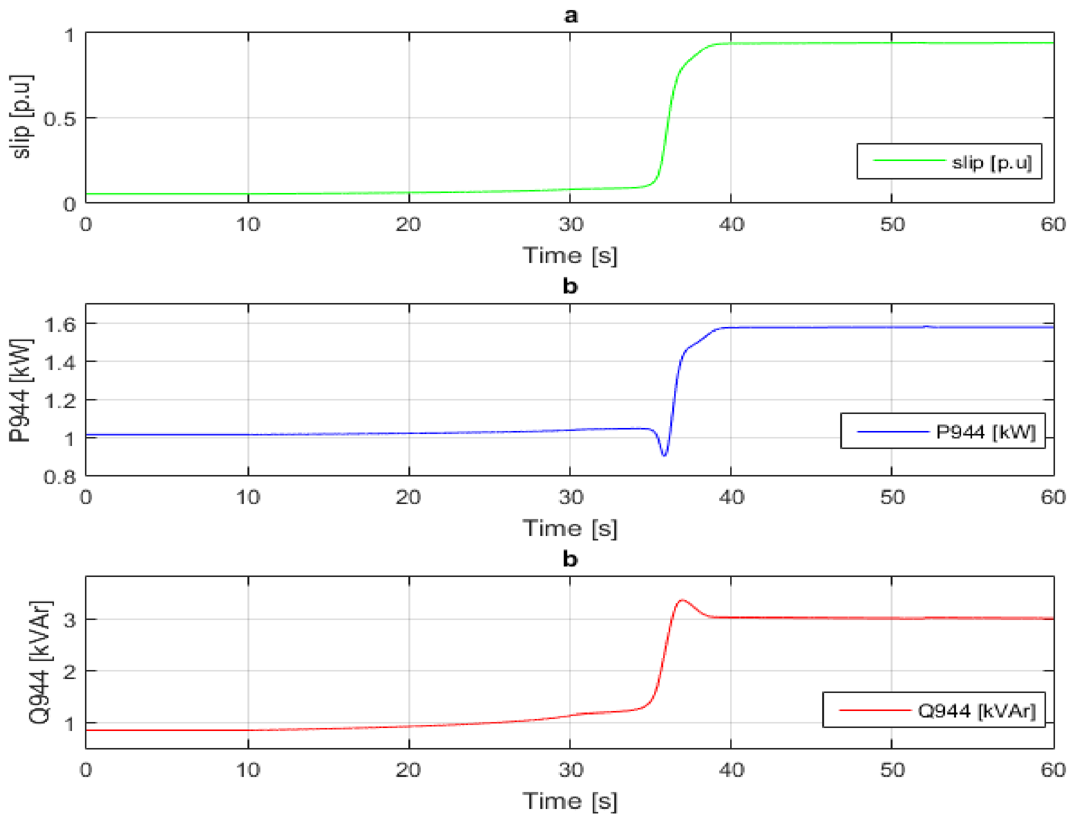

Figure 4.13: Induction motor at bus B944; a: slip, b: Active/Reactive power

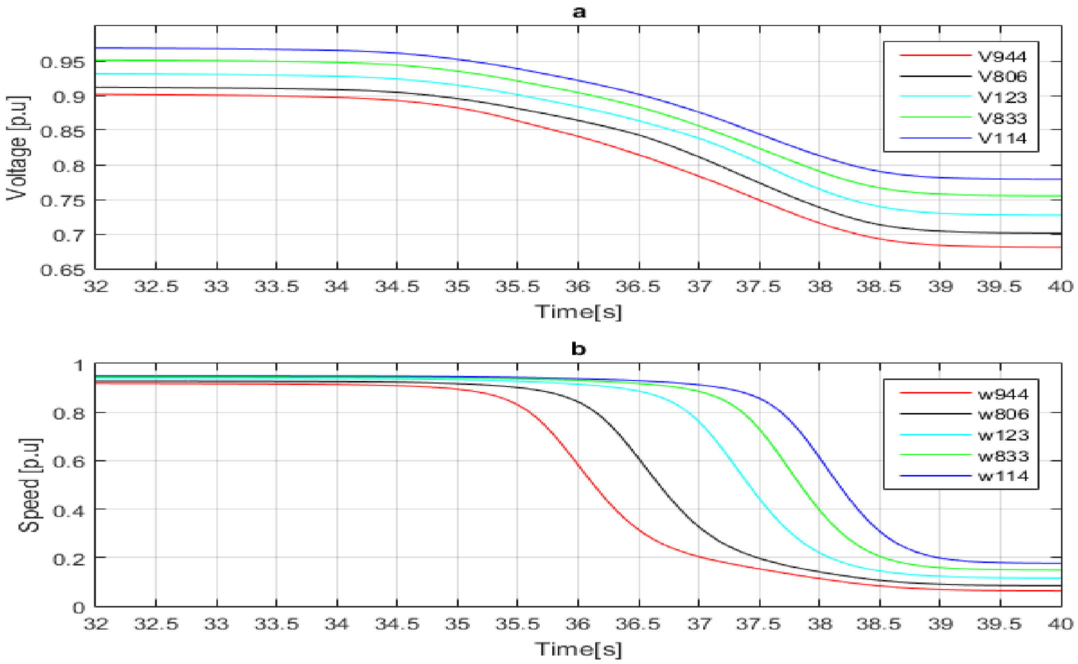

Figure 4.14: Selected induction motors in the network; a: voltage, b: speed

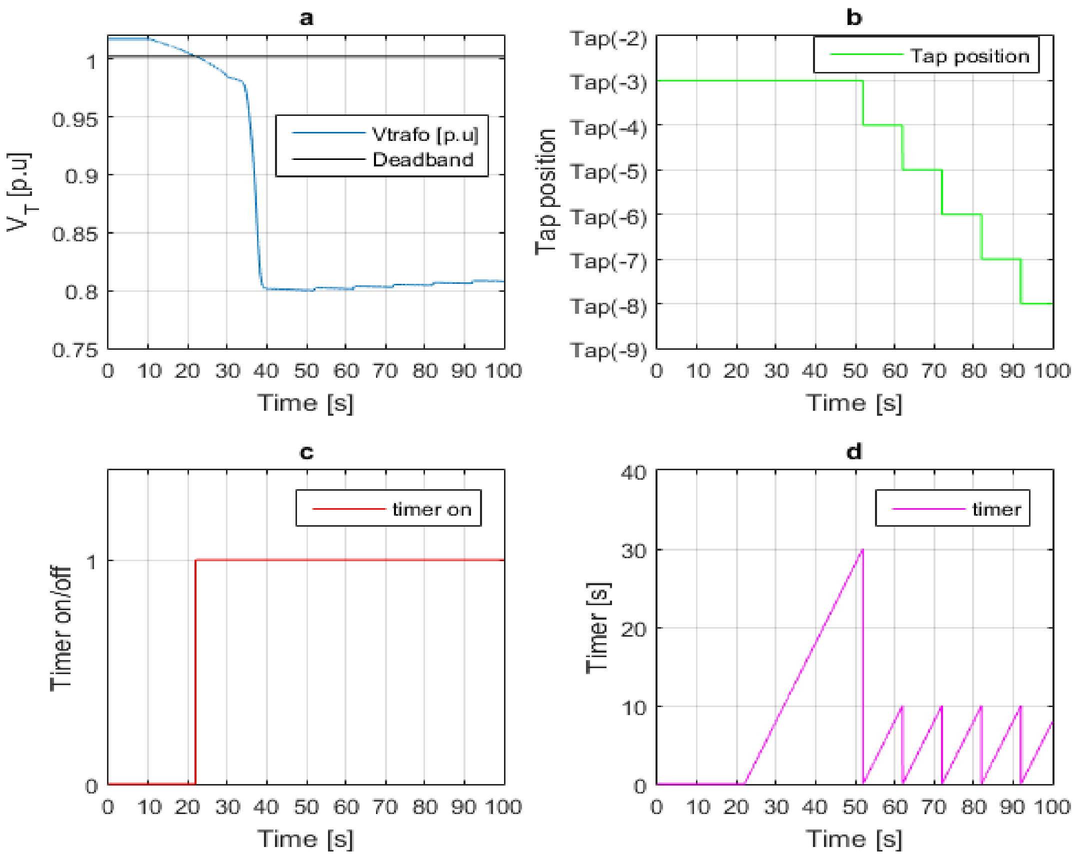

Figure 4.15: Regulating transformer's reaction for the <u>modified grid</u> with 50% PV integration

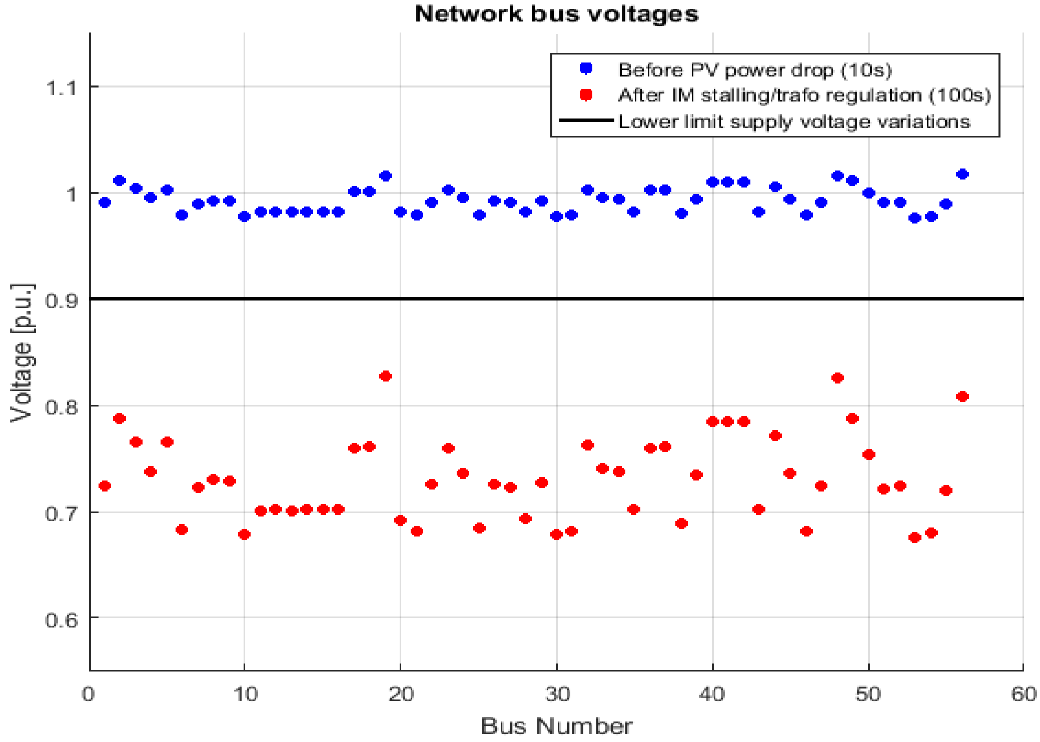

Figure 4.16: System's bus voltages for the modified grid with 50% PV integration

During the time the inductions motors connected load have stalled, the demand for active and especially reactive power has increased substantially. Figure 4.17 shows the active and reactive power demand at the substation MTT0546. As it can be seen, after induction motors have stalled, its demand for reactive power has tripled pointing out the sensitivity of the induction motors regarding the reactive power.

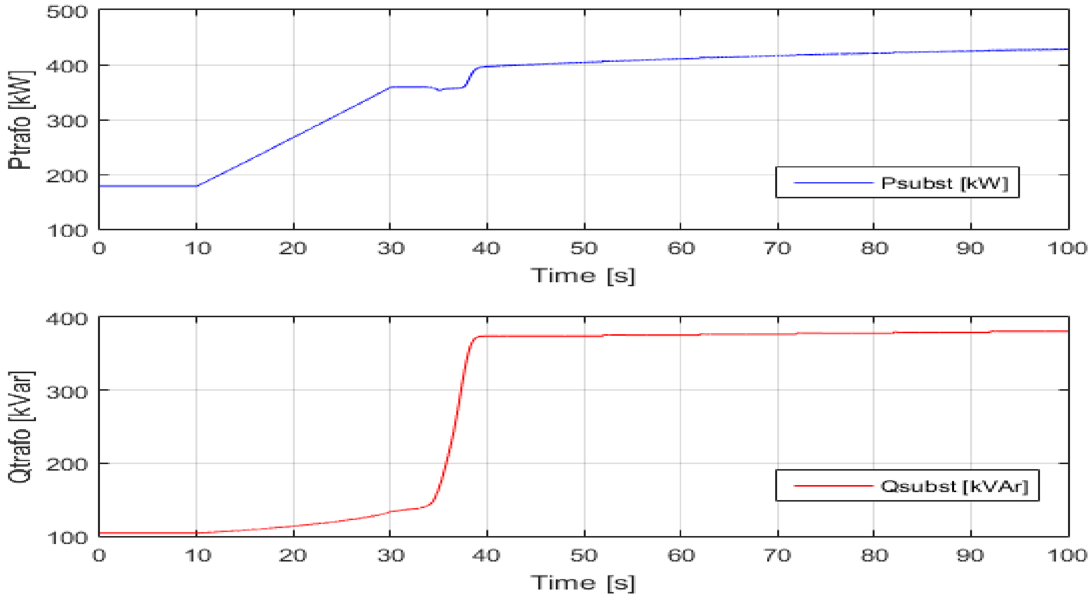

Figure 4.17: Active and reactive power demand at the substation MTT0546

Due to the fact that the stalled motors required high amount of reactive power in order to reaccelerate, it can be rationalized that even if the clouds will start to unveil the PV systems, it is highly improbable that the grid will recover from the voltage instability.

4.2.6 Case with 50% PV penetration and thermal protection of the IM

As explained in Chapter 3, section 3.6.1, most of the residential induction motors are equipped with only over-thermal relays which disconnect the stalling induction motors after a specified amount of time which depends on the amount of heat dissipated in the motor. The thermal protection has been implemented at each motor in the simulation to trip the motors within 5 seconds after the stalling process.

One of the motors to trip first, is the induction motor connected at the bus B941. This is as expected as bus 941 has one of the worst voltage profiles due to the fact that is located far away from the substation. As it can be seen in Figure 4.18, as soon as the induction motor has stalled, it drawn as 3 times rated current. At around 39 seconds, the thermal protection is turned on and at 44 seconds it tripped the motor from the grid.

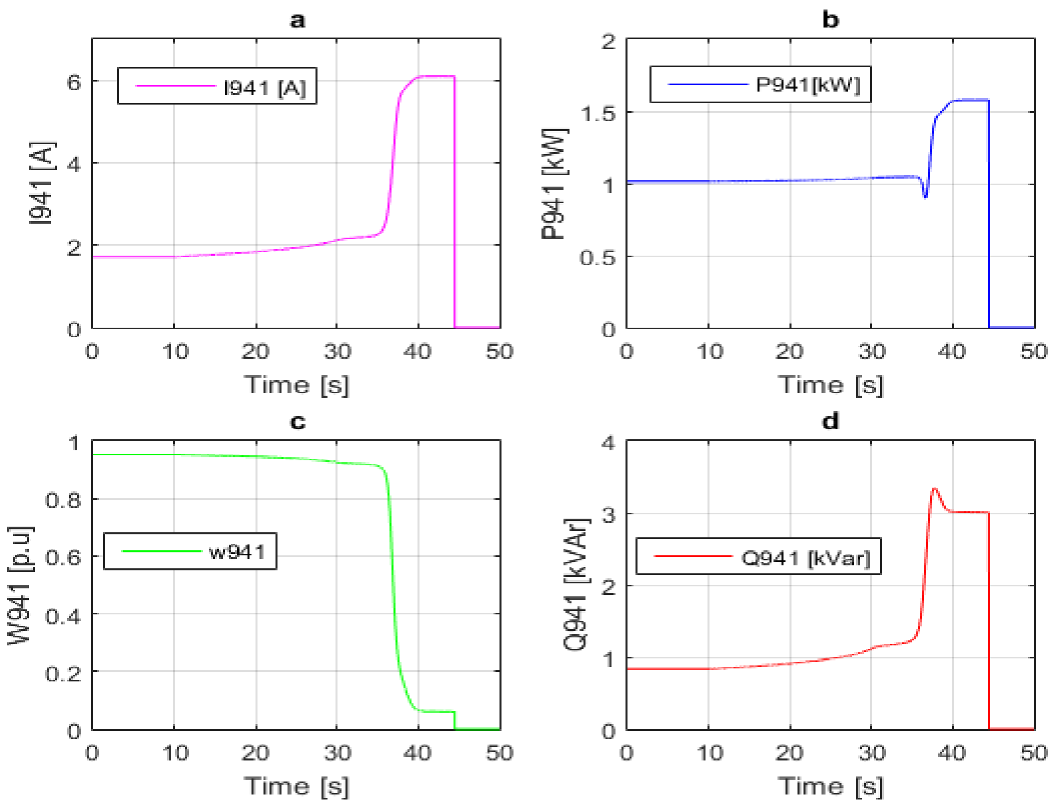

Figure 4.18: Induction motor parameters at bus B941

Figure 4.19 and Figure 4.20 show the transient behavior which occurred at the substation. As soon as the voltage at the secondary side of the transformer has crossed the lower limit deadband, the transformer relay was turned on (around 22 s) and the clock started to count. However, at around 44 seconds all of the induction motors have tripped, due to the action of the thermal relays protection. The voltage at the secondary side of the transformer recovers suddenly and violates the higher deadband limit. At around 45 seconds, the regulating transformer's relay is turned on again, and it changed the tap position until the voltage is brought within the imposed deadband (around 124 seconds).

As it can be seen in Figure 4.19 and Figure 4.20, the regulating device changed its tap position 6 times, from Tap=-3 to Tap=3 in order to bring the voltage value within the limits. In Figure 4.21, it can be seen the occurred transient behavior of some selected buses into the network due to the thermal protection action as well due to the regulating transformer action.

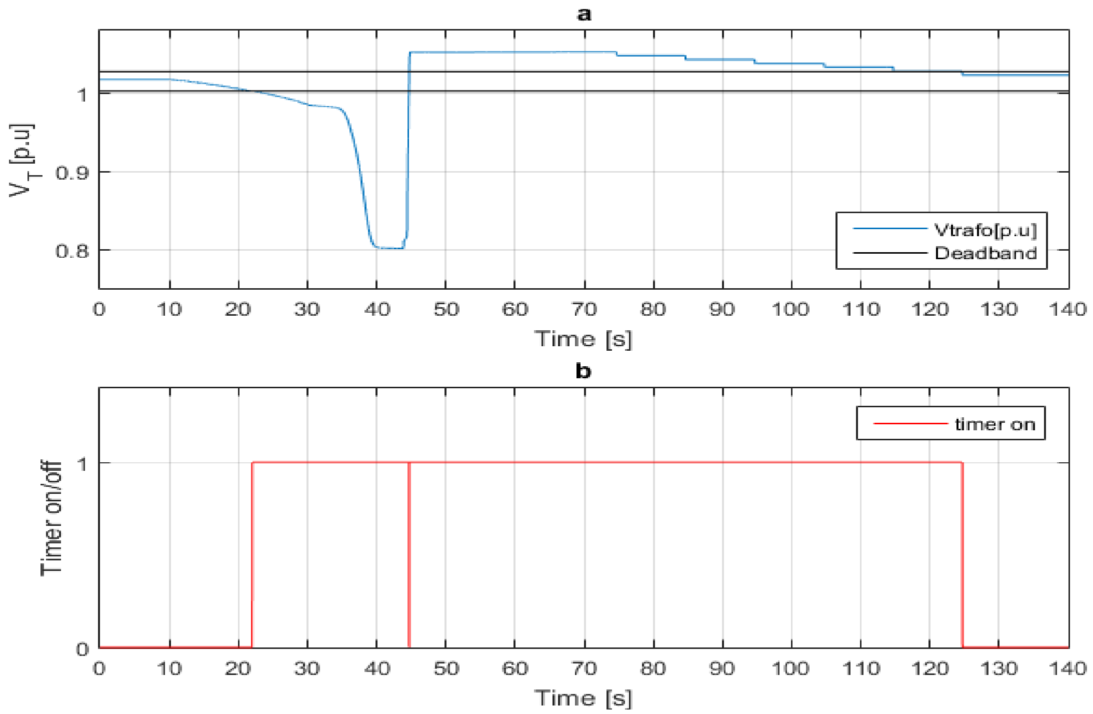

Figure 4.19: Regulating transformer's reaction for the <u>modified grid</u> with 50% PV integration and thermal protection implementation

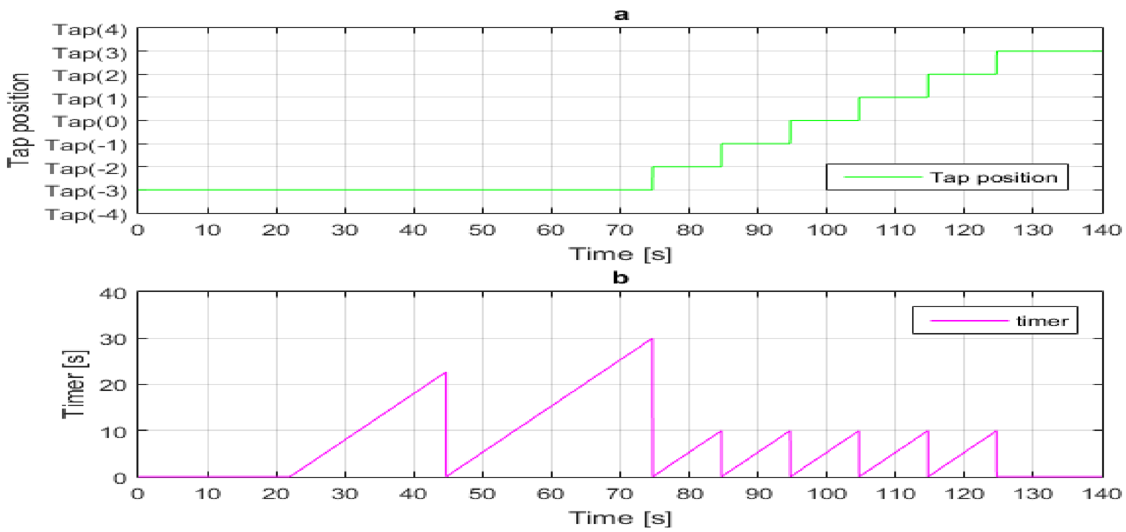

Figure 4.20: Regulating transformer's reaction for the <u>modified grid</u> with 50% PV integration and thermal protection implementation

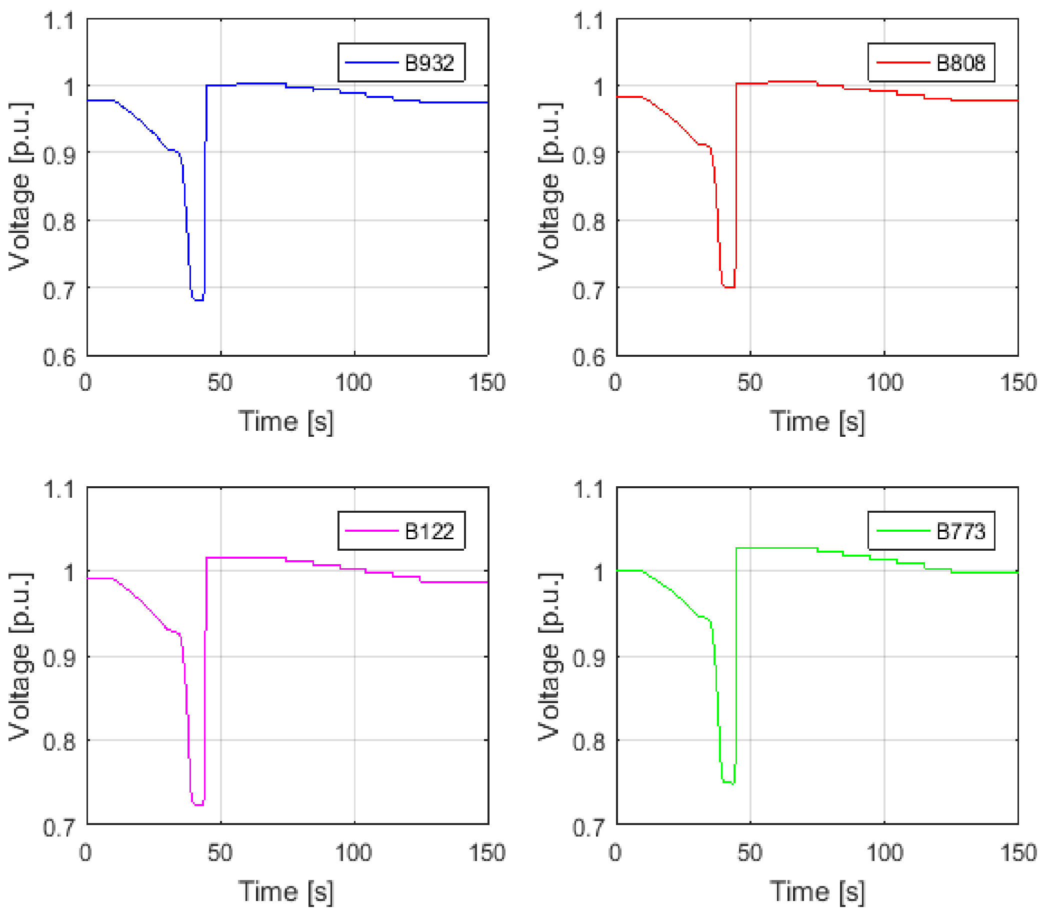

Figure 4.21: Sensitive bus voltages for 50% PV integration and thermal protection

4.2.7 Case with 50% PV penetration using Static Load Models (ZIP).

For the 50% PV penetration level, the voltage stability concern has been investigated by implementing detailed load models. However, if the static load models are being used, voltage instability cannot be identified. The static model comprised 70% constant power loads and 30% constant impedance load.

The simulation was conducted using the same characteristics as in the previous case: same PV disturbance, same PV penetration level and the same nominal load power. The Figure 4.22 shows the transient behavior which occurred at the substation. As it can be seen, the regulating transformer operated two times to bring the voltage level within the limits and therefore was able to maintain the system voltage stable.

As illustrated in Figure 4.23, before clouds began to cover the distribution grid (t=10s), the steady-state voltage level results were almost the same for both ZIP models and detailed dynamic models. However, in the case of ZIP model, after the clouds covered the entire grid, the lowest voltage value occurred was 0.91 p.u., and which after the regulating transformer action, was stepped to higher values.

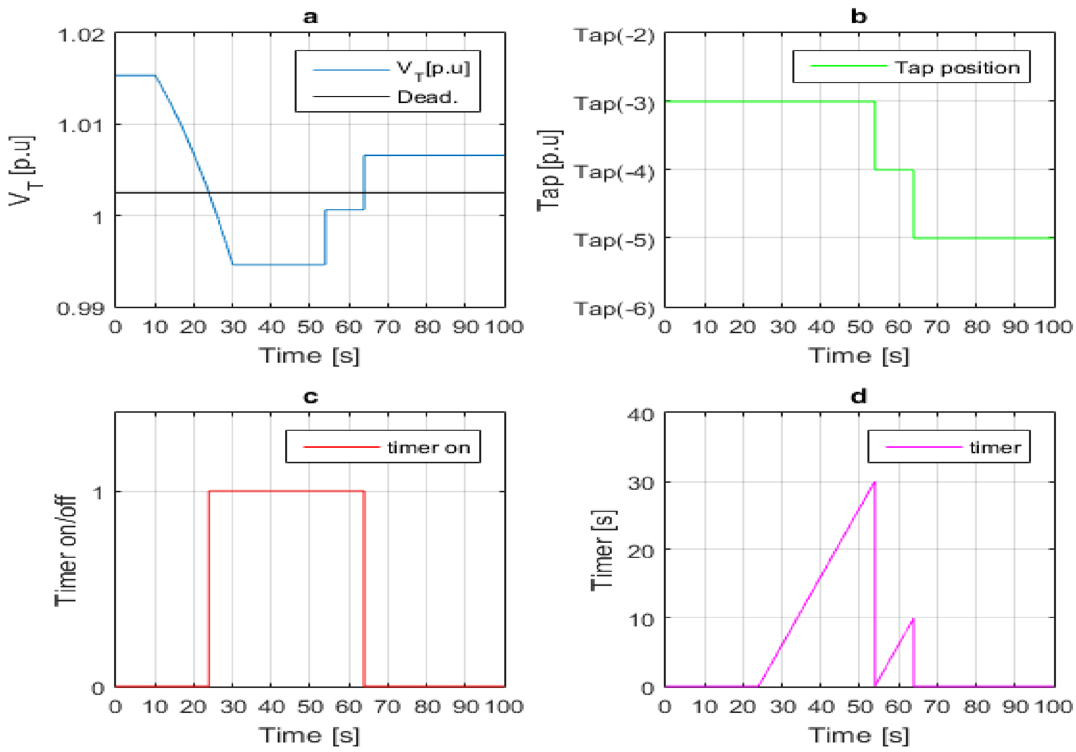

Figure 4.22: Regulating transformer's reaction for the <u>modified grid</u> with 50% PV integration using ZIP model

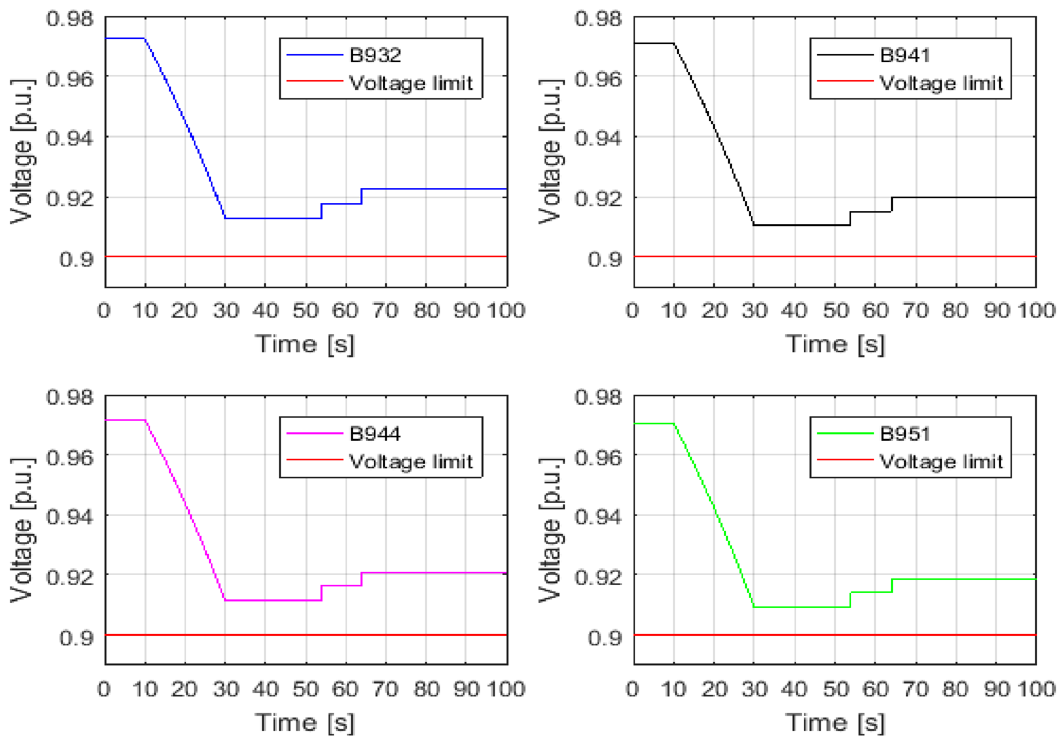

Figure 4.23: Sensitive bus voltages for 50% PV integration using ZIP model

It can be concluded that the ZIP model failed to give accurate results compared with the dynamic model and therefore no voltage instability occurred for the 50 % PV penetration level. This is mainly because of the implementation and the characteristics of the load models in the simulation during and after PV disturbance:

- In the case of ZIP models, during PV power drop, the consumed power will be reduced for constant impedance loads and no change will occur for constant power loads. In summary, the total power demand will decrease and to some extent, this alleviates the voltage drop phenomenon.
- In the case of the dynamic models, the response for constant impedance loads is the same as compared with the ZIP models. However, the constant power loads have different characteristics in this case. Thermostatic loads will start to recover slowly their pre-disturbance power causing additional voltage drops due to the higher demanded current. Induction motor loads are the driving factors which causes voltage instability. As the voltage level decreases due to the PV power drop, the induction motor power demand increases and causes additional voltage drop in the system. The extreme case is reached when the motor loads begin to stall. As illustrated in Figure 4.13, when the induction motor has stalled, its demand for reactive power has tripled and caused voltage instability in the grid.

4.3 Simulation summary

The simulations have shown that the real network was able to maintain its voltage stability when cloud induced power swings occurred in the network. The reasons behind this is that the real grid is designed to be a relatively strong grid, with high short-circuit capacity and short line branches which makes it invulnerable to PV power output fluctuations. In addition, the grid is operated under low load condition during the summer period.

However, if a potential different distribution grid, with lower short-circuit capacity and higher load condition is investigated, the grid might be voltage vulnerable to PV power fluctuations.

Therefore, in this study, the voltage stability was investigated for a relatively small modified residential grid with PV energy integration when the fast clouds covered the PV units. The cloud effect was simulated for different penetration levels until the network became voltage unstable. Dynamic and static load models for the residential houses were implemented and their differences were explained. The simulation results were summarized in Table 4.1 and the following observations were made:

- The network operated in the base case scenario (NO PV integration) without any voltage related problems.
- The network was able to still maintain voltage stability with 20-40% PV penetration levels when the fast moving clouds covered the residential area.
- For the 50% PV penetration level, the voltage stability could not be maintained under the same irradiation disturbance. Gradually, all the induction motors have stalled due to the occurred low voltage values before the voltage support action of the regulating transformer.
- The same problem could not be identified when the loads were modeled as static loads (ZIP model).

Table 4.1: Voltage Profiles with different PV Penetration Levels and Load Models

Load Model	Penetration level	Voltage status	Lowest Voltage Value (p.u.)		
			t=10s	t=30s	t=100s
Dynamic	0%	Stable	0.934	-	-
Dynamic	20%	Stable	0.954	0.924	0.935
Dynamic	30%	Stable	0.958	0.913	0.923
Dynamic	40%	Stable	0.967	0.909	0.926
Dynamic	50%	Unstable	0.976	0.903	0.676
Static	50%	Stable	0.98	0.91	0.931

5 MITIGATING SOLUTIONS

*This chapter proposes different mitigating solutions for improving the voltage stability of the system when cloud-induced power swings occur for the instable case scenario **(50 % PV integration**) in the modified network. SVC, D-STATCOM, ESD devices are implemented and simulated in the model. The potential differences between their operation and interaction with the network is analyzed and explained as well.*

5.1 Possible Counter-Measurements

Voltage instability for the modified network with 50 % PV integration has occurred mainly because of PV power fluctuations caused by the clouds' coverage of the PV systems. Referring to section 2.4 and 2.5, different mitigation solutions could be implemented in order to improve the voltage stability of the network with relatively large amount of solar PV integrated into the system. Among those, ESD, FACTS devices and reactive power support of the PV inverters could enhance the penetration level and therefore could be beneficial in terms of voltage stability of the network.

5.1.1 Energy Storage devices

One of the possible measurements to counteract voltage instability is to use energy storage devices (ESD). However, this is an expensive solution. Currently, a zinc-bromine flow battery unit with a capacity of 5 kVA-20kWh costs around 20000 AU$ [23], [28].
According with [23], [28] the optimal location of the ESD should be located in the close proximity of the loads. This is indeed the optimal location, since locating the energy storage devices closed to the loads will provide local energy support to the loads and less power will come from the upstream network. This will lead to less voltage drops in the network when clouds will start to cover the PV panels and the voltage profile will be improved. Two storage units of 12 and 14 KVA were modeled in the simulation. The location for the storage units was selected in the downstream part of the network, at busses SK0808 and SK2194.

5.1.2 FACTS Devices

Another solution is to use reactive power support from the FACTS devices as SVC and STATCOM. The reported price is roughly 50-55 US $/kVAr for small STATCOM units [23], so this might be a cheaper choice compared with the storage devices. This possible mitigating solution is however questionable regarding its efficiency since the distribution systems are characterized by high R/X ratio of the electrical lines. In other words, the injection or absorption of reactive power into the system in order to counteract the voltage deviations due to the cloud induced power swings of the PV units might not be beneficial from voltage stability point of view. Nevertheless, this possible solution should be investigated due to the lower purchasing and maintenance price of these devices and therefore it is integrated and simulated in the model.

The Neplan simulation tool [29] has the ability to determine the optimal capacitors placement into the network. The program proposes locations for the placement of shunt capacitors with the purpose of reducing the losses in the network. After performing this calculation, the bus SK2859 was found to be the optimal location for the installation of the SVC and the

STATCOM units. Both the SVC and STATCOM units were selected to have the same rating power of 35 kVA.

5.1.3 PV inverter reactive power support

The most economical solution is to use reactive power support from the PV inverters. This solution does not require any additional investment and is the most cost-beneficial. Currently, PV inverters are overdesigned and work at 80% of their rated capacity which makes room for reactive power support for the grid [23]. Moreover, in the case when the potential clouds could cover the PV arrays, the active power of the PV units will decrease, which in turn, it will increase substantially the capacity of reactive power support from the PV systems. As for the FACTS devices, the reactive power support of the PV inverters is questionable due to the high R/X ration of the electrical lines at the distribution level. Nevertheless, due to the overall distributed effect of the PV inverters, this countermeasure could be viable and it is economically attractive.

5.1.4 Implementation in Neplan

The SVC, STATCOM and ESD were integrated in the model to be simulated. Figure 5.1 shows the placement of the devices in the modified grid. The simulation tool is equipped with these devices (are integrated in the software's library) and the user has the ability to model and control their dynamic transient response. Their control systems were based on different blocks, different designing stages and different algorithms which allowed the user to investigate their transient response. The controlled algorithm of these devices was based on d-q synchronous coordination system. By using a d-q coordination system, the active and the reactive power transient response of these devices were independently achieved. This is a major feature of a d-q control algorithm.

5.2 SVC

As explained in section 2.4.1, the purpose of the SVC regulator is to maintain a referenced voltage at the PCC. This is achieved by continuous changing of the SVC's shunt susceptance. The reference voltage for the SVC unit was selected to be 0.98 p.u and the coefficients for the PI controller were set to K_p=100 for the proportional part and K_i=10 for the integrator part.

As can be seen in the figure 5.2 and 5.3, in the interval between 0 and 10 s, the network operated in the steady-state mode and the SVC was not activated. But as soon as the clouds started to cover the network, at around 10 s, voltage drops occurred in the network. The control circuit of the SVC unit, as explained in section 2.4.1, did sense a voltage error and therefore sent the optimal signals to the TCR and TSC to change the total susceptance of the unit in order to maintain the targeted voltage value.

Thereby, between 10-16 s, the SVC unit became an adjustable capacitor and injected reactive power into the network. However, as soon as the unit hit its limits, the voltage control was lost and the SVC became only a fixed capacitor. The capacitor current injected into the grid after the SVC hit its limits, as can be seen in the figure 5.3.d, started to decrease pointing out the drawbacks of the SVC units compared with the STATCOM devices.

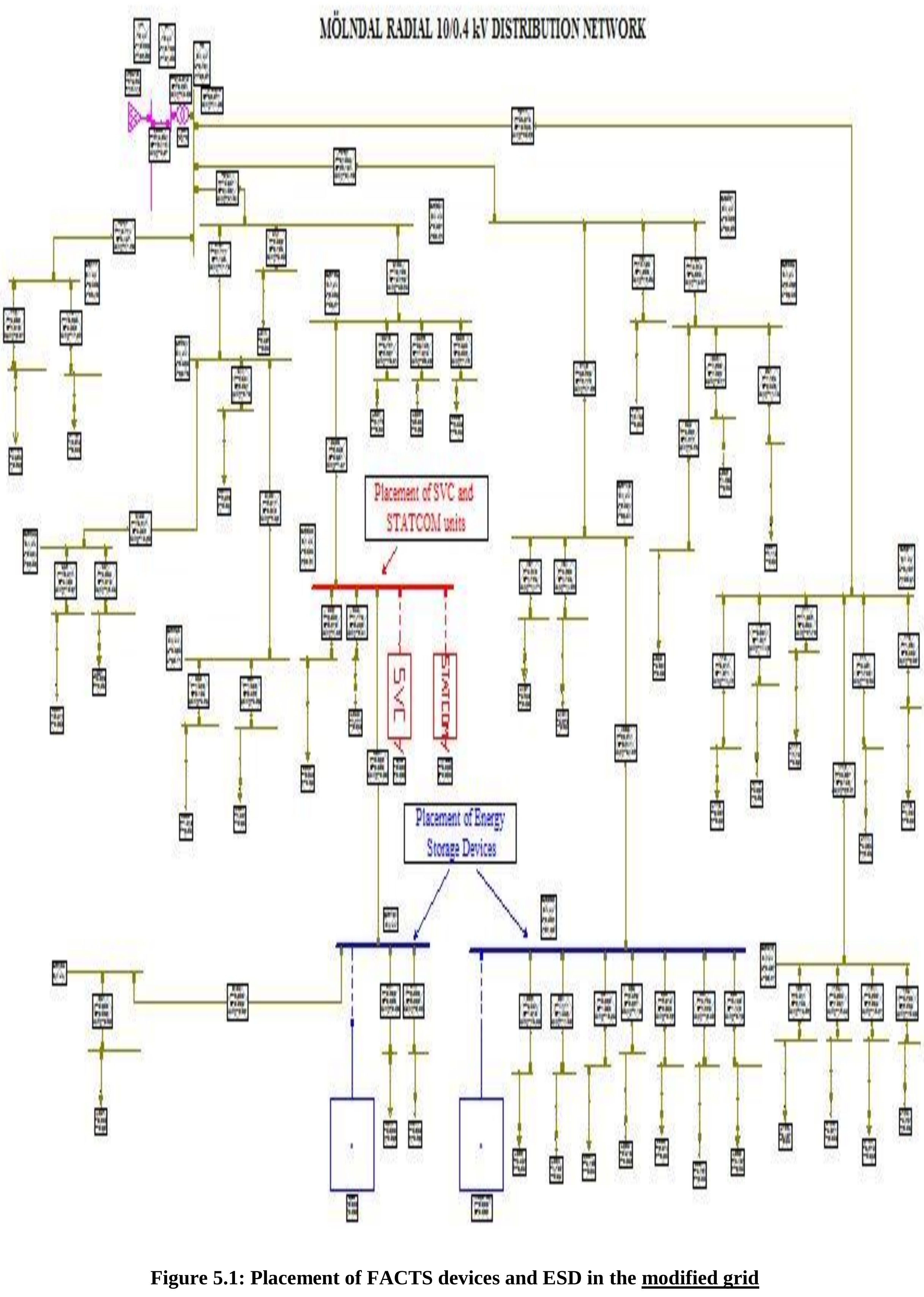

Figure 5.1: Placement of FACTS devices and ESD in the modified grid

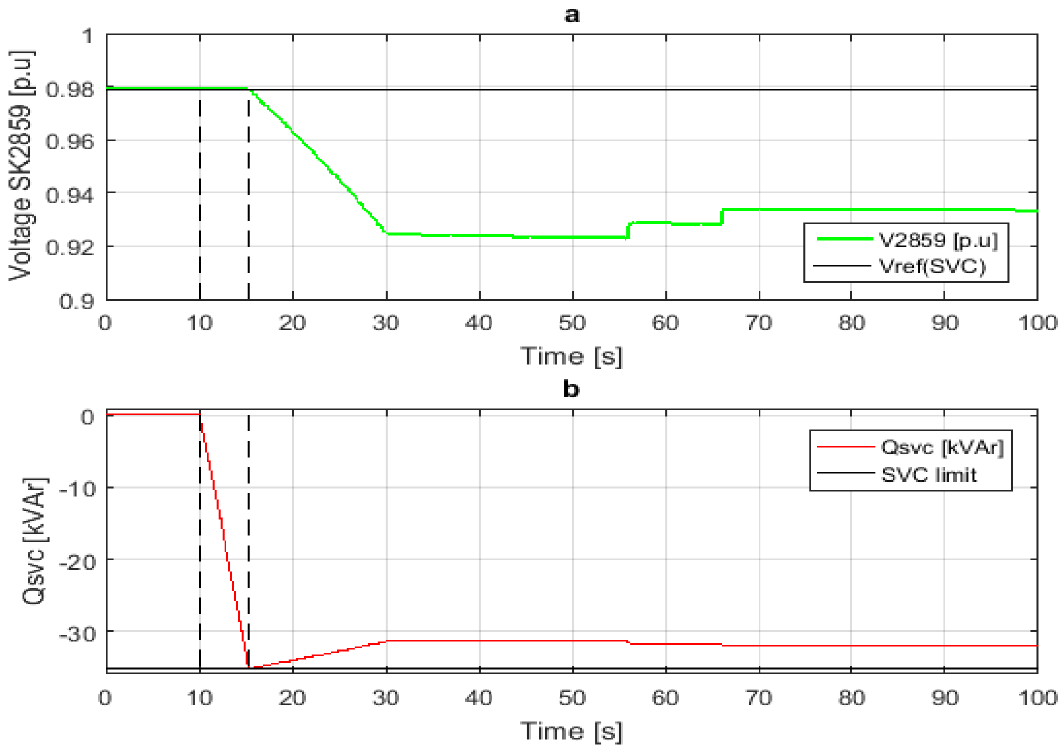

Figure 5.2: Voltage (a) and reactive power (b) of the SVC unit at bus SK2859

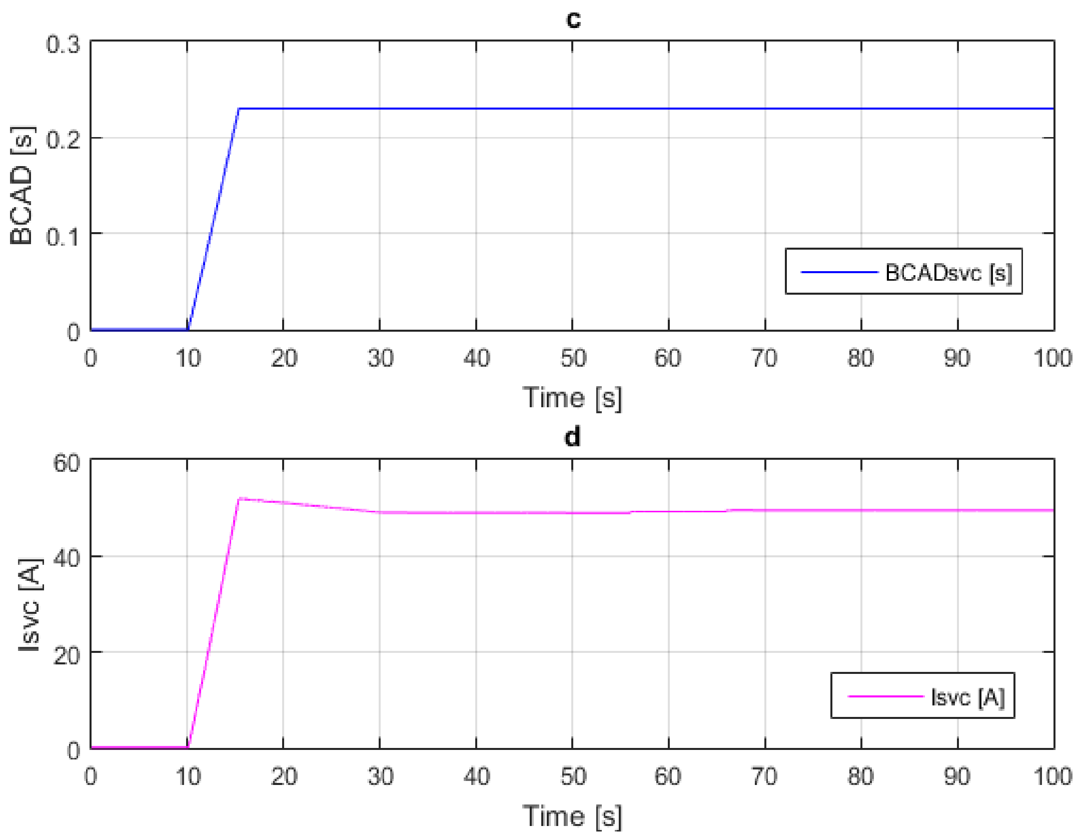

Figure 5.3: Susceptance (c) and Current (d) of the SVC unit at bus SK2859

Since PV power production works at the unity power factor, the voltage drop is due to the loss of active power from the PV generation systems into the grid. As the investigated network has higher R/X ratio implies that more reactive power has to be injected at the controlled node of the SVC unit in order to counteract the loss of active power and to maintain a stable voltage value.

However, as soon as the SVC unit starts to inject reactive power at the bus SK2859, the voltage at the secondary side of the transformer started to increase (Figure 5.4). This can be explained as the transformer has a very high X/R ratio (around 4.5) and it is more sensitive to reactive power than active power flowing through it. In other words, the decrease of reactive power through the regulating transformer (due to the action of the SVC) is more pronounced than the increase of active power flow (due to the loss of PV generation) through the transformer and the voltage at the secondary side had to increase.

As soon as the SVC lost its control, the voltage at the secondary side of the regulating device started to decrease and eventually crossed the deadband (around 28 s) and energized the timer. The tap changer performed two times in order to bring the targeted voltage within the imposed deadband.

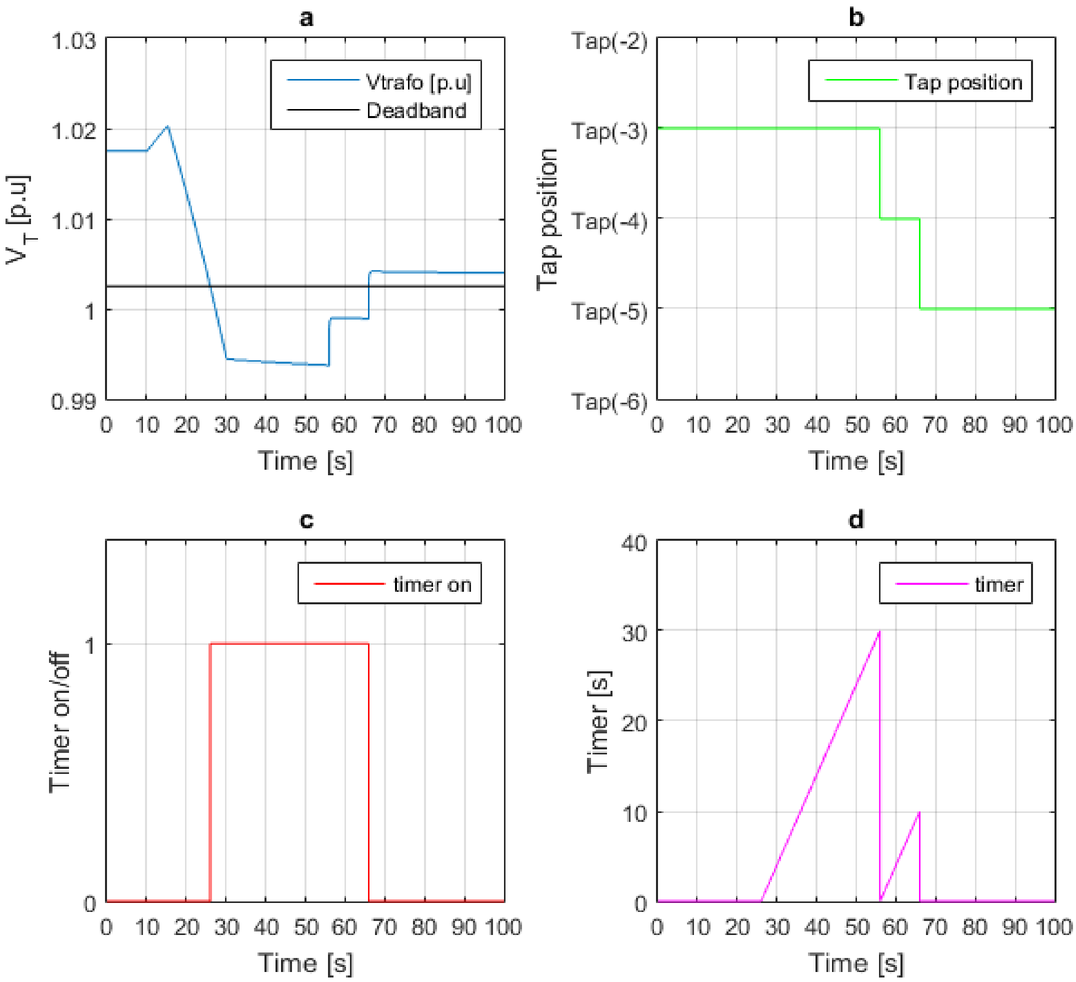

Figure 5.4: Regulating transformer's reaction for 50% PV integration and SVC unit at bus SK2859

Figure 5.5 shows the transient behavior, after the combined effect of PV power loss and SVC reactive power support, at some of the most sensitive busses of the network. The lowest voltage value occurred was 0.92. However, the action taken by the regulating transformer stepped the voltages to higher values and the system was voltage stable.

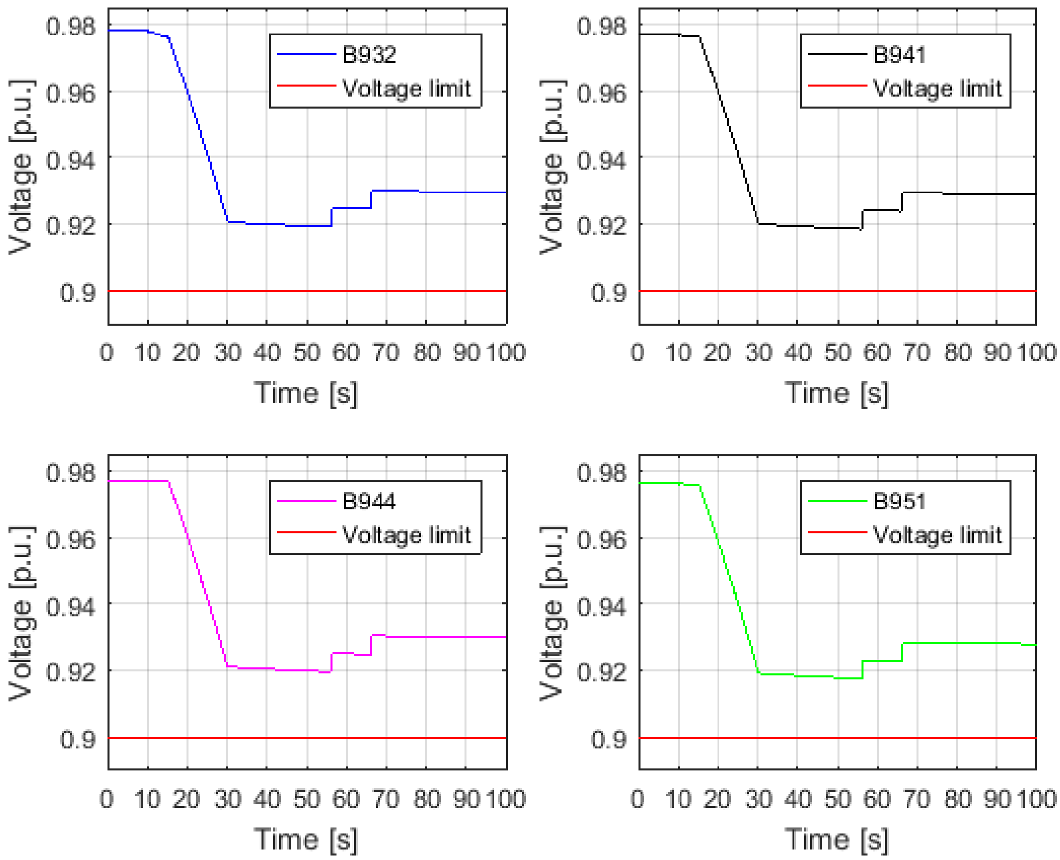

Figure 5.5: Selected system's bus voltages for 50% PV and SVC unit at bus SK2859

5.3 STATCOM&reactive power support of PV inverters

STATCOM devices have the same purpose as the SVC units in that they inject the required reactive power at the PCC in order to maintain the controlled voltage at the desired level. The main difference is that their principle of operation is based on the voltage source inverter which provides a circulating path of the currents to flow through the inductances of the electrical lines. Based on the signs of the injected currents (lagging or leading the voltage at the PCC), the STATCOM units are able to operate in both reactive and capacitive range.

Due to the fact that STATCOM's operation is based on voltage commutated inverter, its principle of operation is very similar of that of a PV inverter. The main difference is that, STATCOM devices are not always equipped with storage devices and therefore, they are able to inject only reactive power into the grid.

Due to the similarities in their operation, the STATCOM device connected at bus SK2859 has been roughly modeled as a potential reactive power support from the PV inverters. The mainly drawback of this approach is that it doesn't inject and prioritize the active power as is the case of a PV inverter. Moreover, the potential reactive power support from the PV inverters was concentrated at one single location in the network which is not the case for real PV inverters (which are distributed across the network). Nevertheless, this approach gives an insight of how the potential reactive power support from the PV inverters is achieved.

The control system, as explained in section 2.4.2, is based on d-q synchronous coordination system. The reference imaginary part of the STATCOM current depends on the grid voltage at the PCC (Figure 5.6) while the real part current depends on the dc power from PV arrays which charges the dc capacitor of the PV generation system.

Therefore, the approach used in this case is based that the reactive power provided by the inverter, is gradually released based on the grid voltages at the PCC. As can be seen in Figure 5.6, the injected current by the STATCOM unit is based on the values of the grid voltage at the PCC.

Therefore, if the voltage at PCC reaches the value of 0.97 and continue to decrease until 0.95, capacitive current is gradually injected by the STATCOM unit. As the voltage at the PCC continues to decrease below 0.95, STATCOM operates fully in the capacitive mode and injects its maximum current. Contrary, when the voltage at the PCC reaches the value of 1.02 and continues to increase to 1.04, reactive current is gradually absorbed from the grid. As the voltage continues to increase above 1.04, STATCOM operates in fully reactive mode and absorbs its maximum current.

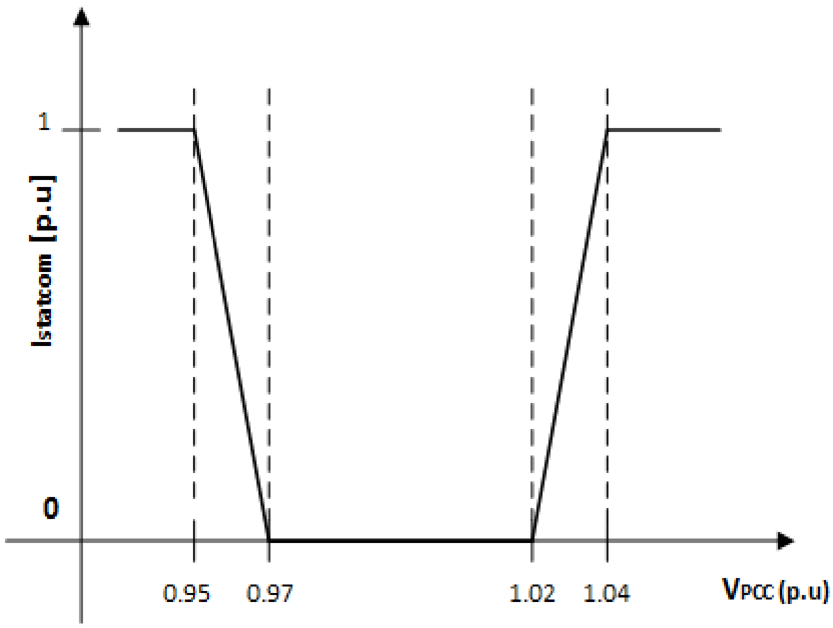

Figure 5.6: Imaginary part of the current as a function of the voltage for STATCOM control

Figure 5.7 shows the simulation results when the developed control strategy is implemented of the STATCOM unit at the bus SK2859. At 10 s, the clouds disturbed the system and the voltage at PCC started to decrease. When it reaches the value of 0.97 p.u (around 13s), reactive power support from the inverter is gradually injected into the grid until it reaches the value of 0.95 (at around 24 s). At this value, the STATCOM hits its power limits and the voltage control is lost.

As can be seen in the figure 5.7.c, the STATCOM has a better dynamic performance compared with the SVC in that, its reactive injected current is not dependent on the value of the voltage at the PCC and remains constant after the SVC hits it limits. This implies that, more reactive power is injected by the STATCOM compared with the SVC for the same ratings.

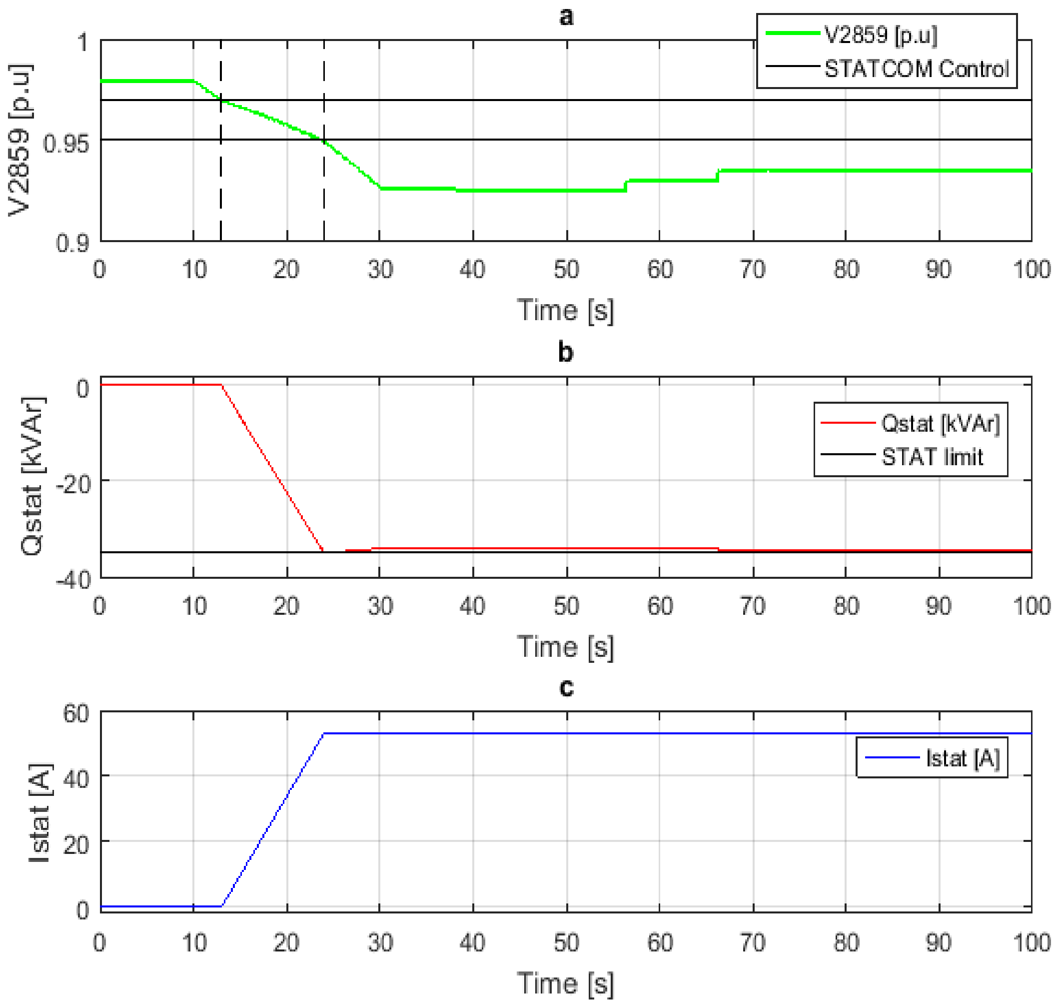

Figure 5.7: STATCOM: Voltage (a), Power (b), Current (c) at bus SK2859

As soon as the STATCOM unit began to inject reactive power into the grid (between 13 and 24 s), the drop rate of the voltage at the secondary side of the regulating transformer was ameliorated (Figure 5.8.a.) and voltage drop for the entire grid was improved. At around 27 s the regulating transformer started to count and performed thereafter two tap operations until the voltage was brought back within the limits.

The lowest voltage after the compensated effect of PV power drop and the action of the STATCOM unit was 0.92. After the operation of the regulating transformer, the voltage level of the entire system is improved, and the voltage level of the investigated busses is raised up as can be seen in the Figure 5.9.

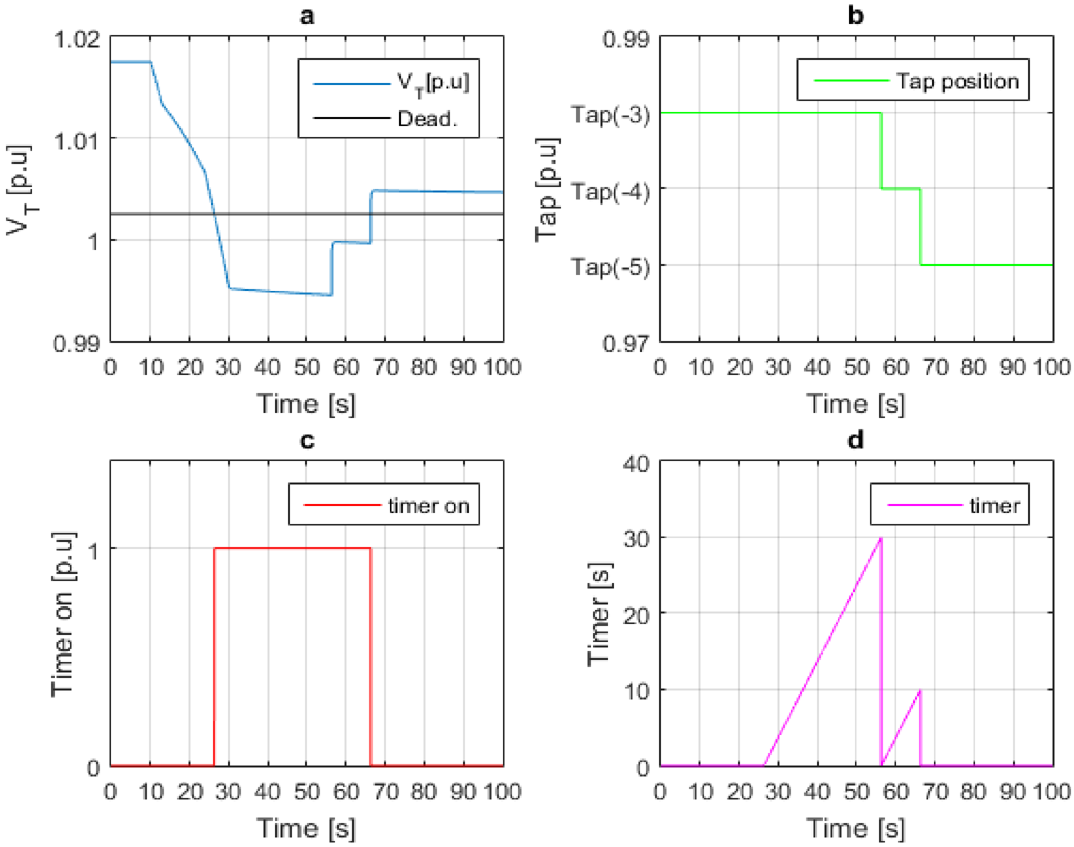

Figure 5.8: Regulating transformer's reaction for 50% PV and STATCOM unit at bus SK2859

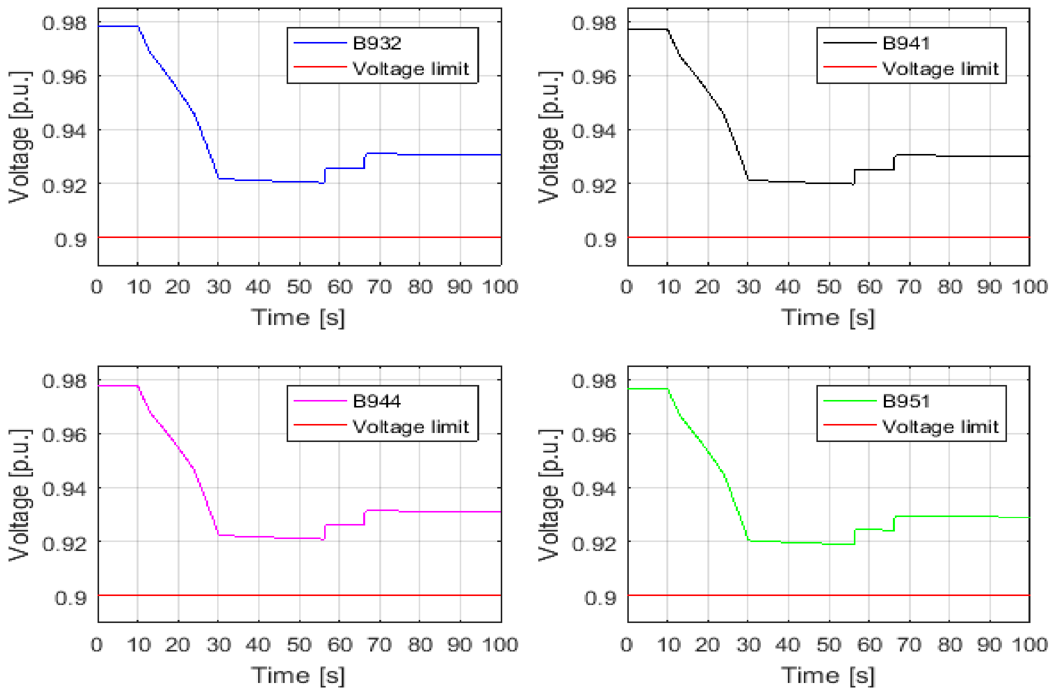

Figure 5.9: Selected system's bus voltages for 50% PV and STACOM unit at bus SK2859

5.4 Energy Storage Devices (ESD)

Energy storage devices operate in the same manner as a PV generation system. The only difference is that they are equipped with batteries instead of PV arrays. Due to the fact that they incorporate an inverter, they are able to inject both active and reactive power into the grid. However, in this study, only active power injection was analyzed. The control system, as in the STATCOM case, is implemented in d-q synchronous coordination system. Based on the grid voltage value at the PCC, the reference real part of the ESD current is calculated and optimal signals are sent to the VSI.

For voltage stability concerns, the energy storage devices are controlled in such a way that they discharge when the grid voltage goes bellow a threshold voltage value and charge when the grid voltage goes above a certain voltage value. Between these two stages, there is a deadband in which no operation is performed. For frequency concerns, the control system might differ.

Therefore, in this study, the control system was implemented that the storage devices are injecting active power if the voltage goes between 0.95 and 0.93 p.u as it can be seen in Figure 5.10. This control system was based on the fact that the discharge/charge rate of the batteries affect strongly their life cycle duration. Currently, Li-ion batteries have a service cycle of 10000 cycles [38]. Therefore, if the voltage level goes below 0.95, energy storage devices will start gradually to inject active power into the grid and will reach its maximum/rated at 0.93 p.u.

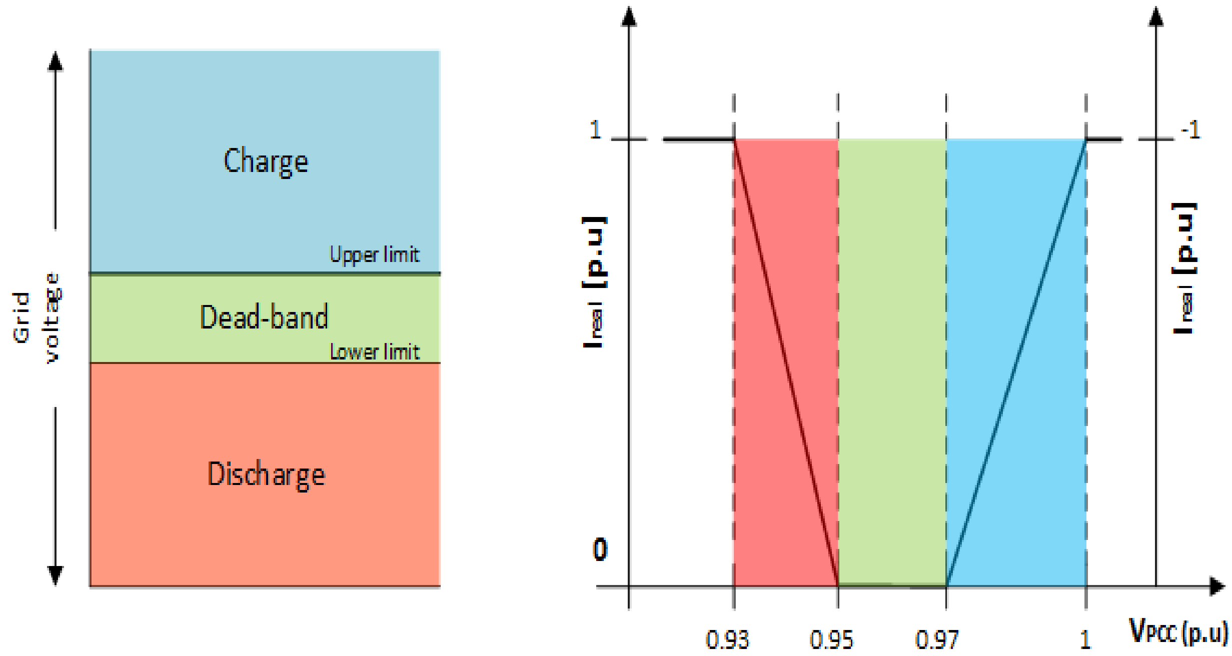

Figure 5.10: ESD charging/discharging control as function of grid voltage

As can be seen in Figure 5.11 and Figure 5.12, as soon as the controlled node voltages at bus SK0808 and Sk2194 reaches the values of 0.95, the energy storage devices start to inject active power into the network which alleviates the drop rate of the voltage and improve the voltage stability of the entire grid.

Worth mentioning here is that, the storage unit located at the bus SK2194 hit its power rating when clouds covered the network and therefore, the voltage control was lost (Figure 5.11). As for the storage unit located at the bus SK0808, the unit was still able to control the voltage range, nevertheless, at the limit (Figure 5.12).

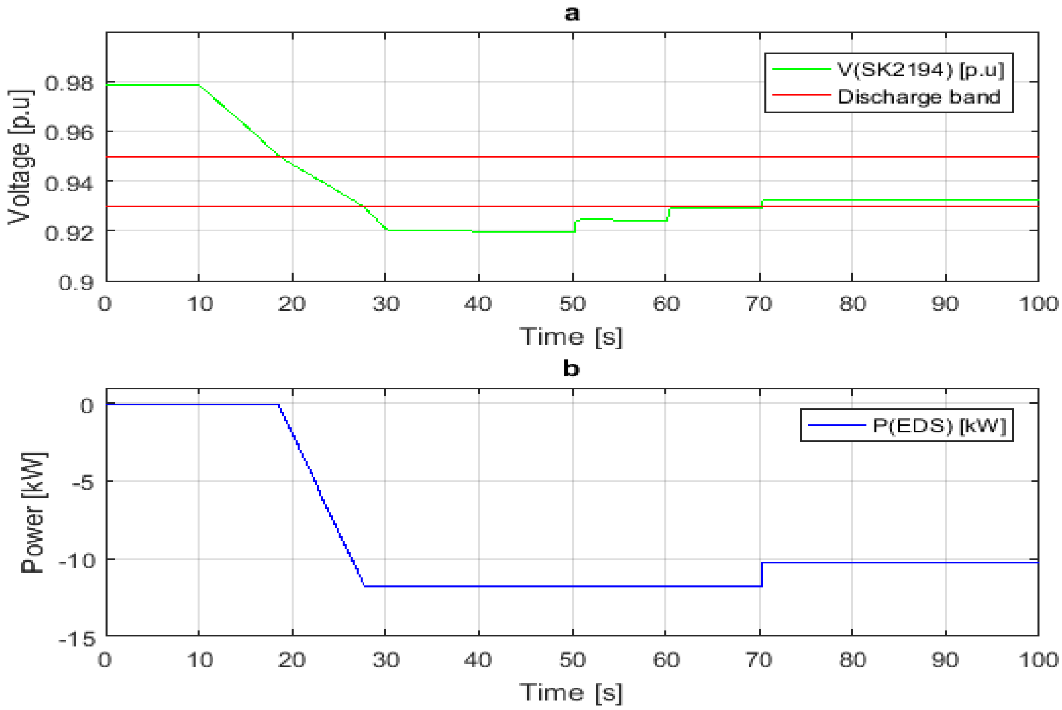

Figure 5.11: Storage device at bus SK2194: Voltage SK2194 (a) and Power SK2194 (b)

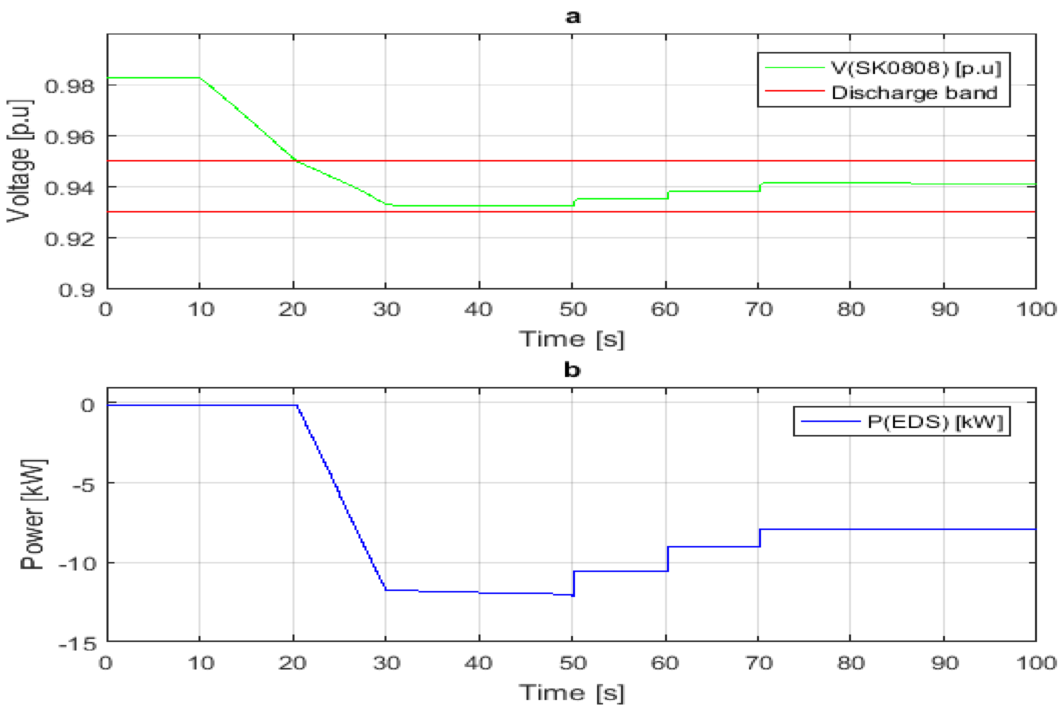

Figure 5.12. Storage devices at bus SK0808: Voltage SK0808 (a) and Power SK0808 (b

Due to the integration of the storage devices into the network, the voltage drop rate at the secondary side of the transformer was improved. As can be seen in Figure 5.13, the transformer operated 3 times in order to bring the voltage within the imposed range.

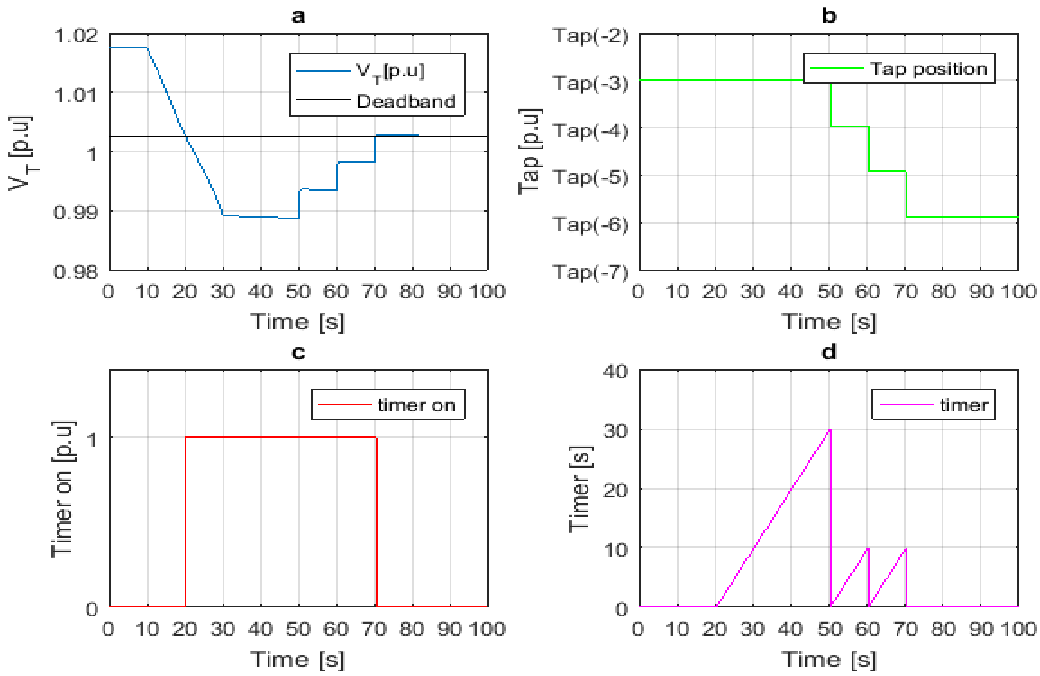

Figure 5.13: Regulating transformer's reaction for 50% PV integration and ESD

Figure 5.14 show the voltage profiles of the investigated busses. The lowest voltage level reached after the disturbance was as 0.917 pu. However, the regulating transformer action raises the voltage levels to higher values and better system performance is obtained.

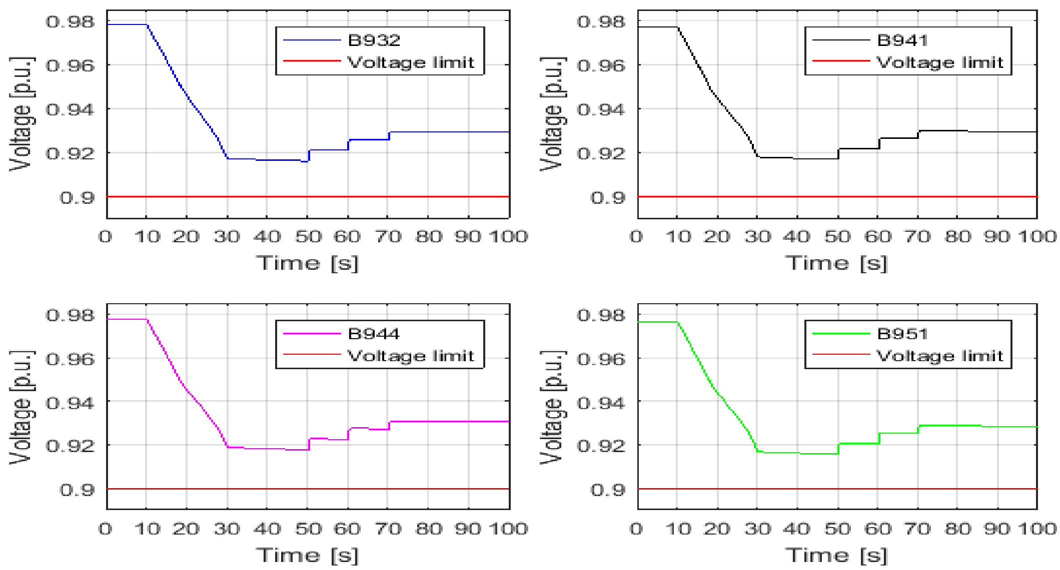

Figure 5.14: Selected system's bus voltages for 50% PV integration and ESD

5.5 Simulations summary

Different mitigating solutions for the voltage instable case scenario (50% PV integration) were proposed and implemented. Their dynamic impact with the system when cloud induced power swings occurred in the network was investigated. The simulations results were summarized in Table 5.1 and the following observations were made:

- The SVC unit was able to maintain the voltage stability of the system. However, correlation between the device and the regulating transformer has to be investigated properly;
- The STATCOM unit was modeled roughly as a potential reactive power support from the PV inverters. It was found that the device was able to maintain the voltage stability of the grid and its dynamic behavior was superior to SVC case;
- ESD were also found to maintain the voltage stability of the network. This is the most efficient method to counteract the PV power fluctuations. However, their high purchasing and maintenance cost make this solution to be economically expensive.

Table 5.1: Voltage status with 50% PV and mitigating devices as function of time

Load Model	**Penetration level**	**Voltage status**	**Lowest Voltage Value (p.u.)**		
			t=10s	**t=30s**	**t=100s**
Dynamic	50% PV+ SVC	Stable	0.977	0.919	0.9284
Dynamic	50% PV+D-STATCOM	Stable	0.977	0.92	0.9295
Dynamic	50%PV+ESD	Stable	0.977	0.917	0.9264

6 CONCLUSIONS AND FUTURE WORK

This chapter presents the conclusion of the conducted work and it proposes different issues/tasks that can be done in the future in order to assess further the impact of integrating renewable resources as PV energy into the distribution grids.

6.1 Conclusions

In this thesis, the voltage stability concern of a distribution network when different PV penetration levels were integrated has been investigated. The voltage stability of the system was analyzed when cloud induced power swings of the PV units occurred in the network. The following conclusions can be made:

1. The residential network located in Mölndal area (the real network) was able to maintain its voltage stability without any concerns when cloud induced power swings occurred in the grid for different penetration levels. However, for the modified grid, the voltage instability occurred with 50% PV power integration. The voltage instability has occurred due to both, extra power flowing from the upstream network (which caused voltage drops within the network) as well due to the longer time delay for the first tap operation of the regulating transformer.

2. For the modified grid with 50% PV power integration, the cloud induced power swings caused voltage instability when the loads were modeled as dynamic loads. This issue has not been properly identified when the loads were modeled as static loads (ZIP model). Therefore, detailed dynamic load models are recommended for further PV integration studies especially when the load composition is predominantly induction motor load.

3. Different mitigation solutions were proposed and implemented for the modified grid with 50% PV power integration. ESD, SVC and STATCOM devices were able to improve the voltage stability of the system. ESD were found to be the most efficient and reliable measures to counteract the PV power loss of the PV units. However, due to the very high costs associated with these devices, alternative solutions as SVC and STATCOM were implemented and analyzed as well. The SVC countermeasure was found to be beneficial for voltage stability concerns. However, the correlation between the regulating transformer and the size of the SVC unit has to be achieved for proper and efficient operation of the system. The STATCOM solution has been modeled roughly as a possible reactive power support from the PV inverters. The method was found effective in reducing the rate of voltage drop and thereby improving the voltage stability limits of the system.

6.2 Future Work

This thesis attempted to analyze the voltage stability concerns in a distribution grid with PV energy integration when fluctuations in the irradiance levels occurred. Additional work that could be further examined include:

1. To model the entire PV generation system in appropriate softwares such as MATLAB and PSCAD. The user can have access to higher information level and can get better insights on the working principle and the involved dynamics inside the inverter. However, this is a tenacious task.

2. To investigate the impacts of the PV energy integration on power quality.
3. To coordinate the potential reactive power support from the PV inverters or/and FACTS devices and the regulating transformer's tap operation during a longer period (e.g., one year) in order to find a suitable balance between system losses and frequency of the tap operations.

REFERENCES

[1] PV Grid,*''Final Project Report''*, August 2014, available at: http://www.pvgrid.eu

[2] J. Kleissl, M. Lave, M. Jamaly, J. L. Bosch, ''*Aggregate Solar Variability*'', Power and Energy Society General Meeting, 22-26 July, 2012.

[3] IEA PVPS Task 14, Subtask 1.3, *''Characterization of the Spatio-Temporal Variations and Ramp Rates of Solar Radiation and PV''*, August 2015.

[4] David Lingfors,*''Solar Variability Assessment and Grid Integration: Methodology Development and Case Studies''*, Licentiate Thesis, Uppsala Universitet, 2015.

[5] M. Paulescu, E. Paulescu, P. Gravila and V. Badescu, ''*Weather Modeling and Forecasting of PV Systems Operation''*, London: Springer-Verlag, 2013.

[6] Solstrålning,*''Sveriges Meteorologiska och Hydrologiska Institut''*, Faktablad Nr. 31, april 2007.

[7] J. Stein, M. J. Reno, C. W. Hansen, *''The Variability Index: A New and Novel Metric for Quantifying Irradiance and PV Output Variability''*, May 14, 2012 Denver, CO.

[8] T. Hoff, R. Perez, *''Quantifying PV Power Output Variability''*, Solar energy, Vol. 84, Nr. 10, October 2010, Pages 1782–1793.

[9] N. Mohammad, M. Quamruzzaman, M. R. T. Hossain, M. R. Alam,''*Parasitic Effects on the Performance of DC-DC Sepic in PV Maximum Power Point Tracking Applications*'', Scientific Research, Smart Grid and Renewable Energy, Vol. 4, Pages 113-121, 2013.

[10] J. Xue, Z. Yin, B. Wu, J. Peng, *''Design of PV Array Model Based On EMTDC/PSCAD*'', Power and Energy Engineering Conference, March 2009.

[11] Nicola M. Pearsall and Robert Hill, Chapter 15, *''Photovoltaic Modules, Systems and Applications''*, Hill and Pearsall edMA3.doc, April 2001.

[12] S. Bhattacharjeea, B. J. Saharia, *''A comparative study on converter topologies for maximum power point tracking application in photovoltaic generation''*, Journal of Renewable and Sustainable Energy, Vol. 6, 053140, pages 1-7, 2014.

[13] F. Iov, F. Blaabjerg, *''Advanced Power Converters for Universal and Flexible Power Management in Future Electricity Network*'', UNIFLEX-PM, 2007.

[14] C. W. Taylor ''*Power System Voltage Stability*'', McGraw-Hill, INC., 1994.

[15] P. Kundur, ''*Power System Stability and Control''*, McGraw-Hill, Inc., 1994 Edition.

[16] T. V. Cutsem, C. Vournas *''Voltage Stability of Electric Power Systems''*, Kluwer Academic Publishers, 1998.

[17] I. R. Navarro, ''*Dynamic Load Models for Power Systems: Estimation of Time-Varying Parameters During Normal Operation*'', Licentiate Thesis, 2002, Lund University.

[18] George K. Stefopoulos, A. P. Meliopoulos ''*Induction Motor Load Dynamics: Impact on Voltage Recovery Phenomena*'', Transmission and Distribution Conference and Exhibition, 21-24 May 2006.

[19] N. G. Hingorani, L. Gyugyi, *''Understanding FACTS: Concepts and Technology of Flexible AC Transmission Systems''*, IEEE Press, 2000.

[20] M. M. Begovici, I. Kim, D. Novosel, J. R. Aguero, A. Rohatgi, *''Integration of Photovoltaic Distributed Generation in the Power Distribution Grid*'', 45th Hawaii International Conference on System Sciences, 4-7 January 2012.

[21] Y. T. Yan, D. Kirschen, *''Impact on the Power System of a Large Penetration of Photovoltaic Generation*'', IEEE Power Engineering Society General Meeting, 2007.

[22] Yan, S. Roediger and T. K. Saha, *''Impact of Photovoltaic Power Fluctuations by Moving Clouds on Network Voltage: A Case Study of an Urban Network*'', Power Engineering Conference (AUPEC), 21st Australasian Universities, 25-28 Sept. 2011.

[23] R. Yan, T. K. Saha, ''*Investigation of voltage stability for residential customers due to high Photovoltaic penetrations*'', IEEE paper, Vol. 27, Nr. 2, Pages 651 – 662, May 2012.

[24] R. Yan, T. K. Saha, *''Investigation of Voltage Variations in Unbalanced Distribution Systems due to High Photovoltaic Penetrations*'', Power and Energy Society General Meeting, 24-29 July 2011.

[25] M. M. Aggarwal, S. K. Gupta and G. Kasal, *''D-STATCOM control in Low Voltage Distribution System with Distributed Generation''*, Third International Conference on Emerging Trends in Engineering and Technology, 19-21 Nov. 2010.

[26] R. Yan, B. Marais, T. K. Saha,'' *Impacts of residential photovoltaic power fluctuation on on-load tapchanger operation and a solution using DSTATCOM*'', Electric Power Systems Research, Vol. 111, Pages 185-193, 2014.

[27] B. B. Zad, J. Lobry and F. Vallee, *''Coordinated Control of On-Load Tap Changer and D-STATCOM for Voltage Regulation of Radial Distribution Systems with DG Units*'', 3rd International Conference on Electric Power and Energy Conversion Systems, Yildiz Technical University, Istanbul, Turkey, 2-4 October, 2013.

[28] M. Zillmann, R. Yan and T. K. Saha,*''Regulation of distribution network voltage using dispersed battery storage systems: A case study of a rural network''*, Power and Energy Society General Meeting, 24-29 July 2011.

[29] NEPLAN AG,"*NEPLAN Software Help Topics User Manual*", Switzerland 2014.

[30] P. Balram, T. Le, O. Carlson, *''Predictive voltage control of batteries and tap changers in distribution system with photovoltaics*'', Power Systems Computation Conference, 2016.

[31] European Standard EN50160 *''Voltage Characteristics of Electricity Supplied by Public Distribution Networks*'', 2007.

[32] E. Mulenga,’’Impacts of Integrating Solar PV Power to an Existing Grid: *Case Studies of Mölndal and Orust Energy Distribution (10/0.4 and 130/10 kV) grids*’’, Master Thesis, Chalmers University of Technology, 2015.

[33] I. Vassileva, *’’Characterization of Household Energy Consumption in Sweden: Energy Savings Potential and Feedback Approaches’’*, Mälardalen University Press Dissertations, No. 129, 2012.

[34] A. Green, K. Ellegård, *’’Consumer behavior in Swedish households: routines and habits in everyday life’’*, Swedish Energy Agency.

[35] K. Linden, I. Segerqvist,’’*Modelling of Load Devices and Studying Load/System Characteristics*’’, Technical report No. 131L, Chalmers University of Technology, 1992.

[36] J. P. Zimmermann,’’*End-use mettering campaign in 400 households in Sweden. Assesment of the potential Electricity savings*’’, Swedish Energy Agency, Sept. 2009.

[37] IEEE Task Force, ’’*Load Representation for Dynamic Performance Analysis*’’, IEEE Transactions on Power Systems, Vol.8, Nr.2, May 1993.

[38] R. S. Meena., ’’*Battery energy storage system in solar power generation*’’, Chapter 4, Jan. 3, 2013.

Appendix1: Cable Data

Nr.	From	To	R_0 [ohm/km]	X_0 [ohm/km]	Length [m]
1	AT0519	T1	0.125	0.0732	760
2	T2	L1743	0.641	0.085	215
3	L1743	SK2477	1.15	0.085	7
4	T2	SK2034	0.206	0.0723	168
5	SK0321	SK2148	0.493	0.075	85
6	SK2255	55-1	1.83	0.088	20
7	SK2255	55-2	0.32	0.075	14
8	SK2195	95-1	1.1	0.084	80
9	SK0808	08-1	1.83	0.088	14
10	SK2811	11-1	1.15	0.079	89
11	SK0321	21-5	0.32	0.082	93
12	SK2477	77-3	1.2	0.091	61
13	SK2034	SK2193	0.206	0.0723	135
14	SK2254	SK2256	0.206	0.0723	200
15	SK2034	SK2254	0.206	0.0723	133
16	SK2254	SK2255	0.206	0.0723	80
17	Sk2194	SK2195	0.206	0.0723	120
18	T2	SK0321	0.206	0.0723	140
19	SK2193	SK2859	0.206	0.0723	102
20	SK2859	SK2194	0.206	0.0723	83
21	T2	SK2811	0.125	0.0732	84
22	SK0808	08-7	1.83	0.088	84
23	SK0808	08-4	1.83	0.0817	53
24	SK0808	08-6	1.83	0.088	61
25	SK0808	08-5	1.83	0.088	61
26	SK0808	08-2	1.83	0.088	66
27	SK0808	08-8	1.83	0.088	57
28	SK2256	56-3	1.83	0.0817	41
29	SK2256	56-4	1.83	0.0817	46
30	SK2254	54-4	1.83	0.0817	54
31	SK2812	12-2	1.83	0.0817	50
32	SK2812	12-5	1.83	0.0817	59
33	SK2812	12-4	1.83	0.0817	26
34	SK2812	12-3	1.83	0.0817	37
35	SK2811	11-3	1.83	0.0817	23
36	SK2811	11-4	1.83	0.0817	23
37	SK2811	11-5	1.83	0.0817	23
38	SK2811	11-6	1.83	0.0817	23
39	SK2193	93-1	1.83	0.088	26
40	SK2193	93-2	1.83	0.088	22
41	SK2194	94-1	1.83	0.088	33
42	SK2194	94-4	1.83	0.088	18

43	SK2859	59-2	1.15	0.079	279
44	SK2859	59-3	1.15	0.079	74
45	SK0321	SK2683	0.32	0.0723	37
46	SK2683	83-1	1.2	0.091	24
47	SK2683	83-2	1.2	0.091	28
48	SK2683	83-3	1.2	0.091	60
49	SK2148	48-1	1.83	0.088	26
50	SK2148	SK0808	0.493	0.075	60
51	SK2811	SK2812	0.32	0.0723	237
52	SK2148	48-4	1.83	0.088	26
53	SK2193	93-5	1.83	0.088	22
54	SK2477	77-2	1.2	0.091	35
55	34-45	SK2034	1.2	0.091	102

Appendix 2: Load data

House Number	**Load**	**Power [kW]**
1	L931	10.86
2	L932	58.64
3	L935	4.10
4	L951	12.31
5	L592	1.37
6	L593	1.91
7	L941	13.15
8	L944	4.35
9	L551	9.41
10	L552	16.73
11	L564	2.09
12	L563	1.76
13	L544	4.07
14	L344	4.00
15	L345	4.00
16	L772	8.99
17	L773	17.45
18	L215	19.79
19	L481	8.46
20	L484	8.53
21	L801	9.39
22	L802	8.95
23	L804	6.66
24	L805	4.08
25	L806	4.72
26	L807	6.04
27	L808	5.62
28	L831	11.42

29	L832	6.75
30	L833	6.25
31	L111	18.80
32	L113	9.59
33	L114	8.60
34	L115	9.57
35	L116	2.00
36	L122	10.45
37	L123	8.16
38	L124	10.09
39	L125	10.90